# Design and Fabrication of Hybrid Auxetic Structure for Energy Absorption and Dimensional Stability


Submitted By

**Nawshin Fairuz Islam**
200012131

**Md. Yabid Hasan Utsha**
200012136

**Mohammod Al Shafin**
200012143

Supervised By
**Prof. Md. Zahid Hossain**


**A Thesis submitted in partial fulfillment of the requirement for the degrees of Bachelor of Science in Industrial and Production Engineering and Bachelor of Science in Mechanical Engineering**


**Department of Mechanical and Production Engineering (MPE)**
**Islamic University of Technology (IUT)**

**October, 2025**

**Candidate's Declaration**

This is to certify that the work presented in this thesis, titled, "Design and Fabrication of Hybrid Auxetic Structure for Energy Absorption and Dimensional Stability", is the outcome of the investigation and research carried out by me under the supervision of Dr. Md. Zahid Hossain, Professor, Department of Mechanical and Production Engineering, Islamic University of Technology.

It is also declared that neither this thesis nor any part of it has been submitted elsewhere for the award of any degree or diploma.

---------------------

**Nawshin Fairuz Islam**
Student No: 200012131

---------------------

**Md. Yabid Hasan Utsha**
Student No: 200012136

---------------------

**Mohammod Al Shafin**
Student No: 200012143

**Recommendation of the Thesis Supervisors**

---

The thesis titled "Design and Fabrication of Hybrid Auxetic Structure for Energy Absorption and Dimensional Stability" submitted by Nawshin Fairuz Islam, Student No: 200012131, Yabid Hasan, Student No: 200012136, and Mohammod Al Shafin, Student No: 200012143; has been accepted as satisfactory in partial fulfillment of the requirements for the degree of B Sc. in Industrial and Production Engineering **on 7th October 2025.**

1. -------------------------------------
   Dr Md. Zahid Hossain (Supervisor)
   MPE Dept., IUT, Board Bazar,
   Gazipur-1704, Bangladesh.

**CO-PO Mapping of ME 4800 -Theis and Project**

| COs | Course Outcomes (CO) Statement | (PO) | Addressed by | |
|---|---|---|---|---|
| | | | | |
| **CO1** | Discover and Locate research problems and illustrate them via figures/tables or projections/ideas through field visit and literature review and determine/Setting aim and objectives of the project/work/research in specific. | **PO2 Problem analysis** | Thesis Book<br>Performance by research<br>Presentation and soft skill | |
| **CO2** | Design research solutions of the problems towards achieving the objectives and its application. Design systems, components or processes that | **PO3 Design/development of solutions** | Thesis Book<br>Performance by research<br>Presentation and soft skill | |
| **CO3** | Review, debate, compare and contrast the relevant literature contents. Relevance of this research/study. Methods, tools, and techniques used by | **PO4 Investigation** | Thesis Book<br>Performance by research<br>Presentation and soft skill | |
| **CO4** | Analyse data and exhibit results using tables, diagrams, graphs with their interpretation. Investigate the designed solutions to solve the problems through case | **PO5 Modern tool usage** | Thesis Book<br>Performance by research<br>Presentation and soft skill | |
| **CO5** | Apply moral values and research/professional ethics throughout the work, and justify genuine referencing on sources, and | **PO8 Ethics** | Thesis Book<br>Performance by research<br>Presentation and soft skill | |
| **CO6** | Perform own self and manage group activities from the beginning to the end of the research/work as a quality work. | **PO9 Individual work and** | Thesis Book<br>Performance by research<br>Presentation and soft skill | |
| **CO7** | Compile and arrange the work outputs, write the report/thesis, a sample journal paper, and present the work to wider audience using modern communication | **PO10 Communication** | Thesis Book<br>Performance by research<br>Presentation and soft skill | |
| **CO8** | Recognize the necessity of life-long learning in career development in dynamic real-world situations from the experience of completing this project. | **PO12 Life-long learning** | Thesis Book<br>Performance by research<br>Presentation and soft skill | |

Student Name /ID:

1……………………………………….

2. ……………………………………….

3. ……………………………………….

Signature of the Supervisor: ……………………………

Name of the Supervisor: ……………………………….

**K-P-A Mapping of ME 4800 -Thesis and Project**

| COs | POs | Related Ks | | | | | | | | Related Ps | | | | | | | Related As | | | | |
|---|---|---|---|---|---|---|---|---|---|---|---|---|---|---|---|---|---|---|---|---|---|
| | | K1 | K2 | K3 | K4 | K5 | K6 | K7 | K8 | P1 | P2 | P3 | P4 | P5 | P6 | P7 | A1 | A2 | A3 | A4 | A5 |
| CO1 | PO2 | √ | √ | √ | √ | | | | | √ | | | | | | | | | | | |
| CO2 | PO3 | | | | | √ | | | | √ | √ | √ | | | | √ | √ | √ | √ | | |
| CO3 | PO4 | | | | | | | | √ | √ | √ | √ | | | | | √ | √ | | | |
| CO4 | PO5 | | | | | | √ | | | √ | | | | √ | | | | | | | |
| CO5 | PO8 | | | | | | | √ | | | | | | | | | | | | | |
| CO6 | PO9 | | | | | | | | | | | | | | | | | | | | |
| CO7 | PO10 | | | | | | | | | | | | | | | | | | | | |
| CO8 | PO12 | | | | | | | | | | | | | | | | | | | | |

Student Name /ID:

1……………………………………..

2. ……………………………………..

3. ……………………………………..

Signature of the Supervisor:

…………………………

Name of the Supervisor:

…………………………….

**List of Sustainable Development Goals (SDGs) Addressed in this Project**

| SDG No. | Goals | Targets | Relevance to the Thesis (put √ if valid) | Remarks |
|---|---|---|---|---|
| 1 | No Poverty | 1.1 Eradicate extreme poverty (people living on less than $1.25/day). | | |
| | | 1.2 Reduce poverty in all its forms by at least half. | | |
| | | 1.3 Implement nationally appropriate social protection systems. | | |
| | | 1.4 Ensure equal rights to economic resources, services, property, inheritance, technology, and financial services. | | |
| | | 1.5 Build resilience of the poor and reduce exposure to climate-related and other shocks. | | |
| | | 1.a Mobilize resources to end poverty. | | |
| | | 1.b Create pro-poor policy frameworks. | | |
| 2 | Zero Hunger | 2.1 End hunger and ensure access to safe, nutritious food year-round. | | |
| | | 2.2 End all forms of malnutrition. | | |
| | | 2.3 Double agricultural productivity and incomes of small-scale producers. | | |
| | | 2.4 Ensure sustainable food production systems and resilient agricultural practices. | | |
| | | 2.5 Maintain genetic diversity of seeds, plants, and animals. | | |
| | | 2.a Increase investment in rural infrastructure, research, and technology. | | |
| | | 2.b Correct and prevent trade restrictions/distortions in global food markets. | | |
| | | 2.c Adopt measures to ensure proper functioning of food commodity markets. | | |
| 3 | Good Health and Well-Being | 3.1 Reduce global maternal mortality ratio. | | |
| | | 3.2 End preventable deaths of newborns and under-5 children. | | |
| | | 3.3 End epidemics of AIDS, tuberculosis, malaria, and neglected tropical diseases. | | |
| | | 3.4 Reduce premature mortality from NCDs and promote mental health. | | |
| | | 3.5 Strengthen prevention and treatment of substance abuse. | | |
| | | 3.6 Halve global deaths/injuries from road traffic accidents. | | |
| | | 3.7 Ensure universal access to sexual and reproductive healthcare. | | |
| | | 3.8 Achieve universal health coverage. | | |
| | | 3.9 Reduce deaths from hazardous chemicals, pollution, and contamination. | | |
| | | 3.a Strengthen tobacco control (WHO FCTC). | | |
| | | 3.b Support R&D of vaccines and medicines. | | |
| | | 3.c Increase health financing and workforce. | | |

| | | | | |
|---|---|---|---|---|
| | | 3.d Strengthen capacity for early warning and risk management. | | |
| 4 | Quality Education | 4.1 Ensure all complete free, equitable, quality primary and secondary education. | | |
| | | 4.2 Ensure access to quality early childhood development and pre-primary education. | | |
| | | 4.3 Ensure equal access to affordable technical, vocational, and higher education. | | |
| | | 4.4 Increase skills for employment and entrepreneurship. | | |
| | | 4.5 Eliminate gender disparities in education. | | |
| | | 4.6 Ensure literacy and numeracy for youth and adults. | | |
| | | 4.7 Ensure learners acquire knowledge/skills for sustainable development. | | |
| | | 4.a Build and upgrade education facilities that are inclusive and safe. | | |
| | | 4.b Expand scholarships for developing countries. | | |
| | | 4.c Increase supply of qualified teachers. | | |
| 5 | Gender Equality | 5.1 End all forms of discrimination against women and girls. | | |
| | | 5.2 Eliminate violence against women and girls. | | |
| | | 5.3 Eliminate harmful practices (child, early, forced marriage, FGM). | | |
| | | 5.4 Recognize and value unpaid care and domestic work. | | |
| | | 5.5 Ensure women's participation in leadership and decision-making. | | |
| | | 5.6 Ensure universal access to reproductive health and rights. | | |
| | | 5.a Undertake reforms to give women equal rights to resources. | | |
| | | 5.b Enhance use of enabling technology to empower women. | | |
| | | 5.c Adopt and strengthen policies and laws for gender equality. | | |
| 6 | Clean Water and Sanitation | 6.1 Achieve universal and equitable access to safe drinking water. | | |
| | | 6.2 Achieve access to adequate sanitation and hygiene. | | |
| | | 6.3 Improve water quality by reducing pollution. | | |
| | | 6.4 Increase water-use efficiency and sustainable withdrawals. | | |
| | | 6.5 Implement integrated water resources management. | | |
| | | 6.6 Protect and restore water-related ecosystems. | | |
| | | 6.a Expand international cooperation in water and sanitation. | | |
| | | 6.b Support participation of local communities. | | |
| 7 | Affordable and Clean Energy | 7.1 Ensure universal access to affordable, reliable, modern energy services. | | |

| | | | | |
|---|---|---|---|---|
| | | 7.2 Increase substantially the share of renewable energy. | | |
| | | 7.3 Double global rate of improvement in energy efficiency. | | |
| | | 7.a Enhance international cooperation on clean energy research/technology. | | |
| | | 7.b Expand infrastructure and upgrade technology for sustainable energy. | | |
| 8 | Decent Work and Economic Growth | 8.1 Sustain per capita economic growth. | | |
| | | 8.2 Achieve higher levels of productivity through diversification, tech, and innovation. | | |
| | | 8.3 Promote policies for decent job creation and entrepreneurship. | | |
| | | 8.4 Improve resource efficiency in production and consumption. | | |
| | | 8.5 Achieve full and productive employment for all. | | |
| | | 8.6 Substantially reduce youth not in employment/education/training. | | |
| | | 8.7 Eradicate forced labour, modern slavery, and child labour. | | |
| | | 8.8 Protect labour rights and safe working environments. | | |
| | | 8.9 Promote sustainable tourism. | | |
| | | 8.a Increase aid for trade support. | | |
| | | 8.b Develop a global youth employment strategy. | | |
| 9 | Industry, Innovation, and Infrastructure | 9.1 Develop quality, reliable, sustainable infrastructure. | | |
| | | 9.2 Promote inclusive and sustainable industrialization. | | |
| | | 9.3 Increase access of SMEs to financial services and integration into value chains. | | |
| | | 9.4 Upgrade infrastructure for sustainability and resource efficiency. | | |
| | | 9.5 Enhance scientific research and technology development. | √ | |
| | | 9.a Facilitate sustainable infrastructure in developing countries. | | |
| | | 9.b Support domestic tech development and value addition. | | |
| | | 9.c Increase access to ICT and internet. | | |
| 10 | Reduced Inequalities | 10.1 Achieve income growth of bottom 40%. | | |
| | | 10.2 Empower and promote inclusion regardless of status. | | |
| | | 10.3 Ensure equal opportunity and reduce inequalities of outcome. | | |
| | | 10.4 Adopt policies for fiscal, wage, and social protection equality. | | |
| | | 10.5 Improve regulation of global financial markets. | | |
| | | 10.6 Ensure enhanced representation in global institutions. | | |

| | | | | |
|---|---|---|---|---|
| | | 10.7 Facilitate safe, regular, and responsible migration. | | |
| | | 10.a Implement special treatment for developing countries. | | |
| | | 10.b Encourage development assistance and investment in least developed areas. | | |
| | | 10.c Reduce remittance costs. | | |
| 11 | Sustainable Cities and Communities | 11.1 Ensure access to adequate, safe, and affordable housing. | | |
| | | 11.2 Provide sustainable transport systems. | | |
| | | 11.3 Enhance inclusive urbanization and capacity for planning. | | |
| | | 11.4 Protect cultural and natural heritage. | | |
| | | 11.5 Reduce disaster impact and losses. | | |
| | | 11.6 Reduce environmental impact of cities (air quality, waste). | | |
| | | 11.7 Provide access to safe, inclusive green/public spaces. | | |
| | | 11.a Support positive links between urban, peri-urban, rural. | | |
| | | 11.b Increase disaster risk reduction strategies. | | |
| | | 11.c Support least developed countries in sustainable building. | | |
| 12 | Responsible Consumption and Production | 12.1 Implement 10-Year Framework on sustainable consumption/production. | | |
| | | 12.2 Achieve sustainable management and use of resources. | | |
| | | 12.3 Halve per capita global food waste. | | |
| | | 12.4 Manage chemicals and waste sustainably. | | |
| | | 12.5 Substantially reduce waste generation. | | |
| | | 12.6 Encourage companies to adopt sustainable practices. | | |
| | | 12.7 Promote sustainable public procurement. | | |
| | | 12.8 Ensure people have relevant information for sustainable development. | | |
| | | 12.a Support developing countries' scientific and technological capacity. | | |
| | | 12.b Develop tools to monitor sustainable tourism impacts. | | |
| | | 12.c Rationalize inefficient fossil-fuel subsidies. | | |
| 13 | Climate Action | 13.1 Strengthen resilience and adaptive capacity to climate-related hazards. | | |
| | | 13.2 Integrate climate measures into national policies. | | |
| | | 13.3 Improve education and awareness on climate change. | | |
| | | 13.a Implement UNFCCC commitments (mobilize $100 billion annually). | | |
| | | 13.b Promote mechanisms for capacity-building in least developed countries. | | |
| 14 | Life Below Water | 14.1 Reduce marine pollution. | | |
| | | 14.2 Sustainably manage and protect marine ecosystems. | | |

| | | | | |
|---|---|---|---|---|
| | | 14.3 Minimize and address ocean acidification. | | |
| | | 14.4 Regulate harvesting and end overfishing. | | |
| | | 14.5 Conserve at least 10% of coastal and marine areas. | | |
| | | 14.6 Prohibit harmful fisheries subsidies. | | |
| | | 14.7 Increase economic benefits from sustainable marine resources. | | |
| | | 14.a Increase scientific knowledge and marine technology transfer. | | |
| | | 14.b Provide access for small-scale artisanal fishers. | | |
| | | 14.c Implement international law for oceans. | | |
| 15 | Life on Land | 15.1 Conserve terrestrial and freshwater ecosystems. | | |
| | | 15.2 Promote sustainable management of forests. | | |
| | | 15.3 Combat desertification and restore degraded land. | | |
| | | 15.4 Ensure conservation of mountain ecosystems. | | |
| | | 15.5 Take urgent action to reduce biodiversity loss. | | |
| | | 15.6 Promote fair benefit-sharing from genetic resources. | | |
| | | 15.7 End poaching and trafficking of protected species. | | |
| | | 15.8 Prevent introduction of invasive alien species. | | |
| | | 15.9 Integrate ecosystem values into policies/planning. | | |
| | | 15.a Mobilize resources for biodiversity. | | |
| | | 15.b Finance sustainable forest management. | | |
| | | 15.c Support local communities for forest and wildlife. | | |
| 16 | Peace, Justice and Strong Institutions | 16.1 Reduce violence and related death rates. | | |
| | | 16.2 End abuse, trafficking, and violence against children. | | |
| | | 16.3 Promote rules of law and equal access to justice. | | |
| | | 16.4 Reduce illicit financial/arms flows, organized crime. | | |
| | | 16.5 Reduce corruption and bribery. | | |
| | | 16.6 Develop effective, accountable institutions. | | |
| | | 16.7 Ensure inclusive, participatory decision-making. | | |
| | | 16.8 Broaden participation of developing countries in global governance. | | |
| | | 16.9 Provide legal identity for all (including birth registration). | | |
| | | 16.10 Ensure access to information and protect freedoms. | | |

| | | | | |
|---|---|---|---|---|
| | | 16.a Strengthen national institutions for prevention of violence. | | |
| | | 16.b Promote/enforce non-discriminatory laws and policies. | | |
| 17 | Partnerships for the Goals | 17.1 Strengthen domestic resource mobilization. | | |
| | | 17.2 Developed countries to implement ODA commitments. | | |
| | | 17.3 Mobilize additional financial resources.<br>17.4 Assist developing countries with debt sustainability.<br>17.5 Invest in least developed countries. | | |
| | | 17.6 Enhance access to science, technology, innovation. | | |
| | | 17.7 Promote environmentally sound technologies. | | |
| | | 17.8 Fully operationalize technology bank for LDCs. | | |
| | | 17.9 Enhance international support for capacity-building. | | |
| | | 17.10 Promote a universal, rules-based trading system (WTO). | | |
| | | 17.11 Increase exports of developing countries. | | |
| | | 17.12 Timely implementation of duty-free, quota-free market access. | | |
| | | 17.13 Enhance global macroeconomic stability. | | |
| | | 17.14 Enhance policy coherence for sustainable development. | | |
| | | 17.15 Respect national policy space.<br>17.16 Enhance global partnerships. | | |
| | | 17.17 Encourage multi-stakeholder partnerships. | | |
| | | 17.18 Enhance data capacity of developing countries. | | |
| | | 17.19 Support capacity-building for sustainable development indicators. | | |

# Acknowledgment

This work is done through the grace and guidance of the Almighty.

We are deeply grateful to Professor Dr. Md. Zahid Hossain for his invaluable guidance, constructive suggestions, and continuous support. His insightful feedback and encouragement have greatly shaped the quality of this research and contributed to both its successful completion and our academic development.

We are ever grateful to Asst. Prof. Chowdhury Sadid Alam for his unwavering guidance and constant support throughout this project. At times when we struggled with the research direction, his insightful advice helped us overcome difficulties and avoid errors. Without his presence and mentorship, we could not have learned and accomplished as much as we did. His contributions were instrumental in bringing our work to a meaningful and successful conclusion.

We are grateful to our beloved parents for their love, support and encouragement during our academic journey. They were the wind under our wings, and we will continue to be uplifted by their faith in us.

# Abstract

This thesis has detailed the design, analytical and experimental testing of a new Hybrid Hex-S auxetic structure with S-shaped auxetic cells, which are known to have energy absorbing flexibility, integrated into hexagonal honeycomb-like structure because of its inherent stiffness and structural integrity. The mechanical property of auxetic materials that result in a negative Poisson ratio (NPR) is their ability to expand sideways when under tension and contract when under compression. Such an outstanding aspect gives auxetics unique characteristics of energy absorbing capability and high fracture toughness which are highly desired in areas of application where energy absorption and impact resistance are required. Auxetic materials and NPR materials in particular introduce outstanding advantages into the realms of application such as biomedical equipment and personal protection equipment etc.

Nevertheless, besides the above benefits of such an elastic lattice structure, also common auxetic substructures, such as re-entrant ones, also experience stress concentration at its sharp corner because of which the premature failure and cyclic fatigue operation under real loadings is limited. Such issues are significant shortcomings to the serviceability, and the serviceability itself of the auxetic materials particularly in real application since in many cases they can be subjected to repetitive loading. To resolve these issues, we created the Hybrid Hex-S structure that utilized S-typed auxetic cell to Okamoto hexagonal honeycomb. The uniform S-shaped cells reduce the concentration of the local stress and enhance the uniform deformation to significantly enhance the energy absorption and low cycle fatigue characteristics of the structure.

Based on the discussion and analysis of mechanical behavior, Hybrid Hex-S has superior mechanical properties compared to re-entrant and Aux-Hex structures. The re-entrant geometries have highly localized hot spots under loading which have plastic deformation, whilst the Aux-Hex designs permanently densify at the beginning due to geometry discontinuities. Conversely, Hybrid Hex-S exhibits the prevalence of curvature-based deformation at enhanced compressive loading and enhanced recoveries in comparison with the reducing and recovering of structures with cyclical compression. In particular, under moderate compressive loading, the Hex-S structure demonstrated a stronger load-bearing capability by exhibiting a peak elastic performance that was approximately 6.7% higher than the Aux-Hex design, while remaining only about 4.4% lower than the Re-entrant configuration, all while maintaining good recoverability after unloading.

ASTM standard tests such as compression test, flexural test and tensile test were conducted experimentally on the structures of the Hybrid Hex-S to test the energy absorbency capacity of the material and its fatigue properties. In these experiments, the Hybrid Hex-S is proven to be higher than the conventional auxetic designs in terms of energy dissipation, crack toughness and resilience to cyclic loading. The energy dissipation analysis further indicated that the Hex-S configuration exhibited the lowest dissipation ratio (0.62) compared to the Re-entrant and Aux-Hex designs, which recorded higher ratios of 0.73 and 0.77, respectively. A lower dissipation ratio denotes that less strain energy is lost during deformation, implying that the structure is able to recover more of the stored elastic energy rather than dissipating it as permanent damage.

Therefore, this reduced energy loss behavior highlights the superior elastic recovery and structural stability of the Hex-S geometry under cyclic or repeated loading. Creation of such a structure is of extremely high demand in the field of additive manufacturing (AM), including Fused Deposition Modeling (FDM) 3D printing. The discussion of scalable and manufacturable hybrid auxetic structures is one of the most important new elements of this thesis. In FDM 3D-printing, the paper addresses some of the most troublesome challenges in the production scale, such as [1–6]: fatigue resistance; mechanical robustness; and the ability to print complex and/or auxetic geometries. This study employs the advantages of FDM and TPU to present a scalable pathway to hybrid auxetic materials that can be produced simply with low costs with no expensive geometry ballooning procession to achieve high accuracy to enable such materials to be used in large-scale manufacturing.

Hybrid Hex-S would find very efficient use in impregnable protection gear like helmets and body armor, or even implantable biomedical devices. It is an ideal material in next generation safety products/protection components due to its high energy absorption characteristics and capability to scale-up the manufacturing processes. Lastly, the additively manufactured materials may be designed to fit certain applications and application-specific designs.

This work enhances the mechanical metamaterials and develops the auxiliary materials and their uses. The design goal of the Hybrid Hex-S structure is to satisfy the engineering goal in the material scalability, fatigue, and stress homogenization. It demonstrates its ability to have a wide range of uses. Through the application of the latest methods in additive manufacturing and 4d printing, alongside multiscale modeling, this research provides the basis of the further progress of the next generation materials, adjusted to the needs of the modern industries.

**Keywords:** Additive Manufacturing, Advanced Materials, Mechanical Metamaterials, FDM 3D Printing, Energy Absorption, S-Shaped Cells, Hybrid Auxetic Structures, ASTM Testing, Impact Resistance, Fatigue Resistance, Multiscale Modeling, 4D Printing.

## Summary (For Non-Technical Audience)

This thesis presents a case study on the design and evaluation of Novel Hybrid Structure – Hex-S (where Hexagonal is conventional & S- shaped structure is a relatively new auxetic structure among all), which attempts to integrate two significant mechanical properties: flexibility and stiffness. Auxetic materials are a unique class of material which responds oddly: they widen when stretched and decrease in width while compressed from all directions, unlike typical materials. This special property has made them ideal for use in energy absorption and impact resistance mechanisms, such as protective equipment and car crash vehicle.

In this work, we further improve the performance of the auxetic structures by combining flexibility property of S-shaped auxetic cells and stiffness property of standard Hexagonal structure. What you want to do is make a material that combines the best of these two things, that can dissipate and absorb energy very well but also stay strong and be stable under stress.

In order to pursue this, the thesis has three subgoals as follows.

- The structure of Hex-S Structure: By utilizing hexagonal lattice together with S-shape auxetic cell, it is a new design for the auxetic material. This architecture is designed to enhance energy absorption, dimensional stability and mechanical properties in numerous applications.
- Re-testing Performance: We use cutting – edge computer simulation methods to model the performance of the S- Hex structure under diverse loading conditions compression, impact and others. These simulations are useful for predicting how material would behave in real-world applications. Also, physical characterizations are carried out to test the energy absorption, strength and dimensional stability of the material.
- Comparison with Traditional Structures: The performance of our new Hex-S structure is compared with the traditional auxetic designs viz, Re-entrant and Aux-Hex structures. You can choose various materials to test their impact on system performance, such as TPU and PLA. Such a comparison is useful to illustrate the pros and cons of the new design for energy dissipation improvement but also better stability.

The findings demonstrate that Hex-S retains a high energy absorption, and it keeps its structural integrity under load condition and recovers part of the dissipative energy (which is instead dissipated by traditional materials). This makes it a perfect candidate for applications including armor (helmets), medical devices, implants, lightweight structural components in the aerospace and automotive industries.

# Table of content

Contents


Candidate's Declaration ..... 2
Recommendation of the Thesis Supervisors ..... 3
CO-PO Mapping of ME 4800 -Theis and Project ..... 4
K-P-A Mapping of ME 4800 -Thesis and Project ..... 6
List of Sustainable Development Goals (SDGs) Addressed in this Project ..... 3
Acknowledgment ..... 9
Abstract ..... 10
Summary (For Non-Technical Audience) ..... 12
Table of content ..... 13
List of Tables ..... 1
List of Figures ..... 2
Nomenclatures and Symbol ..... 5
Chapter 1: Introduction ..... 6
Chapter 2: Literature Review ..... 7
2.1 Fundamentals of Auxetic Structures ..... 7
2.2 Classical and Emerging Auxetic Structures ..... 8
2.2.1 S-Shaped Cellular Architectures ..... 8
2.2.2 Hexagonal Honeycomb Structures ..... 9
2.2.3 Re-entrant Auxetic Structures ..... 11
2.3 Hybrid Auxetic Structures and Aux-Hex Design: A Delicate Equilibrium ..... 12
2.3.1The Hybrid Structure: Rationale and Advantages ..... 12
2.3.2 Aux-Hex Hybrid Structures ..... 13
2.4 Tailoring Mechanical Behavior through Positive and Negative Poisson's Ratio Regions ..... 13
2.5 Materials for Additive Manufacturing of Auxetic Structures ..... 15
2.5.1 Thermoplastic Polyurethane (TPU) ..... 15
2.5.2 Polylactic Acid (PLA) ..... 16
2.6 Additive Manufacturing Techniques for Auxetic Fabrication ..... 17
2.6.1 Stereolithography (SLA) ..... 17
2.6.2 Selective Laser Sintering (SLS) ..... 18
2.6.3 Fused Deposition Modeling (FDM) ..... 19
2.7 Dimensional Stability of Auxetic Structures ..... 21
2.8 Identified Research Gaps ..... 23
2.8.1 Limited Research on Hybrid Auxetic Structures ..... 23
2.8.2 Lack of Research on Structural Stability of Auxetic Structures ..... 23
2.8.3 Challenges in Scaling FDM Technology for Industrial Applications ..... 23
Chapter 3: Research Objectives & Methodology ..... 24
3.1 Objectives ..... 24
3.2: Methodology ..... 25
Chapter 4: Validation ..... 27
4.1 Geometric modeling: ..... 27

4.2 Numerical Analysis: .......... 28
4.2.1 Validated Results: .......... 30
Chapter 5: Material Selection, Design & Fabrication .......... 32
5.1 Material Selection: .......... 32
5.2 Design: .......... 35
5.3 Fabrication: .......... 36
Chapter 6: Modelling and Simulation .......... 39
6.1 Material Defining: .......... 39
6.2 Contacts Defining: .......... 39
6.3 Meshing: .......... 40
6.4 Boundary Conditions Defining: .......... 42
Chapter 7: Results and Discussion .......... 44
7.1 Simulation results: .......... 44
7.2 Experimental results .......... 71
7.2.1 Load vs Displacement Results Comparison .......... 71
7.2.1.1 TPU Load vs Displacement Results .......... 72
7.2.1.2 PLA Load vs Displacement Results .......... 72
7.2.1.3 Comparison Between PLA and TPU Structures .......... 72
7.2.2 Stress-Strain results Comparison .......... 73
7.2.2.1 TPU Stress-Strain Behavior .......... 74
7.2.2.2 PLA Stress-Strain Behavior .......... 74
7.2.2.3 Comparative Discussion .......... 74
7.3 Comparison of Different Structures Printed with PLA for Different Displacements .......... 76
7.4 Comparison of Dimensional Stability .......... 82
7.5 Material Comparison .......... 85
Chapter 8: Future Work and Conclusion .......... 87
8.1 Conclusion .......... 87
8.2 Future Scope .......... 88
References .......... 89

# List of Tables

**TABLE 1** ..........27

**TABLE 2** ..........27

**TABLE 3** ..........30

**TABLE 4** ..........31

**TABLE 5** ..........34

**TABLE 6** ..........35

**TABLE 7** ..........35

**TABLE 8** ..........35

**TABLE 9** ..........83

# List of Figures


FIGURE 1- (A) UNIT CELL S-SHAPED STRUCTURE (B) WHOLE S-SHAPED STRUCTURE........... 8
FIGURE 2- WHOLE HEXAGONAL STRUCTURE........................................................................ 9
FIGURE 3: WHOLE RE-ENTRANT STRUCTURE ..................................................................... 11
FIGURE 4: WHOLE AUX-HEX STRUCTURE........................................................................... 13
FIGURE 5 : COMPARISON OF NPR, PPR & ZPR.................................................................. 15
FIGURE 6: STEREOLITHOGRAPHY ........................................................................................ 18
FIGURE 7:SELECTIVE LASER SINTERING (SLS) METHOD .................................................. 19
FIGURE 8:FUSED DEPOSITION MODELING (FDM) METHOD .............................................. 20
FIGURE 9: METHODOLOGY FLOWCHART .............................................................................. 25
FIGURE 10: UNIVERSAL STANDARD TESTING MACHINE ..................................................... 26
FIGURE 11: (A) UNIT CELL OF S-SHAPED STRUCTURE WITH DIMENSIONS, (B) FRONT VIEW OF S-SHAPED STRUCTURE, AND (C) ISOMETRIC VIEW OF S-SHAPED STRUCTURE........ 27
FIGURE 12:(A) UNIT CELL OF RE-ENTRANT STRUCTURE WITH DIMENSIONS, (B) FRONT VIEW OF RE-ENTRANT STRUCTURE, AND (C) ISOMETRIC VIEW OF RE-ENTRANT STRUCTURE ........................................................................................................ 28
FIGURE 13:CONVERGED MESH RESULT FOR (A) RE-ENTRANT STRUCTURE AND (B) S-SHAPED STRUCTURE ........................................................................................... 28
FIGURE 14:. FINITE ELEMENT MESH OF (A) RE-ENTRANT STRUCTURE AND (B) S-SHAPED STRUCTURE ........................................................................................................ 29
FIGURE 15:BOUNDARY CONDITIONS FOR (A) RE-ENTRANT STRUCTURE AND (B) S-SHAPED STRUCTURE ........................................................................................................ 29
FIGURE 16: EQUIVALENT STRESS RESULT FOR RE-ENTRANT STRUCTURE OF (A)REFERENCE, AND (B) SIMULATION.......................................................................................... 30
FIGURE 17: EQUIVALENT STRESS RESULT FOR S-SHAPED STRUCTURE OF (A)REFERENCE, AND (B) SIMULATION.......................................................................................... 31
FIGURE 18:. ASTM D695 FOR PLA (A)SPECIMEN DESIGN, (B)EXPERIMENTAL SETUP, AND (C)SPECIMEN BEFORE AND AFTER TEST .......................................................... 33
FIGURE 19: ASTM D695 FOR TPU (A)SPECIMEN DESIGN, (B)EXPERIMENTAL SETUP (DURING TESTING), AND (C)SPECIMEN AFTER TESTING............................................ 33
FIGURE 20: EXPERIMENTAL RESULTS OF ASTM D695 FOR (A)PLA, AND (B)TPU ............. 34
FIGURE 21: (A) UNIT CELL OF HYBRID HEX-S WITH DIMENSIONS, (B) ISOMETRIC VIEW OF HYBRID HEX-S UNIT CELL, (C) FRONT VIEW OF HYBRID HEX-S, AND (D) ISOMETRIC VIEW OF HYBRID HEX-S.................................................................................. 36
FIGURE 22: FDM 3D PRINTER................................................................................................ 37
FIGURE 23: 3D PRINTING SAMPLES OF HEX-S STRUCTURE USING (A)TPU, AND (B)PLA .... 38
FIGURE 24: MATERIAL PROPERTIES DEFINED IN THE ANSYS FOR (A)TPU, AND (B)PLA .. 39
FIGURE 25: (A) 3D MODEL OF THE LOAD, AND (B)FINITE ELEMENT MESHING OF THE LOAD ........................................................................................................................ 40
FIGURE 26: FINITE ELEMENT MESHING OF AUX-HEX STRUCTURE WITH LOAD APPLIED (A) ISOMETRIC VIEW, AND (C) FRONT VIEW ........................................................... 40
FIGURE 27: FINITE ELEMENT MESHING OF RE-ENTRANT STRUCTURE WITH LOAD APPLIED (A) ISOMETRIC VIEW, AND (C) FRONT VIEW ............................................. 41
FIGURE 28: FINITE ELEMENT MESHING OF HEX-S STRUCTURE WITH LOAD APPLIED (A)

Isometric View, and (c) Front view ..... 41
Figure 29: Fixed Support applied on (a) Re-entrant Structure, (b) Aux-Hex Structure, and (c) Hex-S Structure ..... 42
Figure 30: Unidirectional displacement applied on (a) Re-entrant Structure, (b) Aux-Hex Structure, and (c) Hex-S Structure ..... 43
Figure 31: Aux-Hex structure with Displacement of 2mm printed with PLA (a) Stress Result, and (b) Stress vs Time Graph ..... 45
Figure 32: Aux-Hex structure with Displacement of 5mm printed with PLA (a) Stress Result, and (b) Stress vs Time Graph ..... 46
Figure 33: Aux-Hex structure with Displacement of 15mm printed with PLA (a) Stress Result, and (b) Stress vs Time Graph ..... 47
Figure 34: Aux-Hex structure with Displacement of 15mm printed with TPU (a) Stress Result, and (b) Stress vs Time Graph ..... 48
Figure 35: Aux-Hex structure with Displacement of 30mm printed with TPU (a) Stress Result, and (b) Stress vs Time Graph ..... 49
Figure 36: Re-entrant structure with Displacement of 2mm printed with PLA (a) Stress Result, and (b) Stress vs Time Graph ..... 50
Figure 37: Re-entrant structure with Displacement of 5mm printed with PLA (a) Stress Result, and (b) Stress vs Time Graph ..... 51
Figure 38: Re-entrant structure with Displacement of 15mm printed with PLA (a) Stress Result, and (b) Stress vs Time Graph ..... 52
Figure 39: Re-entrant structure with Displacement of 15mm printed with TPU (a) Stress Result, and (b) Stress vs Time Graph ..... 53
Figure 40: Re-entrant structure with Displacement of 30mm printed with TPU (a) Stress Result, and (b) Stress vs Time Graph ..... 54
Figure 41: Hex-S structure with Displacement of 2mm printed with PLA (a) Stress Result, and (b) Stress vs Time Graph ..... 55
Figure 42: Hex-S structure with Displacement of 5mm printed with PLA (a) Stress Result, and (b) Stress vs Time Graph ..... 56
Figure 43: Hex-S structure with Displacement of 15mm printed with TPU (a) Stress Result, and (b) Stress vs Time Graph ..... 57
Figure 44: Aux-Hex structure with Displacement of 2mm printed with PLA (a) Deformation Result, and (b) Deformation vs Time Graph ..... 58
Figure 45: Aux-Hex structure with Displacement of 5mm printed with PLA (a) Deformation Result, and (b) Deformation vs Time Graph ..... 59
Figure 46: Aux-Hex structure with Displacement of 15mm printed with PLA (a) Deformation Result, and (b) Deformation vs Time Graph ..... 60
Figure 47: Aux-Hex structure with Displacement of 15mm printed with TPU (a) Deformation Result, and (b) Deformation vs Time Graph ..... 61
Figure 48: Aux-Hex structure with Displacement of 30mm printed with TPU (a) Deformation Result, and (b) Deformation vs Time Graph ..... 62
Figure 49: Re-entrant structure with Displacement of 2mm printed with PLA (a) Deformation Result, and (b) Deformation vs Time Graph ..... 63
Figure 50: Re-entrant structure with Displacement of 5mm printed with PLA

(a) Deformation Result, and (b) Deformation vs Time Graph ........................ 64
Figure 51: Re-entrant structure with Displacement of 15mm printed with PLA (a) Deformation Result, and (b) Deformation vs Time Graph ........................ 65
Figure 52: Re-entrant structure with Displacement of 15mm printed with TPU (a) Deformation Result, and (b) Deformation vs Time Graph ........................ 66
Figure 53: Re-entrant structure with Displacement of 30mm printed with TPU (a) Deformation Result, and (b) Deformation vs Time Graph ........................ 67
Figure 54: Hex-S structure with Displacement of 2mm printed with PLA (a) Deformation Result, and (b) Deformation vs Time Graph ........................ 68
Figure 55: Hex-S structure with Displacement of 5mm printed with PLA (a) Deformation Result, and (b) Deformation vs Time Graph ........................ 69
Figure 56: Hex-S structure with Displacement of 15mm printed with TPU (a) Deformation Result, and (b) Deformation vs Time Graph ........................ 70
Figure 57: Experimental results of Hex-S structure printed with (a)TPU and (b)PLA ........................ 71
Figure 58: Stress-Strain graphs for 30mm displacement of – (a) TPU (b) PLA .... 73
Figure 59: Force vs Displacement Graph of 2mm Strain rate for (a)Re-entrant (b) Aux-Hex (c) Hex-S ........................ 76
Figure 60: Force vs Displacement Graph of 5mm Strain rate for – (a) Re-entrant, (b) Aux-Hex, and (c) Hex-S ........................ 77
Figure 61: Force vs Displacement graph of 15mm strain rate for – (a)Re-entrant (b)Aux-Hex ........................ 78
Figure 62: Energy Absorption and Dissipation Curve for PLA structures for (a) Re-entrant, (b) Aux-Hex, (c) S-Hex ........................ 82
Figure 63: PLA-printed Hex-S structures of displacement- (a)2mm and (b)5mm. 85
Figure 64: TPU-printed Hex-S structures of displacement- 15mm ........................ 85

# Nomenclatures and Symbol

| Abbreviation | Nomenclature |
|---|---|
| ABS | Acrylonitrile Butadiene Styrene |
| AM | Additive Manufacturing |
| ASTM | American Society for Testing and Materials |
| Aux-Hex | Hybrid Auxetic-Hexagonal Structure |
| CAD | Computer-Aided Design |
| EA | Energy Absorbed |
| ED | Energy Dissipated |
| FDM | Fused Deposition Modeling |
| FEA | Finite Element Analysis |
| FGM | Functionally Graded Materials |
| FLC | Full Latent Heat Capacity |
| Hex-S | Hybrid Hexagonal-S-shaped Structure |
| NPR | Negative Poisson's Ratio |
| PLA | Polylactic Acid |
| PPR | Positive Poisson's Ratio |
| SDG | Sustainable Development Goal |
| SLA | Stereolithography |
| SLS | Selective Laser Sintering |
| TPU | Thermoplastic Polyurethane |
| UV | Ultraviolet |
| ZPR | Zero Poisson’s Ratio |

| Symbol | Meaning |
|---|---|
| $A$ | Cross-sectional Area |
| $E$ | Young's Modulus (Elastic Modulus) |
| $F$ | Force |
| $F_{loading}$ | Force during loading phase |
| $F_{unloading}$ | Force during unloading phase |
| $H$,$L$,$T$,$W$ | Geometric dimensions (Height, Length, Thickness, Width) |
| $I$,$p$,$M$,$R$ | Geometric dimensions for Hex-S unit cell |
| $l_0$ | Original length |
| $\Delta l$ | Change in length |
| $x$ | Displacement |
| $x_1$ | Initial Displacement |
| $x_2$ | Final Displacement |
| $\alpha, \theta_{1,} \theta_2$ | Angles in geometric models (degrees) |
| $\varepsilon$ | Strain |
| $\sigma$ | Stress |

# Chapter 1: Introduction

Auxetic structures are gaining increasing attention because of their unique mechanical response and versatile structural design. Unlike conventional materials that contract laterally when stretched and expand laterally when compressed, auxetic materials exhibit the opposite deformation behavior. They expand in the transverse direction when subjected to tensile loading and contract when compressed. This counterintuitive response is known as the Negative Poisson's Ratio (NPR) effect, which arises mainly from the geometry of the structure rather than the inherent properties of the material. With carefully engineered unit-cell topologies, auxetic structures can achieve mechanical characteristics that are unattainable in traditional designs, including enhanced flexibility, superior energy absorption, and improved impact resistance.

The auxetic behavior mechanism is entirely geometrical in nature. This is an internal structure of the components that allows deformation to take place through performing a combination of rotation, bending and hinging (instead of stretching axially) is treated as preferable to the construction. When tensile forces act on the geometry, it opens up, placing a lateral growth. Volume compression leads to the same structure closing in the same manner and there is no instability; it is open to densification. The distinctive characteristics of auxetic structures include homogeneous tension distribution; high energy absorption and penetration and localized failure since most are controlled to collapse and these properties make them highly applicable in protective and impact resistant purposes.

The last several decades have seen the study of numerous auxetic geometries in order to achieve a desired set of mechanical properties. The re-entrant as a structure is among the most traditional designs in which the cells have in-slanted walls that bend back and pass down the surface upon load therefore creating powerful NPR behavior. Conversely, S-shaped structure is auxetic, having smooth and curved cell walls which are always flexing in an attempt to allow easier recoverability or damping. By analogy, the overall effect of the hexagonal honeycomb structure is often positive Poisson ratio (PPR) effect, i.e. expanding laterally when compressed and pinching when forced open, which the lateral size does not fully restore and influences both stiffness and flexibility.
The combination of such competing geometries has led to the formation of the hybrid auxetic structures that contain both auxetic (NPR) and non-auxetic (PPR) structures in a single frame. Stereotyping with a variety, e.g. re-entrant as well as S-shaped and regular hexagon shaped stereotyping gives a good trade-off between strength, ductility and energy dissipation. These structures are however being investigated on a variety of advanced applications like the protective armor, aerospace damping system and biomedical implant where light weight is needed alongside toughness.

As a result, understanding of the geometry deformation mechanisms in auxetic structures can be used as a fundamental point which will be used to design and study a combined S-shaped/hexagonal (auxetic-honeycomb) structure whose purpose is to offer improved compressive strength, flexibility and energy absorption action.

# Chapter 2: Literature Review

## 2.1 Fundamentals of Auxetic Structures

Auxetics are a class of synthetic materials with negative Poisson's ratio (NPR), these materials expand laterally while stretched and contract laterally when compressed. The bizarre setting that these structures exhibit is not in the material, but inherent to their internal structure. Various geometries have been developed so far to generate auxetic response, such as re-entrant, S-shape, rotating unit, chiral and hybrid honeycombs.

The re-entrant geometry is one of the most popular auxetic geometries. It is made up of inwardly projecting cell angles, so that under load, these collapse and expand simultaneously with each other thereby opening and closing laterally during compression. This geometry has been investigated for improved energy absorption and deformation management under quasi-static or dynamic loading (Ardebili et al., 2018 [1]; R.P Bohara et al, 2024 [2]). The structural feature of re-entrant cells is that it can collapse continuously in the face of external force, and stress can be distributed uniformly, which are very suitable for impact protection, damping materials applications (Choi et al., 2022 [4]).

The S-shaped auxetic structure, also referred to as the "S-structure," benefits from a smooth deformation path with minimal stress concentration and good recoverability when compared with sharp re-entrant designs. Its smooth curve provides more bending power, the ability to withstand side loading. Theoretical and numerical studies revealed that the S-shaped design can balance the stiffness and energy dissipation for the crushing state (Etemadi et al., 2024 [7]; Jin et al., 2021 [9]).

In addition to traditional pure single-type geometries, hybrid auxetic materials have been proposed to integrate various deformation tactics in common structural configurations. These include re-entrant and hexagon combinations, which are combined to form mixed (Aux-Hex) geometry and other mixed geometries where at least one component may provide for improved load distribution or other desired attributes such as being able to control stiffness. Such structures also exhibit better trade-off between lateral expansion and energy absorption, in charity of the auxiliary-connected non-auxetic cells these results them as suitable for multi-directional impact resistance and high-strain applications (Lagoda and Gabor, 2018 [12]; Joseph et al., 2021 [11]). The hybrid design not only expands the entire landscape of reachable mechanical response but also enables designers to tailor deformation pathways through varying the geometry instead of modifying the parent material.

More recently, geometrically optimized and architecturally inspired auxetic structures have also been proposed, with the performance of which is influenced by the structure's own form. Examples are rotating square-based cell systems, and tunable re-entrant networks that show distinctive deformation modes supporting high compressive strain recovery and stability (Li et al., 2019 [13]; Plewa et al., 2022 [19]; Pothier et al., 2022 [20]). These design-guided advancements demonstrate the role of geometric architecture in directing auxetic behavior and open up possibilities for second-generation mechanical metamaterials with tunable and predictable deformation responses.

In general, the auxetic geometry shows great scale and load adaptability. Their shape memory properties are also geometry-activated and lead to more effective impact absorbing/impact resistant mechanisms as well as design options for aerospace, protective gear, or medical engineering (Rufo-Martín et al., 2025 [24])

## 2.2 Classical and Emerging Auxetic Structures

A large variety of geometrical structures presented up to date exist for auxetic, having different mechanical and performance characteristics. Such configurations are able to take advantage of the negative Poisson's ratio (NPR) effect, through which the structures display lateral expansion while being stretched and contraction in the transverse direction when compressed. Such properties are of much importance for their applications in various fields such as protection materials, bio medicaments. In the following, we describe a selection of well-known and emerging auxetic topologies, from traditional to recently discovered ones, discussing their main features and applications.

### 2.2.1 S-Shaped Cellular Architectures

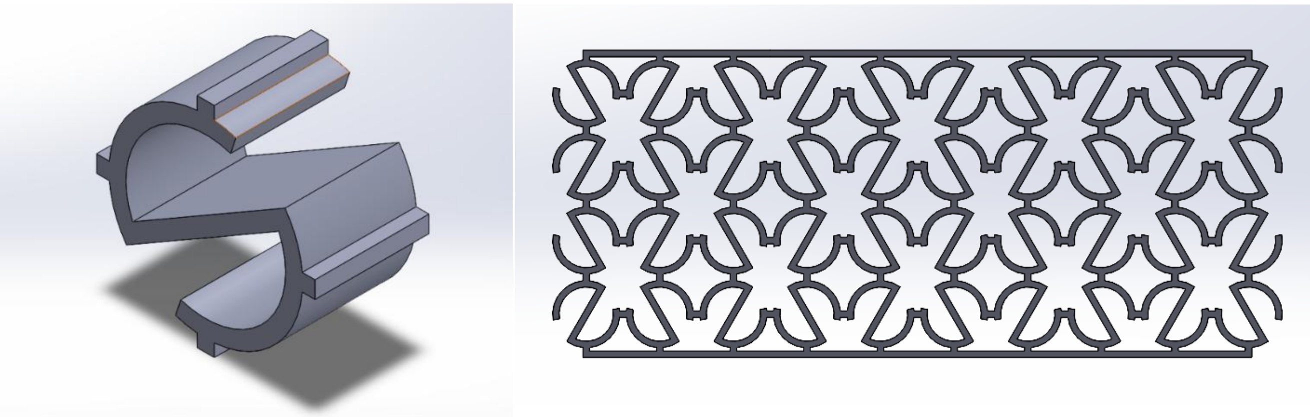

**(a)** **(b)**

***Figure 1:(a) Unit cell S-Shaped Structure, (b) Whole S-shaped structure***

Auxetic S-shapes have been developed as a move beyond conventional re-entrant designs which may suffer from corner failures when stress concentrations become too high. The addition of smooth, continuous curves in the S-shaped cell geometry helps to solve this problem by providing a more rugged structure that is able to better resist fatigue failure due to cyclic loading.

Meena and Singamneni (2019) [16]: By considering S-shaped auxetic cells fabricated as elastomer structures, it was systematically shown that such a cell possesses larger cyclic strains and much less stress-focusing phenomena compared to the RBM case. The gentle curvature of the S-shape makes stress easier to distribute throughout the structure, so more energy can be absorbed. This feature is of particular interest for applications involving multiple loading and unloading cycles, such as protective clothing or wearables.

It should be noted that Namvar et al., 2022 [18]) have shown how the continuous curvature characteristic of an S-shaped design resulted in a ~ 50% reduction in peak von-Mises stress with respect to typical re-entrant formed shapes. This decrease in peak stress is associated with a marked improvement in the materials structural fatigue performance, rendering S-shaped auxetics suitable for use in extreme-performance technologies that require high fatigue resistance, e.g. robotic actuators and padding systems. Moreover, NPR values as low as -2.5 can be obtained with these geometries, which compares very favorably with conventional re-entrant designs (NPR around -1.2), significantly extending their potential for utilization in wearable technology and biomedical implants investigated in Meena et al. [16]

S-shaped auxiliary cells can provide smooth deformation as well as better energy absorption, and thus potentially Ideal structure in a large number of fields such as industries with cyclic loading which require durability of material body among lots of applications.

### 2.2.2 Hexagonal Honeycomb Structures

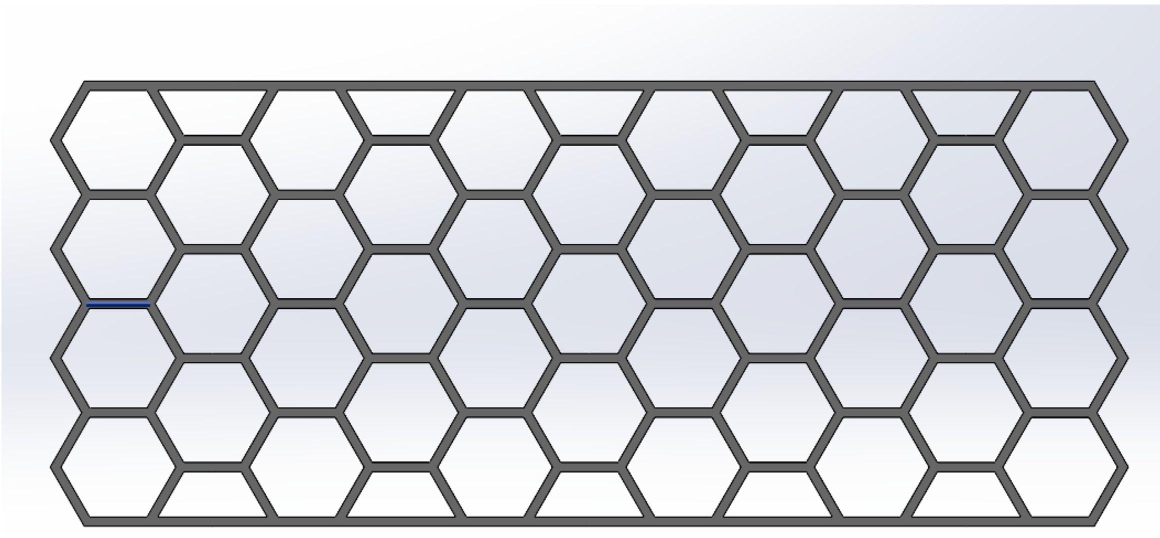

***Figure 2: Whole Hexagonal Structure***

Some of the most commonly used and earliest shaped cellular structures are hexagonal honeycomb truss, and known to be of high stiffness-to-weight ratio and in-plane load transfer preference. They use such buildings where there would be a light-weight application, but where the strength level is required to be high e.g. aerospace, automotive or building industries. They are able to share stresses that would conveniently be used in load-bearing purposes that need light and powerful structure (Plewa et al., 2022 [19]).

In addition to these competitive advantages, the hexagonal honeycombs do possess PPR property, which, when compressed, expands laterally, and when in tension, expands laterally. Although it is a valuable property in most structural use, it limits the ability of the honeycomb to absorb energy in impact conditions. Such a positive ratio of the structure in Poisson will result in a reduced energy dissipation capacity, which is required but is not desired in an application that needs a larger region of energy uptake such as in a protective system or shock isolation structure (Pothier et al., 2022 [20]).

Honeycombs are highly utilized as they have structural performance efficiency, high compressive strength and low weight ratio particularly in aerospace and automotive structures (Qiao and Chen 2015 [22]). However, rigidity of such structures is basically related to the nature of energy absorption of such structures and thus their operation in various impact resistant applications could be comparatively poor.

The hexagonal honeycomb is a structure with geometric properties (high mechanical strength and even distribution of loads), which are quite convenient to use when the structural rigidity is needed with a minimum weight. As one example, a construction structure (sandwich panels with hexagonal honeycomb cores) (Ren et al., 2018 [23]; Rufo-Martin et al., 2025 [24]) and a lightweight component of an aircraft and vehicle crash-worthiness equipment can be offered because this type of honeycombs can be loaded in compression without significant plastic deformation.

Finally, in case a honeycomb with the hexagonal cell is implemented, the strength to weight ratio and the structural efficiency of this cell remains insightful in all types of loads-carrying applications. Yet, a Poisson ratio that is positive of these honeycombs poses negative challenges to their application as a component in applications that require high-energy absorption and hybrid structural designs that use honeycomb and auxetic components to be deployed to increase impact mitigation have recently been investigated (Xu et al., 2019 [30])

### 2.2.3 Re-entrant Auxetic Structures

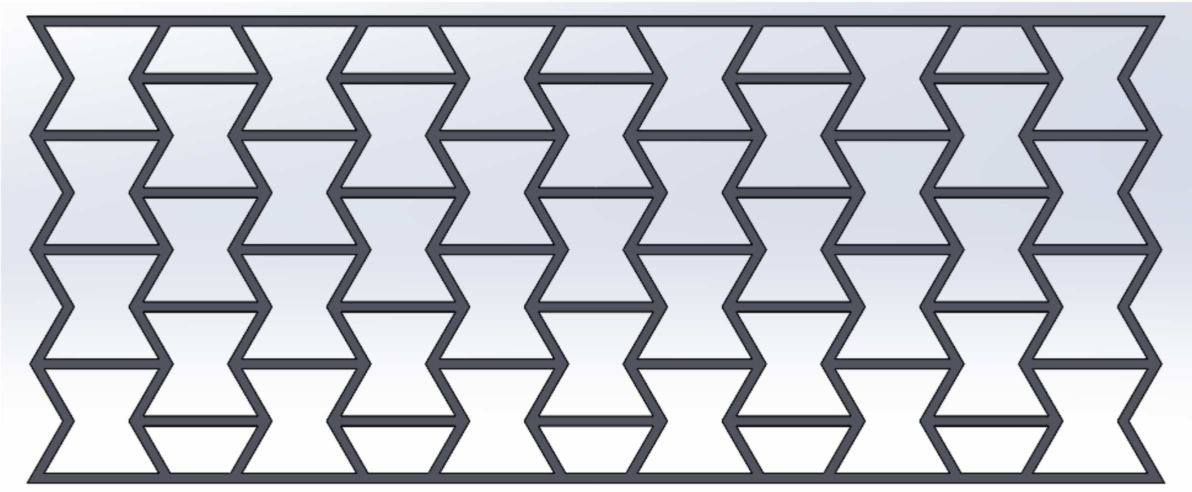

***Figure 3: Whole Re-entrant Structure***

One of the most familiar families of auxetic structure are re-entrant structures where the inclination of their ribs is inwards so that when stressed laterally they elongate and when stressed compressively they contract. They were originally theorized in Choi et al., 2022 [4], in which, through geometry manipulation of the unit cell, were able to enable a negative Poisson ratio (NPR). A number of studies have since been devoted to optimizing rib angles, wall thickness and unit cell geometries to higher levels so as to maximize the NPR effect and to optimize the mechanical performance of the material.

Usually, NPR of re-entrant geometries falls in a range of -0.2 to -0.6. Though these values are minor compared to the ones of other auxetic structures, the cavities bring much benefit to the energy absorption and stress distribution. Stress concentration however is among the harsh limitations of the re-entrant structures, particularly when the cells are sharp ended, and it can lead to local failure with the high strain. Duncan et al., 2018 [6] noted that this issue was solved by the fact that local sharp geometries and stress concentrations can lead to premature failure of the design, especially when the load is cyclic.

To avoid this, Etemadi et al., 2024 [7] recommended that the structure should be modified such as by tapering the ribs and fillets at corners to prevent the occurrence of a non uniform distribution of stress. This change is able to feel the stress concentration and increase the material durability. Moreover, additive manufacturing (and, specifically, FDM with TPU) has enabled the creation of such auxiliary patterns as re-entrant type auxetic structures getting less and less primitive and offering more advantageous mechanical characteristics and enhanced strength.

There is practical use in re-entrant geometries which are exotic in their behavior and are applicable in flexibility and energy absorption namely, protective materials, medical implants, and energy-absorbing materials in automotive and aerospace. Their major property is the capability to change shape under stresses exerted on them and simultaneously maintain structural integrity which makes them a prospective candidate of possible applications.

## 2.3 Hybrid Auxetic Structures and Aux-Hex Design: A Delicate Equilibrium

The hybrid patterns have been explored to overcome the limitations of the auxetic or non-auxetic ones. NPR areas offer energy and produce some form of elasticity, well PPR areas provide an increase to the overall structure of the structure in terms of stiffness and stability. The resulting stiffness uniformity in space creates anisotropic stiffness, which slows down the speed of its failure and fatigue strength (Jin et al., 2021 [9]; Johnston and Kazancı, 2021 [10]).

Aux-Hex which incorporates auxetic re-entrant unit cell and regular honeycomb is one of the most noticeable hybrid methods. According to Joseph et al., 2021 [11], the Aux-Hex structures have higher energy absorption leading to high impact resistance. Duncan et al., 2018 [6], and Joseph et al. (2022)[11] further expounded that the rigid hexagonal shapes ED with the units of the material facilitate an improvement in the crash energy absorbing capability and compression response of the material. The Aux-Hex structures also demonstrate a superior indentation resistance compared to monolithic honeycombs (Mondal/R., 2024 [17]) the Aux-Hex structures also demonstrate a superior indentation resistance compared to monolithic honeycombs. Combined these findings indicate the trade-off in which Aux-Hex introduces between the flexibility and energy dissipation of auxetics and the rigidity and structural resistance of hexagonal cells.

### 2.3.1 The Hybrid Structure: Rationale and Advantages

From the concept of Aux-Hex, further enhancements have been developed by using curved auxetic geometries (such as "S"-shaped cells). In contrast to re-entrant geometries where there are sharp U-turns, here for the S-like structures bending transitions dominate. Such model helps in decreasing stress concentration factor and thereby improving fatigue resistance (Meena & Singamneni, 2019 [16]). Because S-shaped cells provide the possibility of increased NPR up to -2.5 when compared to re-entrant designs (-1.2), peak von Mises stresses decrease, and crack initiation is delayed. The observed performance of NPR was similar to Qiao & Chen (2015) [22], in which curved double-arrowhead geometries were studied and a reduced ligament displacement while demanding constant NPR is exhibited.

Moreover, the S-shaped auxetic units and hexagonal is joint to Hybrid Hex-S structure in current work. Studies reported by Ren et al., 2018 and Rufo-Martín et al. [24] have observed that when auxetic structures are incorporated into hexagonal cells they experience an increase in compressive strength, energy absorption and indentation resistance.

### 2.3.2 Aux-Hex Hybrid Structures

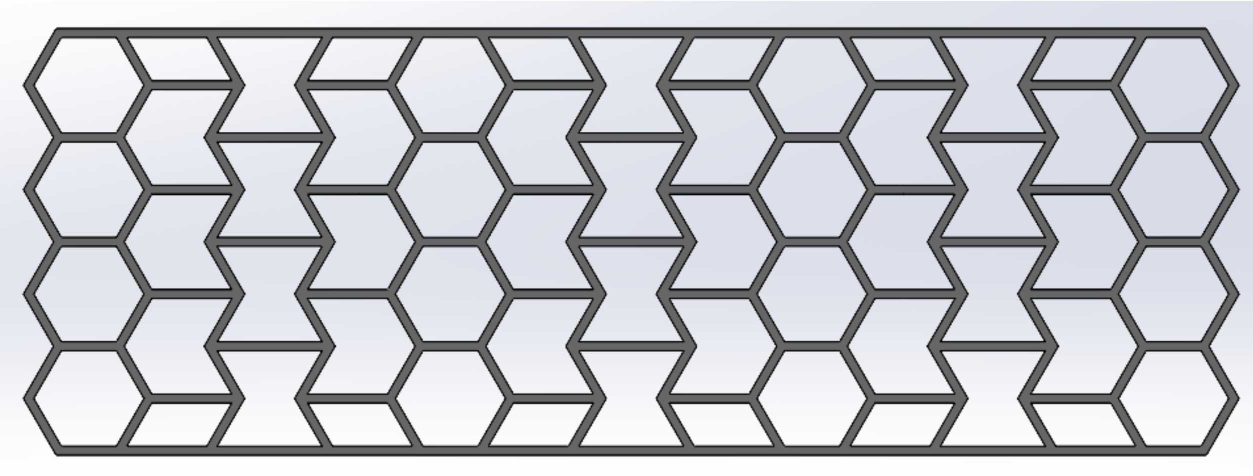

***Figure 4: Whole Aux-Hex Structure***

The Aux-Hex is comprised of a mixed structure that consists of auxetic re-entrant sub-units and conventional hexagon-shaped structures. This hybrid structure enables a compromise between flexibility and rigidity, which is ideal for applications needing energy absorption as well as dimensional stability. The advantages of both geometries are well combined within the Aux-Hex design; i.e., energy dissipation benefits for yarns L11 a la the auxetic cells and carrying load capacity of hexagonal honeycombs.

Gong et al., 2021 [36] and Bai et al., 2017) [37], this hybrid topology can be designed to endow the material with stiffness control, resulting in a more customized performance. The honeycomb structure will also have auxetic cells like the interconnect, which greatly increases the indentation resistance and impact energy absorption of the material. Zhang et al., 2018 [38] experimentally showed that the energy absorption of FDM-made Aux-Hex structures was up to 45% higher in compression than for standard hexagonal structures.

The addition of the Auxetic structure within the hexagonal reinforces it without compromising its flexibility, and so Aux-Hex presents application to protective clothing/ gear as well as energy absorption applications including automobile crash protection, lightweight aerospace cores, and structures that require both strength but also energy dissipation.

## 2.4 Tailoring Mechanical Behavior through Positive and Negative Poisson's Ratio Regions

Positive Poisson ratio (PPR) and negative Poisson ratio (NPR) The concepts of mixing with positive Poisson ratio (PPR) or negative Poisson ratio (NPR) in one structure provides a flexible method of using mechanical properties in structures. The hybrid carbon structures provide an excellent stiffness and energy absorption that is of much interest in devices requiring performance optimization between stresses. NPR and PPR region combination allow one to develop structures that have multifunctional qualities that can be specific to different applications like flexibility, rigidity and energy dissipation.

Among the most significant outcomes of a combination of two PPR and NPR regions into a same structure is appearing of Zero Poisson Ratio (ZPR) region. ZPR region is the one where when the body is strained or pressurized, not laterally contracted or expanded due to any tensile or compressive loading. This causes isotropic mechanical response hence enhancing stability and mechanical integrity. The fact, that it is plausible to construct and incorporate into a hybrid reticulated lattice, the idea of designing and originating ZPR regions, is a significant development in the construction of auxetic structures and gives a greater degree of control to structural architecture.

Samanta 2020 [25] proposed a geometrically nonlinear finite element method for creating hybrid auxetic structures with directional-dependent mechanical behaviour using computational tools. The hybrid structure of NPR, PPR, and ZPR in these hybrids contribute to the suppression of crack propagation, stress singularity, or fatigue. The ZPR sectors in particular are also crucial for the improvement of structural stability of the material. Combining with NPR region and PPR regions make the ZPR region stable, uniform stress responsive without lateral deformation up until breakiog load, so that this can be adapted for dimensional stability under net/oscillating loads.

Plewa et al., 2022 [19] showed that FDM-fabricated TPU objects with NPR-PPR combinations maintained more than 90% of the damping applicability after multiple load cycles. This showed long-term performance under dynamic conditions is possible, especially in application demanding high fatigue strength. The possibility of architecture which combines NPR and PPR regions to generate ZPR structures make it possible to both maximize beam flexibility and stiffness in the same structure. For instance, the NPR regions serve to absorb energy and provide flexibility, whereas PPR regions contribute to overall rigidity of the structure. This combination is such that the structure can remain tailored to its mechanical response as a function of given application requirements.

The distinct mechanical features of the NPR-PPR-ZPR hybrid structures have particular advantages in multifunctional utilization. For instance, in the case of soft robotics where the structure must deform and accommodate different loads, the NPR regions present in this multiresolution scheme will give necessary flexibility. On the other hand, in structural elements such as aerospace structures or load-bearing frame members, PPR regions provide a structure with rigidity and yet still incorporate controlled energy dissipation. These ZPR regions in turn serve to lock the dimension-stable shape of the structure under tension and compression (and thus are important in applications such as, e.g., stents or bone and tissue implants, where it is imperative that an initial shape set be achieved below which little depreciation of the actual final dimensions accommodated by localized deformation occur).

Furthermore, the cross sectional integration of NPR PPR ZPR region can be employed to tailor the performance for complex mechanical responses required by smart structures or adaptive systems. For instance, 4D printing could be used to design a self-responsive structure that changes its shape or stiffness with environment variation, and where NPR, PPR and ZPR areas can collaboratively act as an adaptive mechanical behavior.

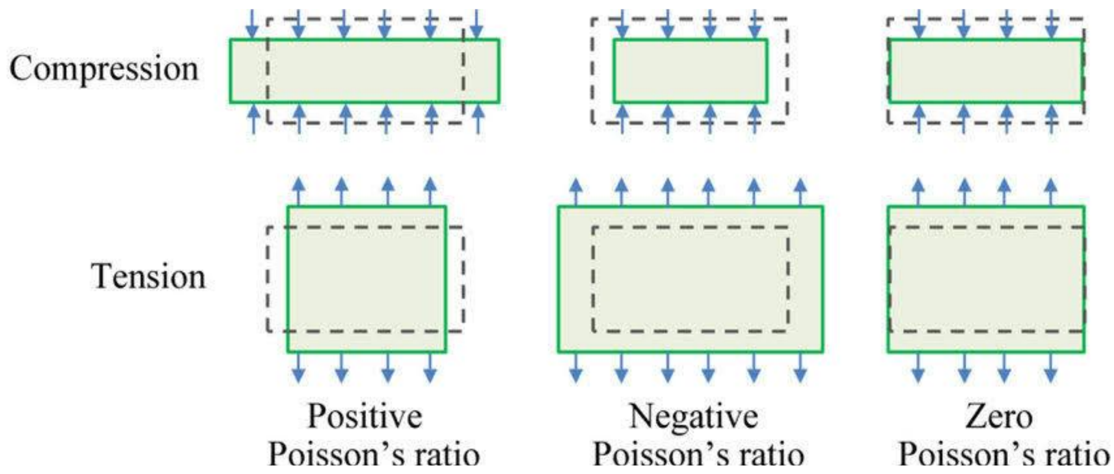


***Figure 5 : Comparison of NPR, PPR, ZPR*** **[43]**

## 2.5 Materials for Additive Manufacturing of Auxetic Structures

The design of auxetic structures for special applications is indeed very closely connected to the material which it is fabricated from, especially when a coordinate technology such as Additive Manufacturing (AM); e.g., Fused Deposition Modelling (FDM) is being employed. The selection of materials greatly influences the overall mechanical performance of an auxetic structure, such as energy absorption, deformation behavior, stiffness and fatigue durability. Material is an important design parameter, which strongly defines the functionality and longevity of the product, in particular when it comes to cyclic loading or impact.

As described above, auxetic structures inherently depend on highly elastic, energy absorbing, and mechanically durable materials to sustain their particular deformation conditions under diverse loading scenarios. Here, we focus on two common materials for the construction of auxetic structures: Thermoplastic Polyurethane (TPU) and Polylactic Acid (PLA), respectively used in additive manufacturing for their unique properties and advantages with respect to other polymers to realize functionally auxetic structures.

### 2.5.1 Thermoplastic Polyurethane (TPU)

TPU has held a prominent position as one of the most pop- ular materials to manufacture auxetic structures, mainly owing to its superior energy absorption capability, elasticity and shape-recoverability. TPU is a flexible material with excellent elasticity and resistance to breaking under high load applications. The vulcanization of TPU and a hysteresis response during cyclic deformation endow it with the ability to resist multiple back-and-forth stretching without major loss of performance, making it durable in dynamic applications.

Bai et al. (2017) [22] were able to show that FDM-printed TPU structures dissipated 58% more energy over a cyclic stretch-release history than the equivalent structures of ABS or PLA. This significant improvement of energy dissipation demonstrates that TPU is a good candidate for impact attenuation including protective apparel, sports equipment and aerospace/automotive vibration damping systems. TPU is an intriguing candidate for such applications since it can absorb high energy per unit volume before failure.

In terms of energy absorption, TPU has long elongation at break (often over 300%), thereby permitting large deformations without loss of mechanical properties. It is these recovery properties that led to the consideration of TPU as a good material for complex auxetic geometries, where shape retention after deformation is very important. With the excellent elongation and reliability of TPU, it is still one popular material for wearable tech as well as bio-medical device which long term deformation and reliability under stress are highly requested by not just user friendly also durance for use.

On the other hand, fatigue resistance of TPU allows for the material to withstand multiple loading-unloading cycles with a little loss of performance. This makes TPU an appropriate choice for something that needs to be used over a long period of time and withstands repetitive stress including robotic actuators, prosthetics, or dynamic cushioning systems.

### 2.5.2 Polylactic Acid (PLA)

Another one of the standard materials used in 3D printing is Polylactic Acid (PLA), a biodegradable thermoplastic derived from renewable sources such as corn starch, and very popular for rapid prototyping and educational activities. PLA is eco-friendly, and an economically viable choice for applications where biodegradability is desired. PLA is finally easy to print in FDM printing technology for new beginners. Very low shrinkage and best layer bonding of any PLA. Notwithstanding, PLA does have its drawbacks which prevent or limit its potential use in demanding applications and especially involving auxetic structures.

One of the main disadvantages of PLA is its brittleness, which makes it inappropriate for highly deformable auxetic structures. PLA usually has a small value of elongation-at-break, leading to cracking or fracturing at high strain. This brittleness is an issue for auxetics materials because they are used in many applications where it's important that the material can deform with force without breaking. The limited ductility, low impact toughness of PLA will not be suitable for applications where substantial energy must be absorbed and high strain recovery is necessary, such as in protection gears or impact-energy dissipating structures.

Notwithstanding these limitations, PLA is still extensively used for design verification and concept proving where the ease of fabrications and low cost cannot be overruled. It is a springboard for prototyping proof-of-principle prototypes, enabling researchers and engineers to quickly prototype and test auxetic structures before moving on to more compliant materials such as TPU for functional applications. It's also excellent for use in eco–friendly designs where the accessibility and biodegradability of a material is important.

In addition, PLA finds its used in low-strain applications where much deformation isn't needed. For instance, elastomer auxetic structure made of PLA is well suited for lightweight non load carrying applications and which has not to be subjected to high cycling stresses or dynamical loading conditions. In these cases, the parameters of PLA are well-balanced for manufacturing and to be able to see auxetics without requiring much more flexibility than, for instance, TPU.

## 2.6 Additive Manufacturing Techniques for Auxetic Fabrication

Additive manufacturing (AM) procedures have been instrumental in the design and additive manufacturing of auxetic structures. AM offers the option of flexibility and high resolution in complex customized geometries than some of the older methods that are not feasible and which would be less attractive in terms of geometry potential. The realization of auxetic structures that require complex structures of structural topology and structural composition in achieving the desired mechanical properties (including negative Poisson ratio (NPR) and energy dissipation) is of great interest. Among all AM processes that are in place today, Stereolithography (SLA), Selective Laser Sintering (SLS) and Fused Deposition Modeling (FDM) have developed to become the methods of choice in manufacturing of auxetic structures. Each of these methods has its uniqueness of advantages and challenges, still, being applicable in specific tasks depending on its mechanical characteristics and production needs.

### 2.6.1 Stereolithography (SLA)

SLA 3D printing is done with the help of ultraviolet (UV) light and a tank that contains a photopolymer resin. The benefits of SLA are that it has high-precision geometry and can produce very fine and complicated auxetic components with complex features that other AM methods may not produce easily. SLA is also of high resolution and accuracy, which makes it the ideal solution to the production of prototypes or models with a tight tolerance, which is needed in the design validation phase of the development.

The significant disadvantage of SLA, however, is that it is extremely dependent on the nature of the photopolymer resins used in this 3D printing method. These resins are typically weak and lack impact strength required by functional auxetic structures despite their high level of effectiveness in creating very small features and good surface finish. So, SLA is quite applicable in applications such as design validation, concept prototypes and aesthetic, but in general not functional auxetic structures as it requires high toughness and resistance when loaded with cyclic loadings. In particular, SLA printed auxetic may be affected by the unavoidable failure or cracking at low impact to make them inappropriate in the applications that need high resilience and energy absorption like protective clothing, mobile elements of a dynamic structure.

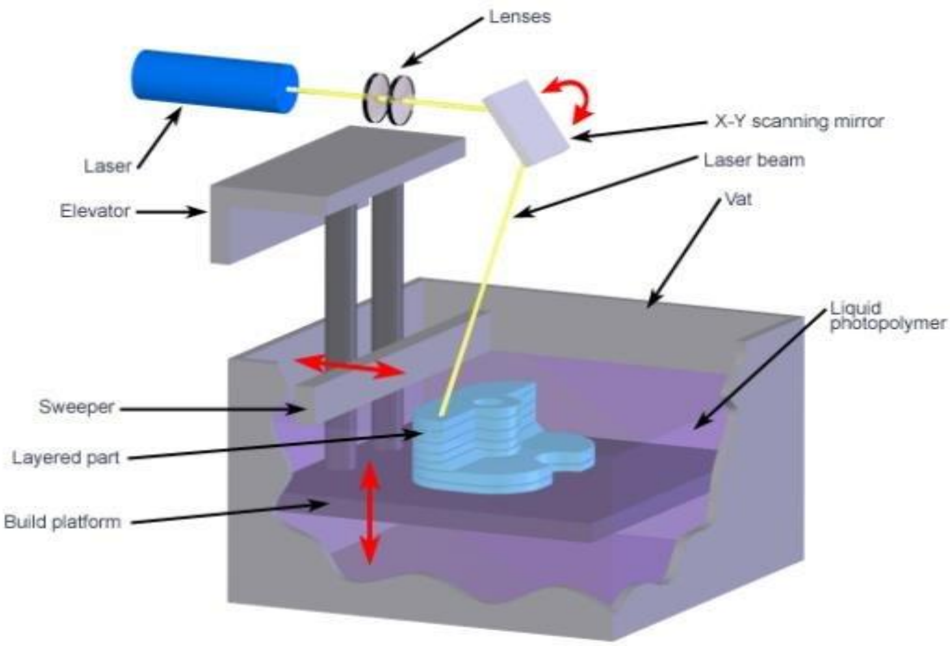


***Figure 6: Stereolithography*** **[44]**

## 2.6.2 Selective Laser Sintering (SLS)

SLS is a 3D printing method that is a powder-based process where polymer powders are sintered to create solid scaffolds layer by layer using a laser. The mechanical performance of SLS is superior to that of the SLA in that SLS materials are more powerful and tougher thus more appropriate to create working auxetic structures. The technique is applicable to most polymer powders including nylon and polyamide TPU. The polymers can be employed to create lower performance mechanical and flexibility auxetic structures.

Among the key benefits of SLS are the fact that the stronger auxetic structures can be printed with a better load bearing capacity and greater deformation than SLA. Strong parts with open structures can be made because SLS processed objects have been consolidated and lack the natural vulnerability of binder type prototyping systems, creating components that are perfect to functional prototypes which demand impact strength and energy absorption. Besides, the SLS does not have to bear structures because the unused powder of the build area supports itself through printing that clearly reduces material waste and post processing remedies.

However, despite all its miracles, SLS has its problems. The SLS equipment are also typically costly, with poor surface finish of the printed components that may impede its further adoption, particularly in certain uses. Depending on an desired quality or smoothness of the part that might be desired in process or as a result of such things as sanding or coating, a post-processing might be required, which may complicate the total manufacturing time, and also it may increase cost. Nevertheless, SLS remains an attractive future in the production of allowable auxetic structures especially in aerospace and automotive parts and protective system sectors where durability and/or strength is paramount.

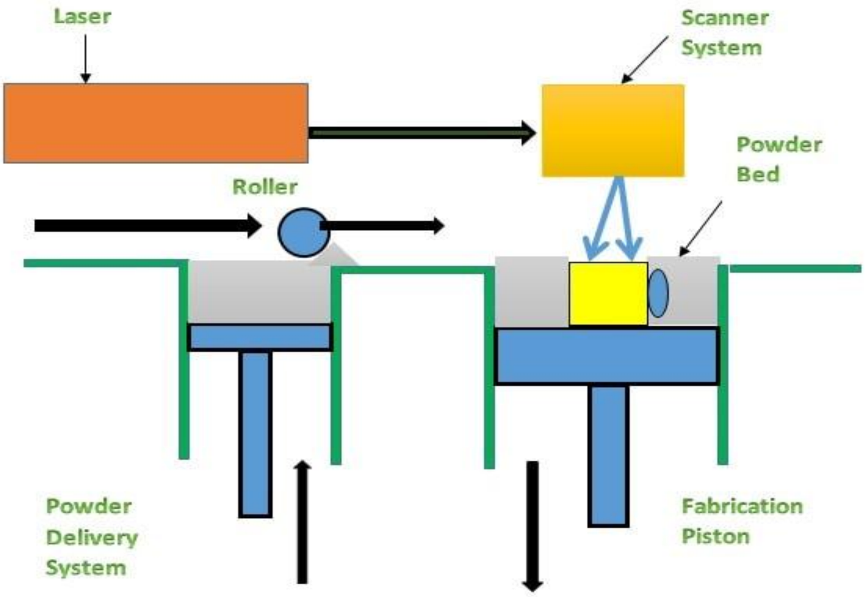


***Figure7: Selective Laser Sintering (SLS) Method [45]***

## 2.6.3 Fused Deposition Modeling (FDM)

One of the famous Additive Manufacturing process that can be used to produce auxetic structure is Fused Deposition Modeling (FDM). FDM printer operates by forcing the molten material through a hot end and layer-by-layer filling the object. This sequential printing allows the computer-controlled assembly of intricate geometries like auxetic lattices, which would be difficult, or even impossible, to make by conventional manufacturing methods. FDM is more versatile because it can produce complex models using less wastage materials besides offering a cheap and less time-consuming production in case of printing desired structures.

The flexibility of FDM is informed by the fact that the printing parameters can be adjusted to suit mechanical response of the printed structure. The important parameters are parameters like the orientation of layers, extrusion temperature and infill density. The orientation of the layer determines the anisotropic characteristics of strength and energy dissipation of the printed structure. Extrusion temperature influences the bond strength of layers and hence the interlayer adhesion behavior which are important to hold the mechanical properties and the stability in geometry as an entirety. Density of infill percent also enables customizing the firm to convey support to maximize energy receive or load-resisting.

The other notable advantage of FDM is the fact that it can be scaled and used in prototyping and production. Taking into consideration the fact that FDM has the capability of dimensional control, it can be utilized to replicate the same design thus achieving a uniform mechanical property among all the printed components. It is especially applied in the industries where high performance applications require tailor made solutions including automotive crash protection or biomedical implants where reliability and repeatability of mechanical response is of concern.

Multi-material designs can also be produced with FDM, as the different materials with varied mechanical properties can be applied to different parts of the same structure. The property allows the creation of hybrid auxetic structures, with harder materials being additively manufactured in areas that need stiffness and areas that need flexibility and energy dissipation being additively manufactured with softer materials. A single print enables mixing of materials to produce auxetic lattices, print material that is optimally designed to achieve maximum strength and energy absorption.

Moreover, FDM may be undertaken on a high number of materials including thermoplastics and composite filaments that may be utilized to create structures that are application specific. Technology has also been discovered to be an important means of doing rapid prototyping and low volume production which has been known to be an effective method of trying out new designs and functional material prior to the large-scale production.

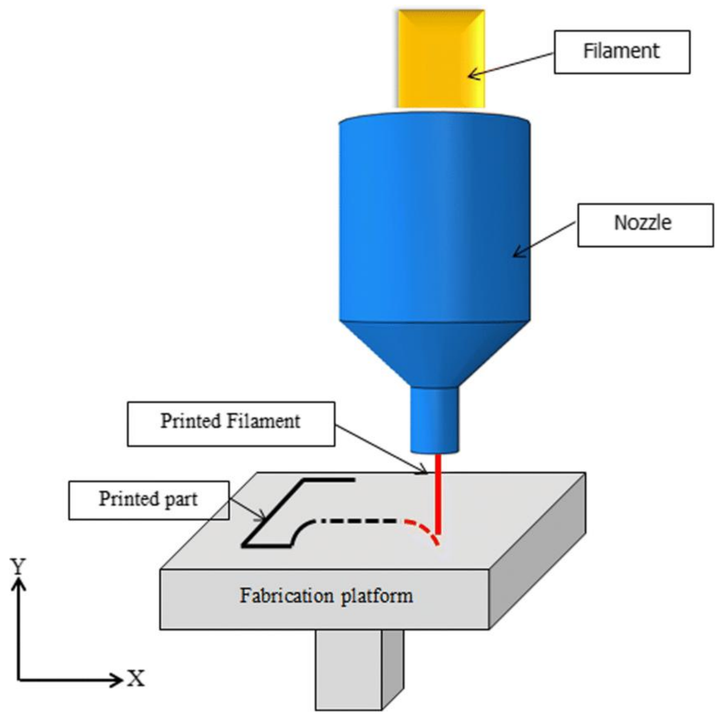


***Figure 8: Fused Deposition Modeling (FDM) Method [46]***

## 2.7 Dimensional Stability of Auxetic Structures

More critical to any structure, particularly one that possesses non-linear behavior of deformation under the load, namely an auxetic structure is that Dimensional Stability. Dimensional stability refers to the ability of a material to maintain its initial size and shape in reference to a force acting on it, environmental variation (change in temperature, humidity or stress). The rigidity of the complex structure is especially of concern to additive manufacturing technique of auxetic structures, when a layer is to be deposited on top of another and this may lead to internal stress or warpage during deposition as a result of temperature gradient particularly with TPU or PLA-like material. Therefore, dimensional stability is not only significant to the auxetic structures to retain their mechanical functionality but also their functioning to act in a dependable and steady way as time skills, especially under practical use in the real-world.

Auxetic materials spontaneously creep to form shapes that may change topology in response to external forces, and it is necessary to know how stable they are with time. Non-uniform strain distributions can also be formed through the mechanical behavior of auxetics that have non-traditional deformation mechanisms, including NPR and curvature-induced expansion and can result in shifting of shape or structure upon external forces or various environmental loads (Li et al., 2021 [32]; Sombaty et al., 2019 [33]). Accordingly, dimensional stability of the auxetic cell is a vital concern in their mechanical good performances in the environmental conditions of variations.

The internal stresses which are formed during additive manufacturing play an important role in determining the dimensional stability of the auxetic structures. With additive layer methods such as Fused Deposition Modeling (FDM) or other warping-prone methods, temperature gradients can cause warping, shrinkage or dimensional deformation of these types of printed auxetic fabrication. The behavior of the material under heating, as well as cooling, is of significance as it is directly linked to the ability of the fabricated construction to maintain its target shape (Shah et al., 2020 [34]; Bakar et al., 2017 [35]). Other materials such as TPU are very flexible and hence demonstrate good dimensional stability as they can be returned to a shape upon small distortions. Conversely, the more solid materials, including PLA may experience difficulties in understanding its dimensional stability; constraints that would be increased by cooling stage and the subsequent rapid changes of temperatures that may leave residual stresses (Gong et al., 2021 [36]; Bai et al., 2017 [37]) and warping.

Moreover, architecture helps in the enhancement of dimensional stability in auxetic architectures. The mechanical response can depend on the geometry of the auxetic unit cells in a re-entrant geometry or the S-shaped geometry. The residual stresses could be formed and restraining the structural stability in localized deformation regions, i.e., sharp-bended or inward-angled elements in the averted auxetic structures with negative Poisson ratio. The design of topological units cell geometries and supportive structure design have become useful in the reduction of warping and enhancement of dimensional homogeneity in auxetic structures (Xu et al., 2020 [38], Zhang et al., 2018 [39]).

The importance of post processes is based on the enhancement of the dimensional stability, but they are related to material properties and the characteristics of the instruments utilized. Such techniques as annealing or controlled cooling procedures contribute to the elimination of any intrinsic stressors and fortification of auxetic-structures'. Indicatively, heat treatment has been discovered to reduce the residual stresses of TPU components, thereby supporting its shape recovery, and preserves the mechanical performance of TPU in the long durability of use (Xiong et al., 2020 [40]; Li et al., 2021 [41]). These post-processing parameters are of critical interest to ensure that the end-result auxetic structures in this case are up to the required standard diameter wise during both the manufacturing and operation.

Few researchers have however stated that materials such as PLA are prone to dimensional variations when they are exposed to a change in humidity and temperature hence interfering with mechanical performance and stability (Bakar et al., 2017 [35]; Gong et al., 2021 [36]). Conversely, TPU-based auxetic structures tend to be more dimensionally stable with a wider range of environmental parameters due to the thermoplastic nature of elastomeric TPU rendering them less prone to external environmental forces (Zhao et al., 2020 [42]).

## 2.8 Identified Research Gaps

Despite the acknowledged benefits of integrating auxetic and non-auxetic structures, little work has been done on hybrid auxetic structures, especially in their response to complex loading. There is also little understanding of the structural stability of such architectures under dynamic or cyclic deformation, which makes fatigue resistance to be a concern, as well as long term performance during high stakes applications like aerospace, armor and protection systems. In addition, manufacturing hybrid designs using Fused Deposition Modeling (FDM) has manufacturing problems, such as loss of precision, internal stress state, warping, and mechanical property variation. The problem of reproducibility, dimensional accuracy and cost-effectiveness in large-scale manufacture is thus an important challenge to commercialization.

### 2.8.1 Limited Research on Hybrid Auxetic Structures

The majority of works that have been conducted explore single auxetic geometries - re-entrant, S-shaped, arrowhead, or chiral - and the work of hybrid combinations is still emerging. The combination between different geometries still remains not fully understood, and the techniques of how to optimize the functionality, say increasing the energy absorption or the dimensional stability, are to be further researched.

### 2.8.2 Lack of Research on Structural Stability of Auxetic Structures

Though shock absorbing properties of auxetic structures have been studied extensively, the deformation mechanisms of auxetic structures under repeated or impact loading are not studied properly. Non-linearity of the auxetic deformation poses difficulties in the prediction of the energy storage, fatigue-related behavior, and long-term reliability and should be overcome before the safe application to the real-life systems.

### 2.8.3 Challenges in Scaling FDM Technology for Industrial Applications

Although auxetic structures are easily made by FDM because of material versatility and cost benefits, scaling the method to industrial-scale production leads to a loss of accuracy, stresses, and mechanical variability in multifaceted geometries. The widespread deployment in the industrial fields requires improvements in process control, reproducibility and speed of manufacturing, not to mention cost reduction.

# Chapter 3: Research Objectives & Methodology

The paper will address the design, fabrication and characterization of a new hybrid Hex-S auxetic structure which is a combination of negative Poisson ratio (NPR) and positive Poisson ratio (PPR) architecture.

## 3.1 Objectives

The primary objectives of this research are as follows:

1. **To design and fabricate a novel Hybrid Auxetic Structure (Hex-S), combining negative and positive Poisson's Ratio geometry**:

   The former is to develop a hybrid auxetic structure known as the structure of Hex-S. This structure is a combination of S-shaped auxetic cells and hexagonal structures and as such, it is flexible as the auxetic geometries and rigid as regular honeycombs. The objective of this new design is to balance energy absorption, dimensional stability, and mechanical performance best, as well as correct the issues in the traditional auxetic structures. Both the numerical simulations and the experimental validations will be used to complete the test of the hybrid nature of the design.

2. **To perform numerical simulation and experimental characterization for compressive energy absorption and dimensional stability**:

   The second objective is to execute some numerical simulations to model the behavior of the Hex-S structure in case it is compressed and investigate how well it absorbs energy and remains stable when the load varies. We shall also experiment to determine the stability of dimensions of the material as well as its ability to absorb energy. Both finite element analysis (FEA) and standardized compressive testing will be used to examine such valuable metrics as peak force, energy dissipation, and dimensional recovery.

3. **To compare the performance of the newly designed hybrid structure with conventional structures for different materials**:

   The eventual objective is to make a comparison between the Hex-S structure and the conventional auxetic structures (such as Re-entrant and Aux-Hex structures) composed of other materials, such as TPU and PLA. The comparison will focus on such key parameters as energy absorption, compressive strength, and dimensional stability. The objective is to demonstrate the superiority of the hybrid structure in dissipating energy and still being capable of shifting to its usual shape after being loaded on several occasions.

### 3.2: Methodology

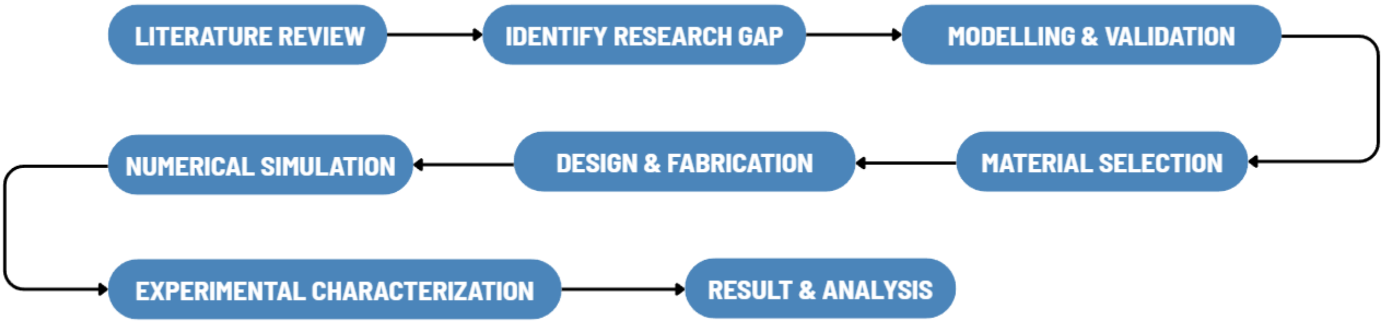


***Figure 9: Methodology Flowchart***

An extensive study was done on the auxetic structures, positive, negative and zero Poisson's ratio, applications, etc. At first, we designed two auxetic structures, the re-entrant structure, which is a widespread auxetic structure and a comparatively new one, the S-shaped structure. We have designed the re-entrant and S-shaped structure according to the dimensions mentioned in the reference literature. It is to be noted that a few dimensions were missing for the S-shaped structure in the reference, for which we had assumed a relevant value. After recreating the structure, we moved on to the numerical simulation, where we used ANSYS static structural analysis. All boundary conditions were followed according to the reference article. Moreover, we validated the results successfully with a minimum amount of deviation. Therefore, it confirms the accuracy of our model, the concept of the S-shaped structure having a better negative Poisson's ratio than the re-entrant structure, meaning that the S-shaped structure shows more flexibility when any load is applied onto it.

From our background research, we have seen minimal study on combining both positive and negative Poisson's ratios in a single structure. Nevertheless, it is certain that this kind of study has immense potential in the field of advanced materials, solid mechanics, and additive manufacturing. We have studied work where they combined a conventional hexagonal structure having a positive Poisson's ratio with a re-entrant structure, resulting in a remarkable energy absorption capability and dimensional stability. As for the materials, PLA and TPU were used. PLA is commonly used for prototyping purposes and provides stiffness, but it is brittle. So, it enables us to easily visualize and study dimensional stability and energy absorption capability in our hybrid structure. Furthermore, TPU is more elastic and rigid and has excellent strain recovery, which allows us to explore the potential application of the newly designed hybrid structure, Hex-S.

We developed the idea of combining a hexagonal shape with S-shaped structures because the S-shaped design exhibits a superior negative Poisson's ratio compared to a re-entrant structure. First, we designed the unit cell of the hybrid structure, and then we combined these unit cells to create the entire framework. After completing the design, we fabricated the structure using Fused

Deposition Modelling (FDM) 3D printing with both TPU and PLA materials.

Next, we conducted numerical simulations to model unidirectional quasistatic loading. We also performed experiments in the laboratory following standardized compression tests to characterize the properties of both PLA and TPU materials accurately. Additionally, we executed unidirectional quasistatic compression tests on our fabricated models.

***Figure 10: Universal Standard Testing Machine***

Finally, we analyzed the results from our numerical simulations and experimental tests, comparing various aspects, such as the structural performance of the Hex-S, Aux-Hex, and re-entrant structures, as well as the material properties of PLA and TPU. We also compared the energy absorption of PLA-printed structures. Our findings led us to conclude that our proposed hybrid Hex-S structure demonstrates significantly better dimensional stability than the Aux-Hex structure and exhibits a higher energy absorption capability compared to conventional auxetic structures, such as the re-entrant structure.

# Chapter 4: Validation

To ensure the right way of analysis, model's accuracy, and reliability, we validated the reference literature of Meena et.al [16]. The detailed steps of the validation are discussed below:

## 4.1 Geometric modeling:

For the validation purpose, we designed two models, a re-entrant structure and an S-shaped structure. The dimensions were used as mentioned in the reference article. We used SOLIDWORKS 2023 for modelling purposes.

***Table 1***

| Unit Cell Dimensions for S-Shaped Structure | | | | | |
|---|---|---|---|---|---|
| ***L (mm)*** | ***R (mm)*** | ***C (mm)*** | ***t (mm)*** | ***W (mm)*** | ***$\theta_1$ & $\theta_2$ (°)*** |
| 14 | 7 | 10.6 | 1.5 | 10 | 30 |

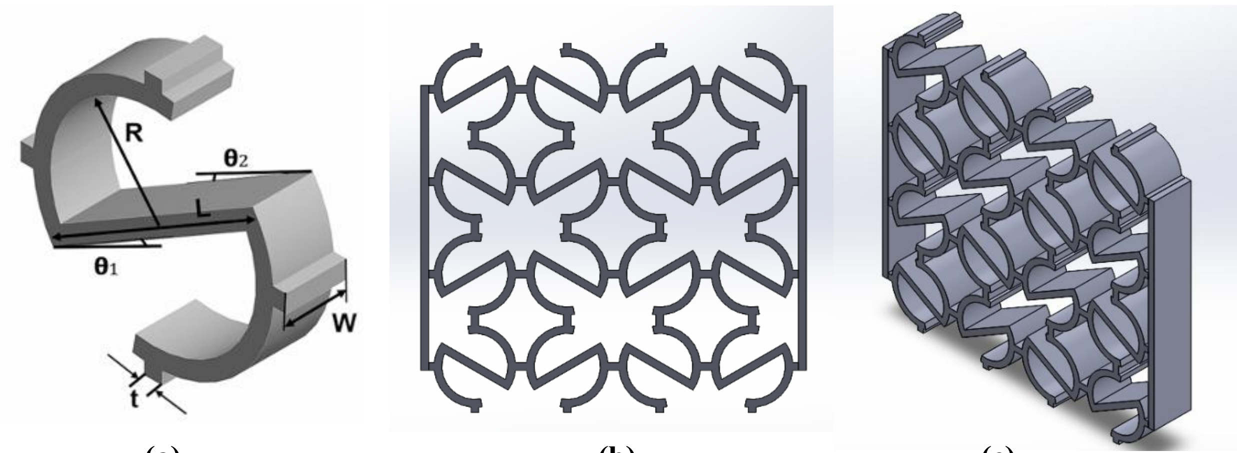


(a) (b) (c)

***Figure 11: (a) Unit cell of S-Shaped Structure with dimensions, (b) Front view of S-Shaped Structure, and (c) Isometric View of S-Shaped Structure***

***Table 2***

| Unit Cell Dimensions for Re-entrant Structure | | | | |
|---|---|---|---|---|
| ***H (mm)*** | ***L (mm)*** | ***T (mm)*** | ***W (mm)*** | ***α (°)*** |
| 14 | 7.25 | 1.5 | 10 | 75 |

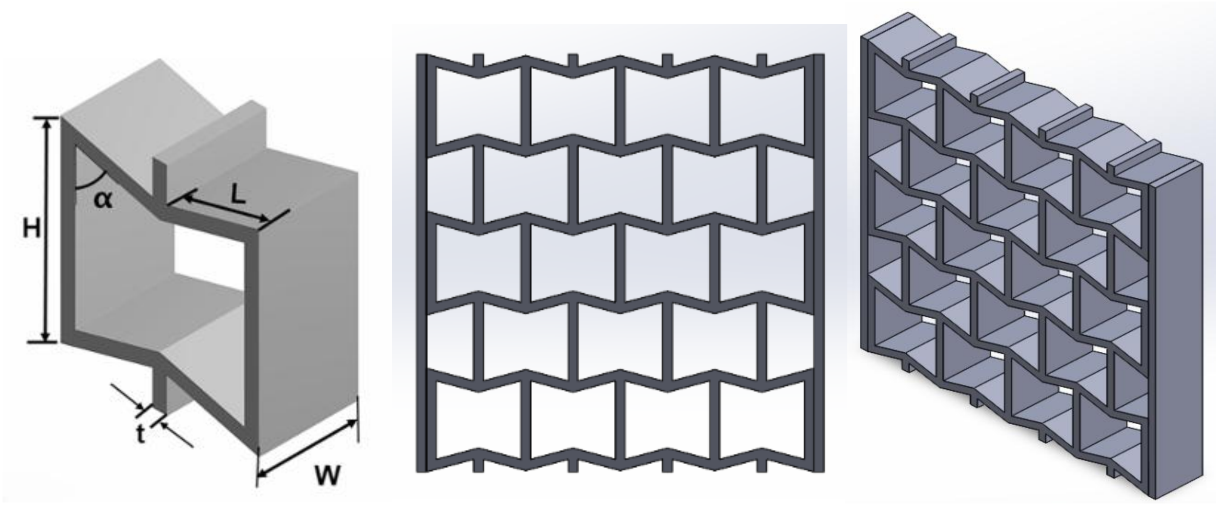


**(a)** **(b)** **(c)**

***Figure 12:(a) Unit cell of Re-entrant Structure with dimensions, (b) Front view of Re-entrant Structure, and (c) Isometric View of Re-entrant Structure***

## 4.2 Numerical Analysis:

We used ANSYS 2021's static structural analysis for numerical analysis. The structure is made of stainless steel 316 L. The reference article said to use the Boundary conditions as they were. The tetrahedral method with an element size of 0.5 mm was used because the mesh convergence analysis showed that it worked. The Augmented Lagrange method was used to define the contacts in the structure. This made sure that the contact elements were as compatible as possible with a frictional coefficient of 0.2. To measure how the structure behaves when it is compressed, a fixed support was put on the -X direction and a displacement of -0.1mm was put in the opposite direction.

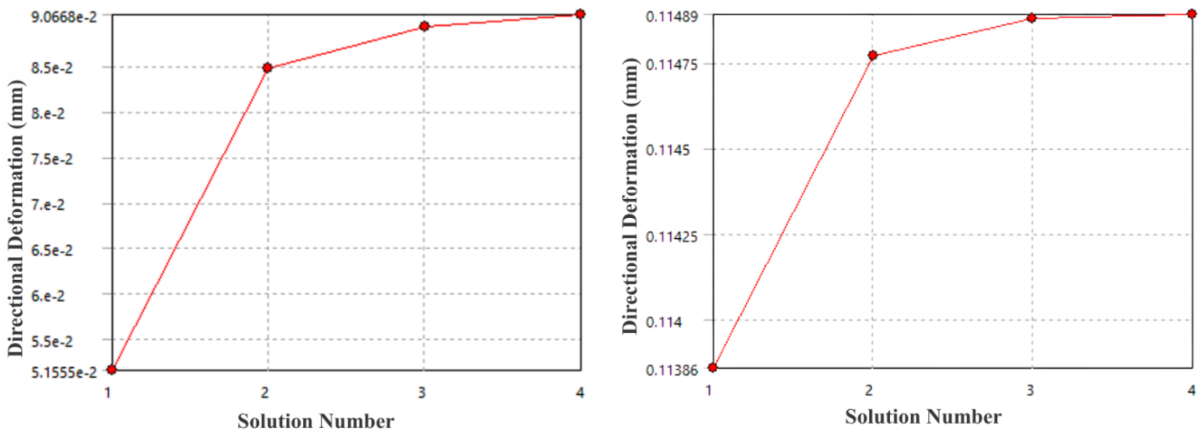


**(a)** **(b)**

***Figure 13:Converged mesh result for (a) Re-entrant Structure and (b) S-Shaped Structure***

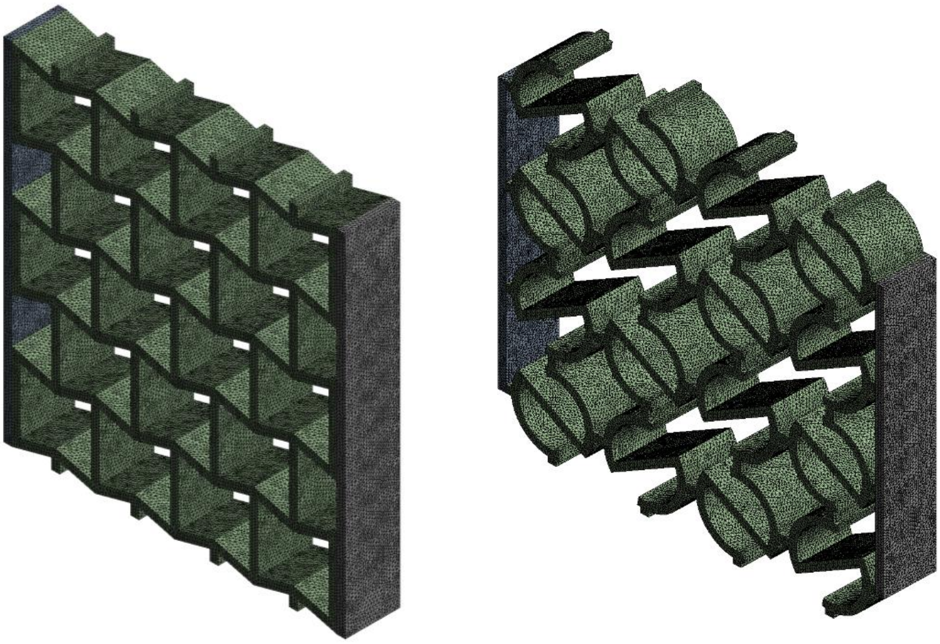

**(a)** **(b)**

*Figure 14:. Finite Element Mesh of (a) Re-entrant Structure and (b) S-Shaped Structure*

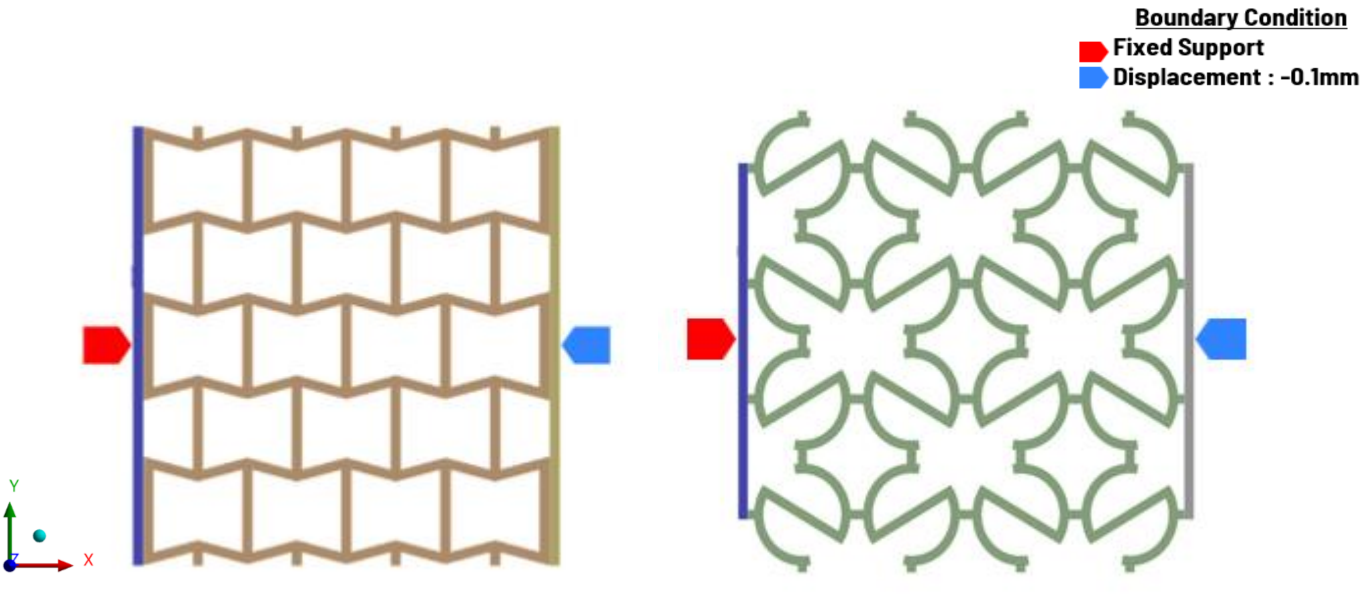


**(a)** **(b)**

*Figure 15:Boundary conditions for (a) Re-entrant Structure and (b) S-Shaped Structure*

### 4.2.1 Validated Results:

After all the necessary boundary conditions were applied, the equivalent stress was found for both the re-entrant and S-shaped structures.

The reference equivalent stress for the re-entrant structure was 834.25 MPa, and the simulation result was 842.72 MPa, which was only 1.015% off, showing that the simulation was much more accurate.

*Table 3*

| *Reference Data (MPa)* | *Simulation Data (MPa)* | *Deviation (%)* |
|---|---|---|
| 834.25 | 842.72 | 1.015 |

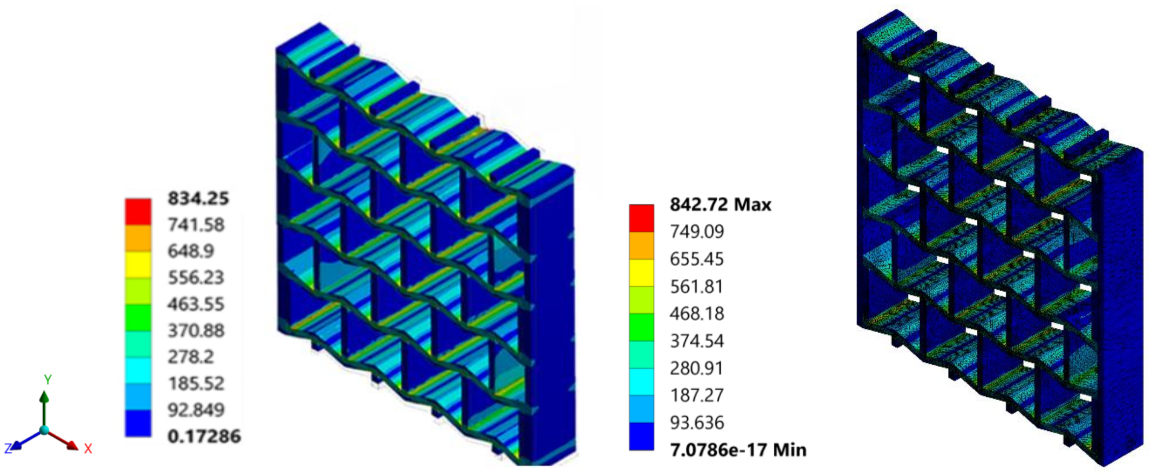


**(a)** **(b)**

***Figure 16: Equivalent stress result for Re-entrant Structure of (a)Reference, and (b) Simulation***

The reference equivalent stress for the S-shaped structure was 336.3 MPa, while the simulation value was 301.38 MPa. Here, the deviation is 10.38%, which is a little higher than for the re-entrant structure because some dimensions need to be guessed. But this difference is still within the acceptable range.

*Table 4*

| ***Reference Data (MPa)*** | ***Simulation Data (MPa)*** | ***Deviation (%)*** |
|---|---|---|
| 336.3 | 301.38 | 10.38 |

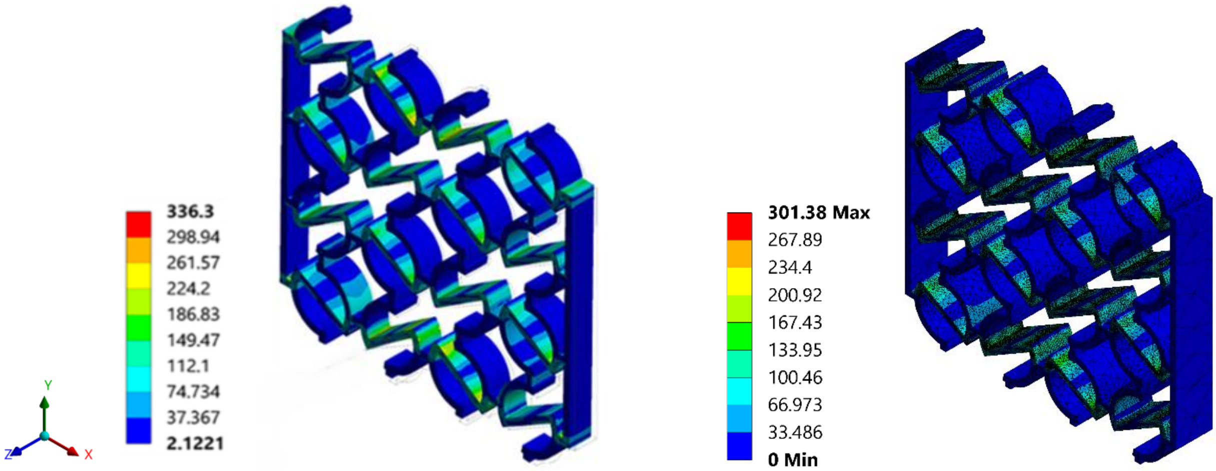


**(a)** **(b)**

***Figure 17: Equivalent stress result for S-Shaped Structure of (a)Reference, and (b) Simulation***

The validation result confirms that our simulation and study methods are correct. Additionally, it enabled us to advance our research based on the premise that the S-shaped structure possesses a superior negative Poisson's ratio compared to the re-entrant structure, suggesting that the S-shaped structure is the optimal choice for our continued investigation into the design of hybrid structures.

# Chapter 5: Material Selection, Design & Fabrication

## 5.1 Material Selection:

Our experiment will be based on two polymeric materials, namely, PLA and TPU, which will be used to measure the efficiency of a newly worked-out hybrid structure Hex-S.PLLA, which is the trending 3D printing material currently. We have selected it primarily due to the reason that it is stiff and well fitting. With these qualities we not only learned when the Hex-S design first failed, but also tested its dimensional stability when compressing the material; it was brittle in nature and did not take to strains, however, in excess of one inch. TPU in its turn possesses its own characteristic profile of mechanical properties. It was robust and more ductile than PLA, and it copes with stress quite well. The Hex-S-structure might be tested to determine the performance at the situations where it is exposed to a big load repeatedly due to the ability of the material to be deformed significantly with no fracturing.

We performed compression tests on PLA material and TPU material and the findings were DR. ASTM D695 is a standard machine in this sphere. This is a technique of verifying the performance of rigid and semiflexible plastics under pressure. This testing was done at constant rate of crosshead displacement of 1 mm/min to ensure that the loading conditions were virtually at zero. To reduce variations the specimens were machined to the size requirements of the standard and to ensure that the geometry and surface polish was the same on all the specimens. Measuring stress and strain was done throughout the tests. This assisted us in the determination of compressive strength, modulus and strain recovery values.ASTM D695 gives us a procedure of comparing the mechanical properties of PLA and TPU in a stable and repeated way. The present batch of tensile testing has shown that all our largest engineering challenges can be successfully faced and conquered with perseverance.

The data received through ASTM D695 tests did not only confirm the strategy in selecting materials applied to select the two materials used in this project, but also gave information about How the hybrid S-Hex structure responded with regards to the absorption of energy and what parameters would result in the absorption of more energy.

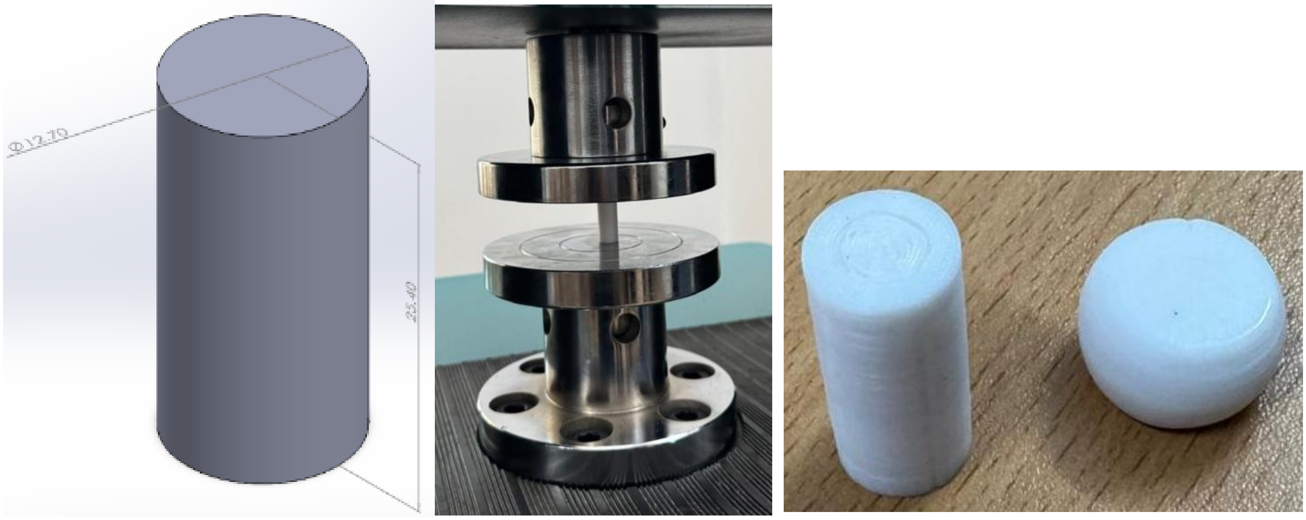


**(a)** **(b)** **(c)**

***Figure 18:. ASTM D695 for PLA (a)Specimen Design, (b)Experimental setup, and (c)Specimen before and after test***

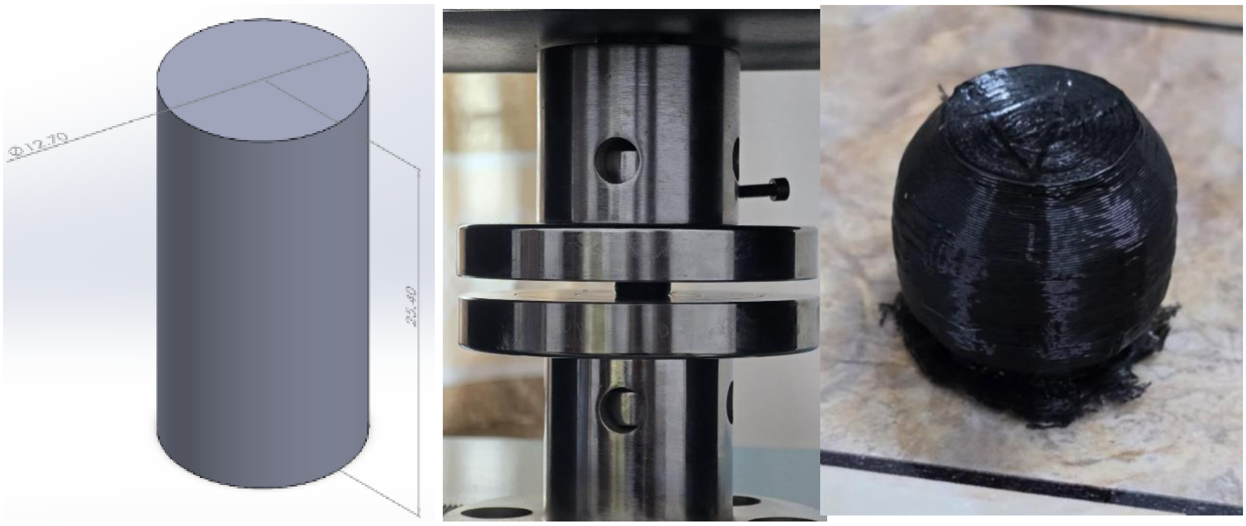


**(a)** **(b)** **(c)**

***Figure 19: ASTM D695 for TPU (a)Specimen Design, (b)Experimental setup (during testing), and (c)Specimen after testing***

Three sets of experiments have been performed for each material and collected the average values for Young’s Modulus, Poisson’s Ratio, Yield Strength and Tangent Modulus for the final results.

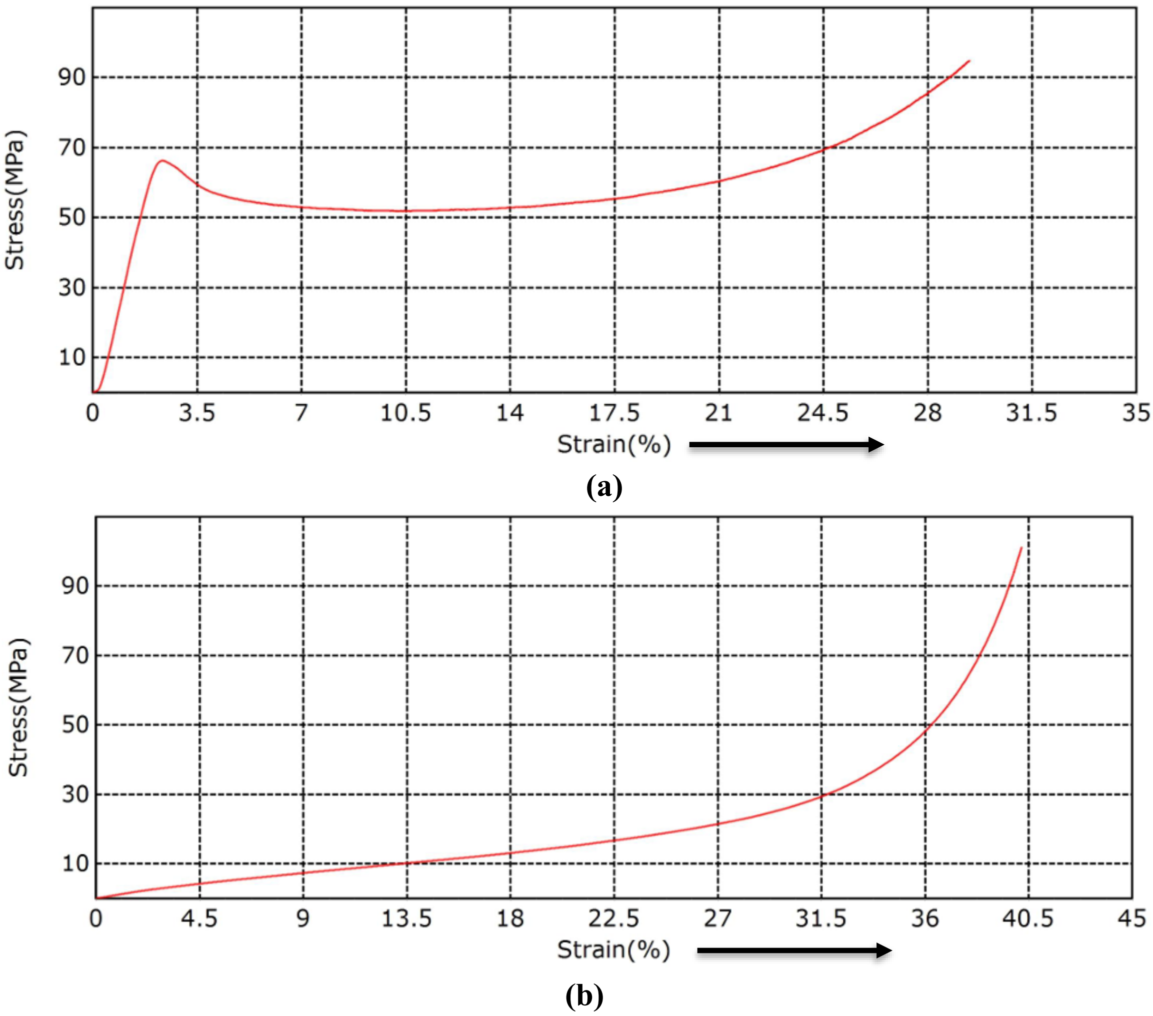


***Figure 20: Experimental results of ASTM D695 for (a)PLA, and (b)TPU***

***Table 5***

| *Material* | *Density (g /cm$^3$)* | *Young’s Modulus (GPa)* | *Poisson’s Ratio* | *Yield Strength (MPa)* | *Tangent Modulus (MPa)* |
|---|---|---|---|---|---|
| **PLA** | 1.24 | 1.9 | 0.36 | 56.3 | 200 |
| **TPU** | 1.22 | 0.2 | 0.45 | 40.5 | 4.8 |

## 5.2 Design:

Design of the hybrid Hex-S structure began with the base unit cell and optimal dimensions are determined. Mainly the main problem was to combine the S-shaped structure with an hexagonal shape. This design comes from many trials and tribulations. The first challenge was to determine the number of S- shapes corresponding to one hexagonal shape for optimal results.

***Table 6***

| No. of S-Shape | Effect |
|---|---|
| **1** | Does not slow enough flexibility when combined with hexagonal structure |
| **2** | Perfect combination of flexibility and stiffness |
| **4** | Becomes too stiff that it doesn't show the auxetic behavior what it must have |

In order to obtain auxetic behavior, we added two S's corresponding to a hexagonal. Combining two S-shaped unit cells and multiplying them transforms the total structure, so four S-shaped structures appear; this is what gives rise to auxetic behavior.

The dimensions were also determined through multiple trials and errors, as well as some from available sources, such as Namvar et al. We mainly made modifications to the angles; for example θ1 (°). We tried different angle values and ran the simulation to figure out what angle has more flexibility by actual subjective feeling, because all angles are the "S" structure's.

***Table 7***

| $\theta_1$ (°) | Effect |
|---|---|
| **90** | The distinct spring like behavior of S-Shape is completely missing |
| **60** | Flexible but limited space for lateral compression |
| **45** | Better flexibility than 60° and more room for deformation |
| **30** | Even better than 45° and the utmost utilization of spring like behavior of S-shaped structure |

Therefore, a 30° angle was chosen for our design purpose. In addition to that, fillets with a radius, R, were added for better energy absorption and dimensional stability.

***Table 8***

| **Unit Cell Dimensions for Hybrid Hex-S Structure** | | | | | | | | |
|---|---|---|---|---|---|---|---|---|
| ***I (mm)*** | ***p (mm)*** | ***M (mm)*** | ***R (mm)*** | ***α (°)*** | ***$\theta_1$ (°)*** | ***$\theta_2$ (°)*** | ***t (mm)*** | ***W (mm)*** |
| 5 | 2 | 7 | 1.22 | 30 | 30 | 10 | 1.5 | 10 |

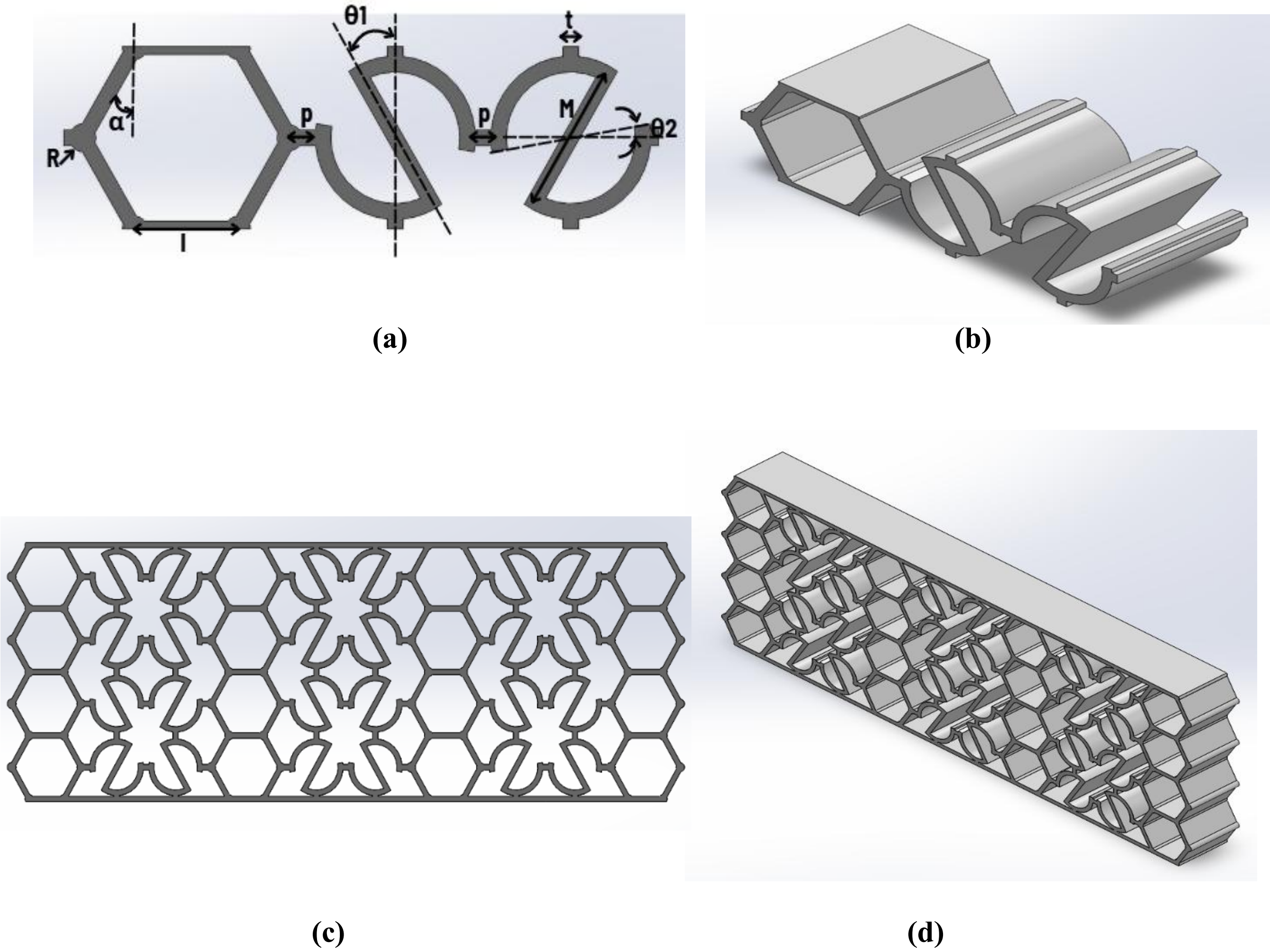


***Figure 21: (a) Unit cell of Hybrid Hex-S with dimensions, (b) Isometric View of Hybrid Hex-S unit cell, (c) Front view of Hybrid Hex-S, and (d) Isometric View of Hybrid Hex-S***

## 5.3 Fabrication:

3D Printing and Fabrication Process An auxiliary process, which had been decided design for the auxetic structures, became popular with Fused Deposition Modeling (FDM). This was because it could provide accessibility, economy, and the fact its polymer-based functional prototypes are just what you need. Multiple benefits were found from FDM in this investigation as compared with Selective Laser Sintering (SLS) and Stereolithography (SLA). The precision of SLS is higher and it uses powder-based materials, but on the other hand it's more expensive to make and the removal of surplus powder is a specialized process that requires its own equipment. Similarly, though SLA delivers a very good surface finish; because it uses photopolymer resins which are brittle and not suitable for mechanical testing of flexible auxetic structures. Meanwhile FDM can print with engineering thermoplastics like TPU and PLA, which mix flexure and durability together as required. It also manages rapid iteration and parameter optimization, making it the best way to make experimental prototypes that have functionality.

With the optimized FDM parameters, the printing process which occured maintained high dimensional accuracy and good mechanical properties. Layer height was set at 0.2mm for an optimal balance between surface resolution and speed of printing. A nozzle diameter of 0.4mm was used to ensure even layer bonding yet preserve fine geometric detail. Infill density was left constant at 100%, while extra thick walls increased the structural strength and load-bearing capacity of objects. The printing temperature was maintained at 210°C, in order to ensure that the filament flow went properly and layers bonded together. Bed temperature was set to 60°C, to keep warping at a minimum and improve adhesion. With an optimized speed of 280 mm/s, the print time is balanced between productivity and part integrity. In addition, the surrounding added 5mm wide banded printing for bed adhesion was also intended to increase part integrity and reduce the tendency of layers peeling apart during printing.

The printed samples were then left at about room temperature (20-25°C) for 30 minutes cooling to make them completely solidified and habituation to stress minimized. Afterwards, the brim was removed manually using an anti-cutter to produce the final geometry without destroying any parts of the structure and maintain its edges. With all these parameters optimized in these ways, the fabricated auxetic specimens had both requisite mechanical strength acquisitions as well as good flexural properties dimensionally stable enough not to shift even over time, so much suitable for further experimental research and analysis.

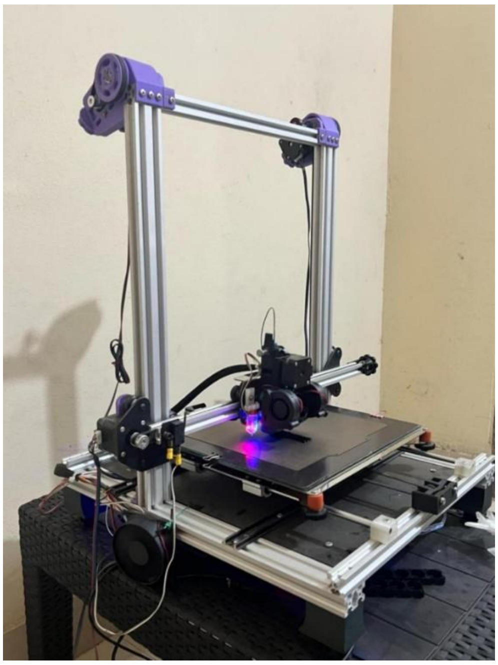

***Figure 22: FDM  3D Printer***

By comparing FDM-printed structures themselves we have learned that the mechanical performance of FDM-printed structures is greatly influenced by the difference in printing direction, filament alignment and interlayer bonding. In this study, specimens were printed in 45 ° and 90 ° orientations to explore its influence on the structure. The results indicate that at the 45° orientation was more favorable in properties than at the 90 ° one.

This improvement may be attributed to 45° being an angle of equilibrium so that the strain is distributed evenly; there is scope for multi-directional filament alignment and better cracking resistance through which a structure has greater capacity before it finally yields due to overstrain. On the other hand, at 90° the falling filaments are perpendicular to loading direction, creating highly ruled interlayer stress points which are difficult to bond together. This can lead shear forces exerted during a certain period of time cause them be stretched apart and split from one another entirely while under load. On the other hand, with a 45° configuration, load is more evenly distributed in the lateral direction on per adjacent layer so as to provide greater interlayer adhesion and tensile strength.

After all, it means that with the 45° orientation the anisotropy which is common in FDM parts is eliminated so that they all have a more uniform response to compression loading or tension. Therefore, 45° printed auxetic structures have a more isotropic and stable mechanical performance, so this direction is suitable for places where strength, energy absorption and dimensional stability are all required.

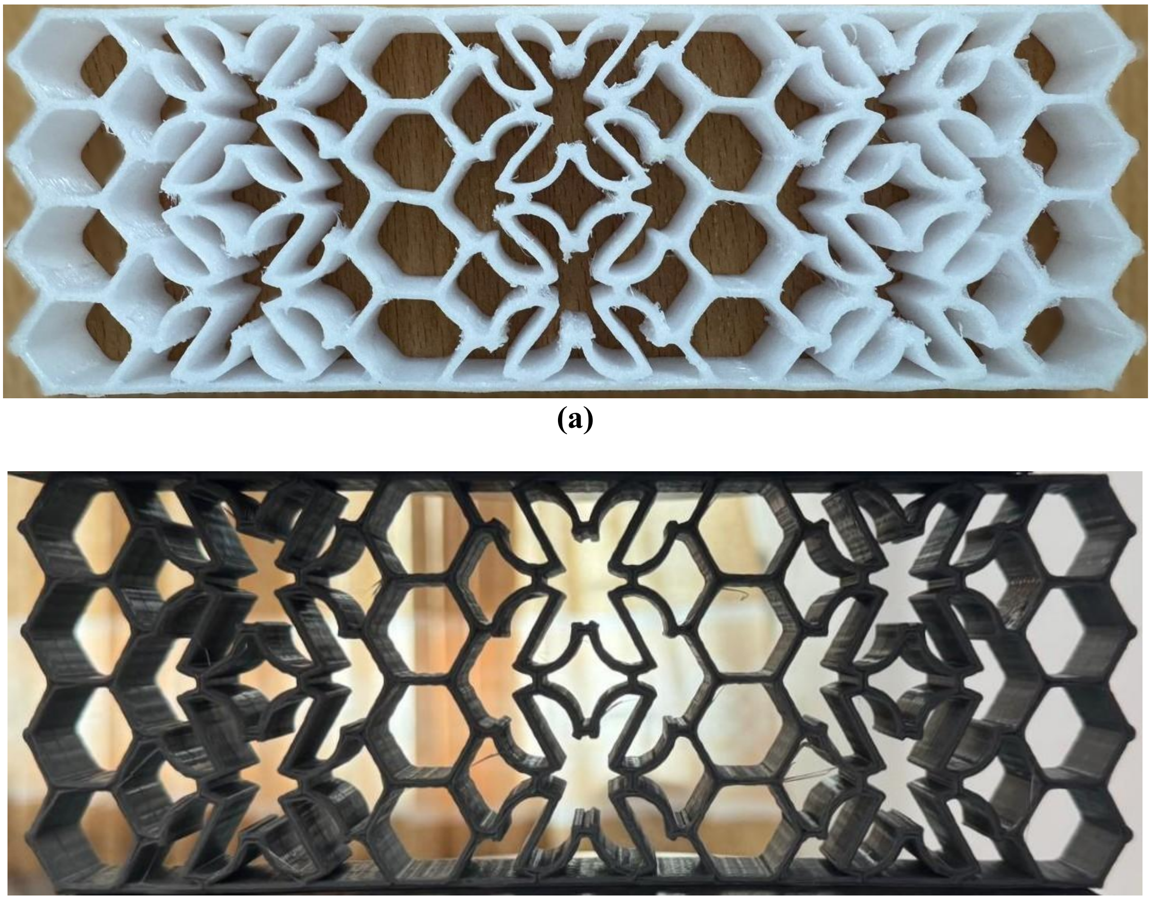

**(a)**

**(b)**

***Figure 23: 3D printing samples of Hex-S structure using (a)TPU, and (b)PLA***

# Chapter 6: Modelling and Simulation

For the numerical analysis, ANSYS 2021 R2 explicit dynamics method was used. Several analyses were performed by changing the structures, boundary conditions and materials for the extensive study.

## 6.1 Material Defining:

Material properties for PLA and TPU were defined before starting the analyses. These properties were obtained from ASTM D695 for TPU and PLA material.

| | A | B | C |
|---|---|---|---|
| 1 | Property | Value | Unit |
| 2 | Material Field Variables | Table | |
| 3 | Density | 1220 | kg m^-3 |
| 4 | Isotropic Elasticity | | |
| 5 | Derive from | Young's Mo... | |
| 6 | Young's Modulus | 0.2 | GPa |
| 7 | Poisson's Ratio | 0.45 | |
| 8 | Bulk Modulus | 6.6667E+08 | Pa |
| 9 | Shear Modulus | 6.8966E+07 | Pa |
| 10 | Bilinear Isotropic Hardening | | |
| 11 | Yield Strength | 40.5 | MPa |
| 12 | Tangent Modulus | 4.8 | MPa |

**(a)**

| | A | B | C |
|---|---|---|---|
| 1 | Property | Value | Unit |
| 2 | Material Field Variables | Table | |
| 3 | Density | 1.24 | g cm^-3 |
| 4 | Isotropic Elasticity | | |
| 5 | Derive from | Young's Mo... | |
| 6 | Young's Modulus | 1.9 | GPa |
| 7 | Poisson's Ratio | 0.36 | |
| 8 | Bulk Modulus | 2.2619E+09 | Pa |
| 9 | Shear Modulus | 6.9853E+08 | Pa |
| 10 | Bilinear Isotropic Hardening | | |
| 11 | Yield Strength | 56.3 | MPa |
| 12 | Tangent Modulus | 200 | MPa |

**(b)**

***Figure 24: Material properties defined in the ANSYS for (a)TPU, and (b)PLA***

## 6.2 Contacts Defining:

A frictional contact with frictional coefficient of 0.3 was applied in between the bottom surface of the load plate and the top surfaces of the re-entrant, Aux-Hex and Hex-S structure.

## 6.3 Meshing:

To replicate the actual experimental setup, a round flat plat 1kg load was designed. As for the load, the meshing method and size was applied the default settings.

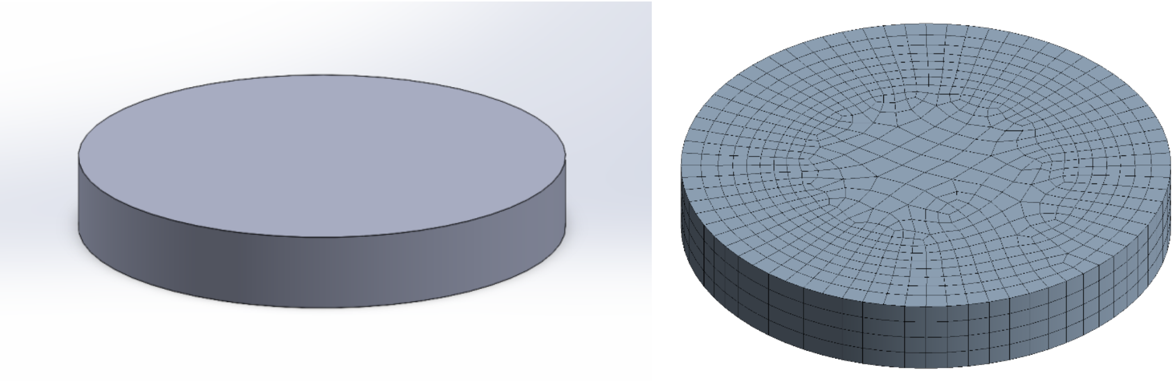

***Figure 25: (a) 3D Model of the Load, and (b)Finite Element Meshing of the Load***

**(a)** **(b)**

Tetrahedral mesh as utilized for all three structures due to its ability to effectively capture stress distribution in complex geometries like the re-entrant, Aux-Hex and Hex-S structure.

Mesh size of 1mm was applied for both Aux-Hex and Re-entrant structures, which was obtained from converging the result. And in case of Hex-S structure, finite element mesh of 1mm was applied. But to capture more accurate results, 0.8mm tetrahedral mesh is used in the fillets within the Hex-S structure.

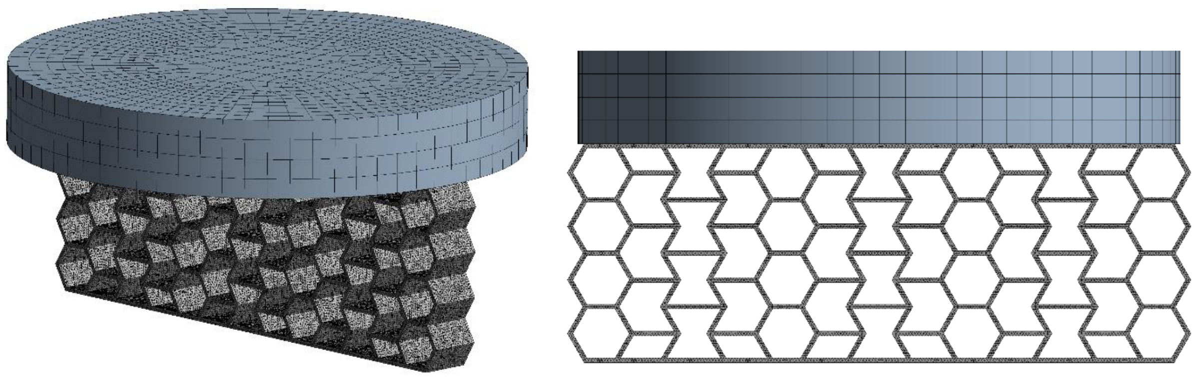

**(a)** **(b)**

***Figure 26: Finite Element Meshing of Aux-Hex Structure with Load applied (a) Isometric View, and (c) Front view***

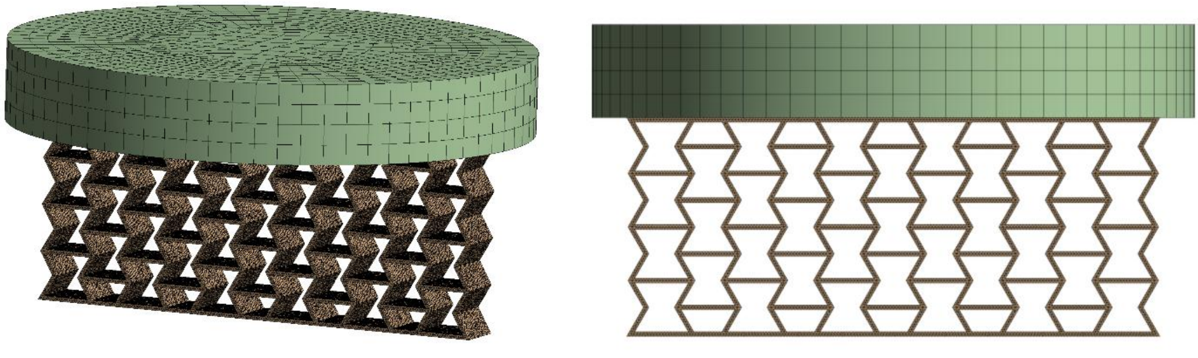

**(a)** **(b)**

***Figure 27: Finite Element Meshing of Re-entrant Structure with Load applied (a) Isometric View, and (c) Front view***

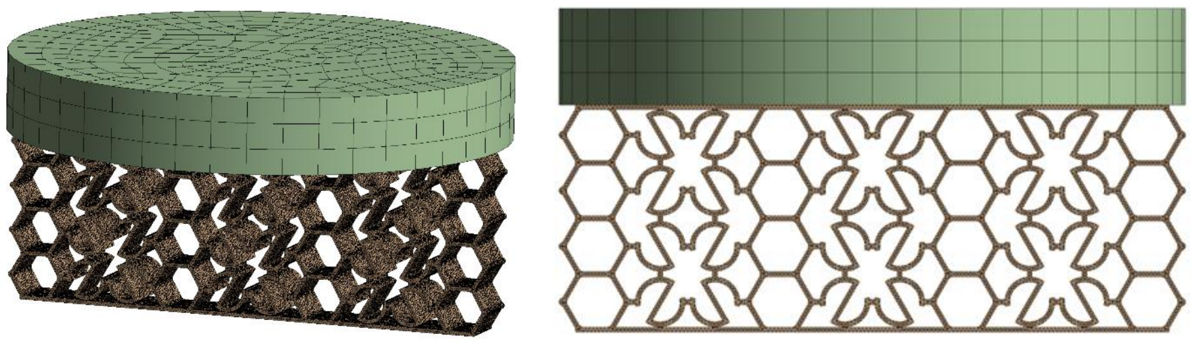

**(a)** **(b)**

***Figure 28: Finite Element Meshing of Hex-S Structure with Load applied (a) Isometric View, and (c) Front view***

## 6.4 Boundary Conditions Defining:

Fixed support was applied on the bottom surface for all three structures, Re-entrant, Aux-Hex and Hex-S structures.

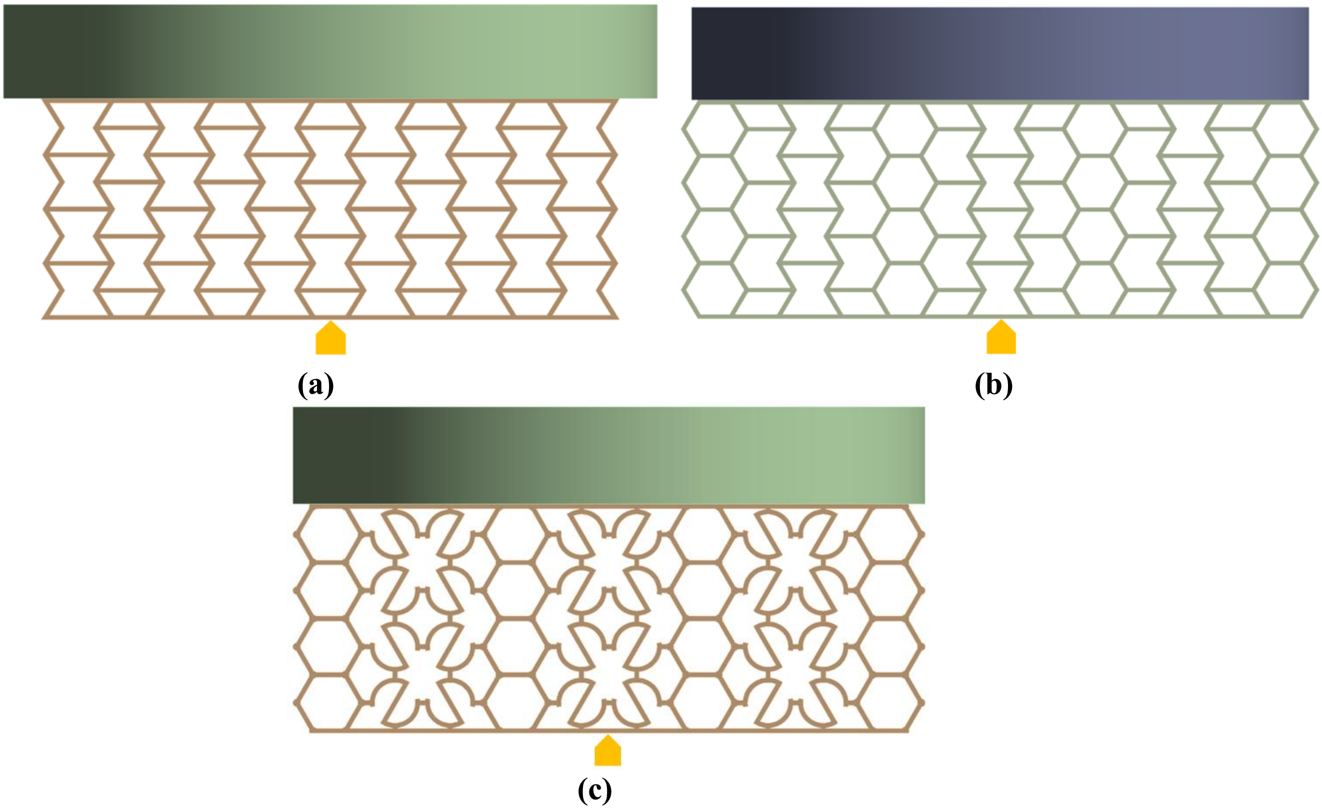


***Figure 29: Fixed Support applied on (a) Re-entrant Structure, (b) Aux-Hex Structure, and (c) Hex-S Structure***

The structure was subjected to an uni-axial stress with a strain rate of 1mm/min. This analysis was carried out in order to simulate the real experimentally existing condition where quasi-static loading is used. Taking our purpose as an example, 2, 5, 15 and 30 millimeters of displacement were added on each structure and we varied them by distance of displacement conducting analyses for this paper.

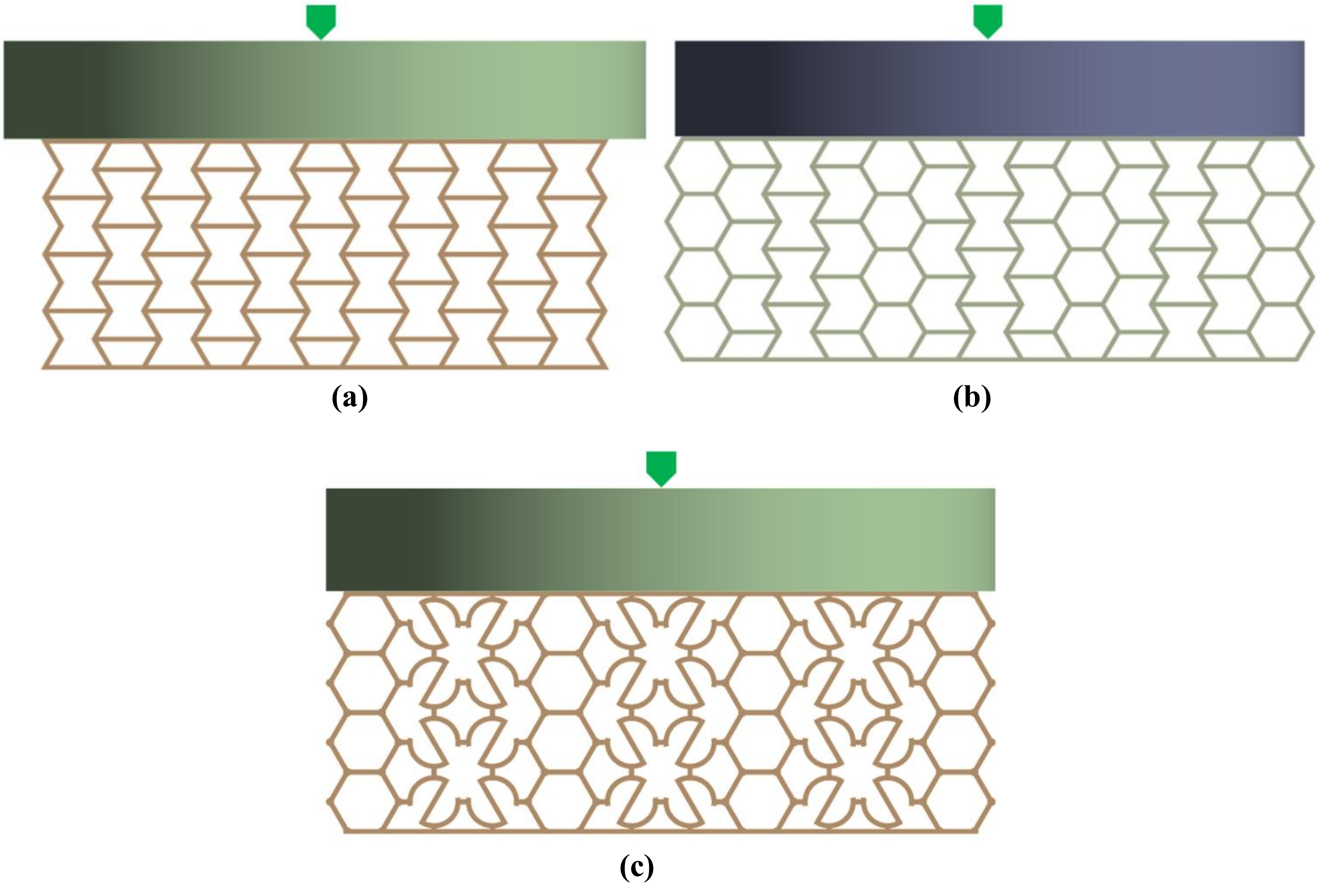


***Figure 30: Unidirectional displacement applied on (a) Re-entrant Structure, (b) Aux-Hex Structure, and (c) Hex-S Structure***

# Chapter 7: Results and Discussion

The entire findings of the experimental tests and simulation of the Hybrid hex-S structure are presented in this chapter with tensile test being the method used in collecting the raw data of Neural aluminum alloy and the structures used in the experiment were the PLA variants of the Hybrid Hex-S structure, Re-entrant structure and Aux-Hex structure. The analysis of these results was done in terms of the energy that is taken up, the distribution of stresses and the behavior of the material when it is subjected to new forms of displacement. It comparatively also evaluates the effectiveness of each design both under simulated and experimental conditions respectively.

## 7.1 Simulation results:

- ***<u>Stress results:</u>***

  - $\boldsymbol{Stress(\sigma) = \frac{Force}{Area}}$
  - $\boldsymbol{Strain(\varepsilon) = \frac{\Delta l}{l_0}}$
  - $\boldsymbol{Young's\ Modulus(E) = \frac{Stress(\sigma)}{Strain(\varepsilon)}}$

*Aux-Hex Structure:*

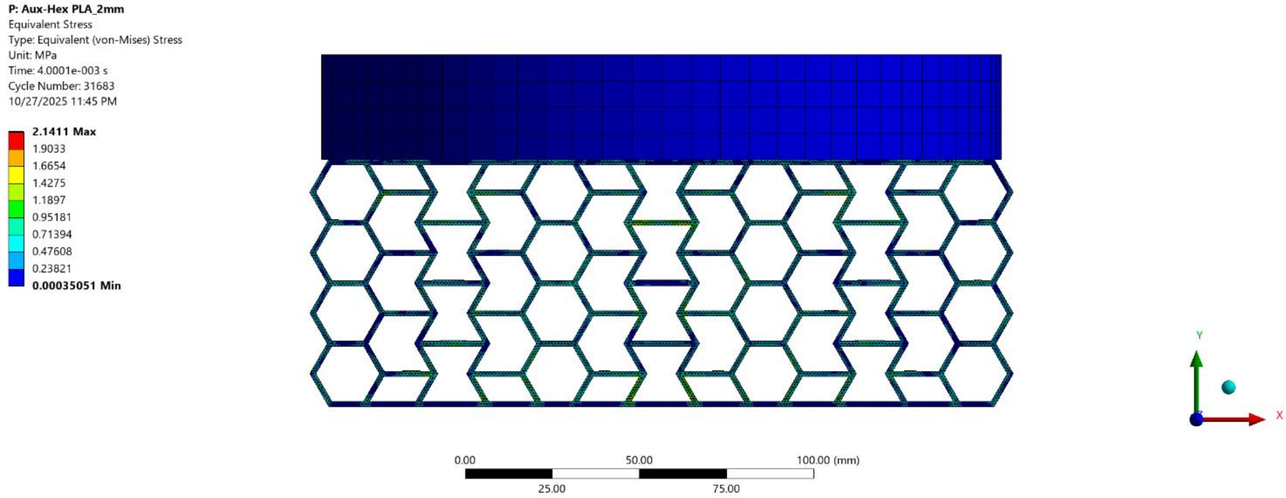


**(a)**

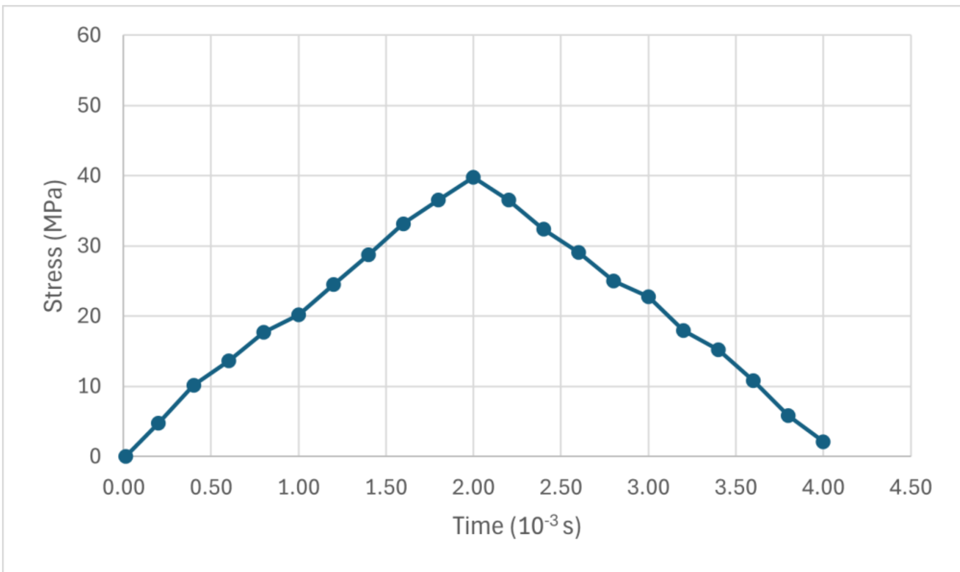


**(b)**

***Figure 31: Aux-Hex structure with Displacement of 2mm printed with PLA (a) Stress Result, and (b) Stress vs Time Graph***

Figure 31(a) indicates that the Aux-Hex PLA sample demonstrated a maximum of 2 mm compressive load in which the sample could not record any residual strain after unloading, hence it exhibited good structural elasticity and shape recovery. On the same note, Figure 31(b) indicates that the stress levels rise progressively as loading progresses up to a peak of about 39.802 MPa at about 2 ms. The values of the stress during unloading go back to the initial point indicating that no significant permanent stress is left within the structure. The fact that the deformation is mostly recoverable is proven by the reason that the stress release is made timely, which enhances the strong energy-absorption and self-recovery properties of the structure.

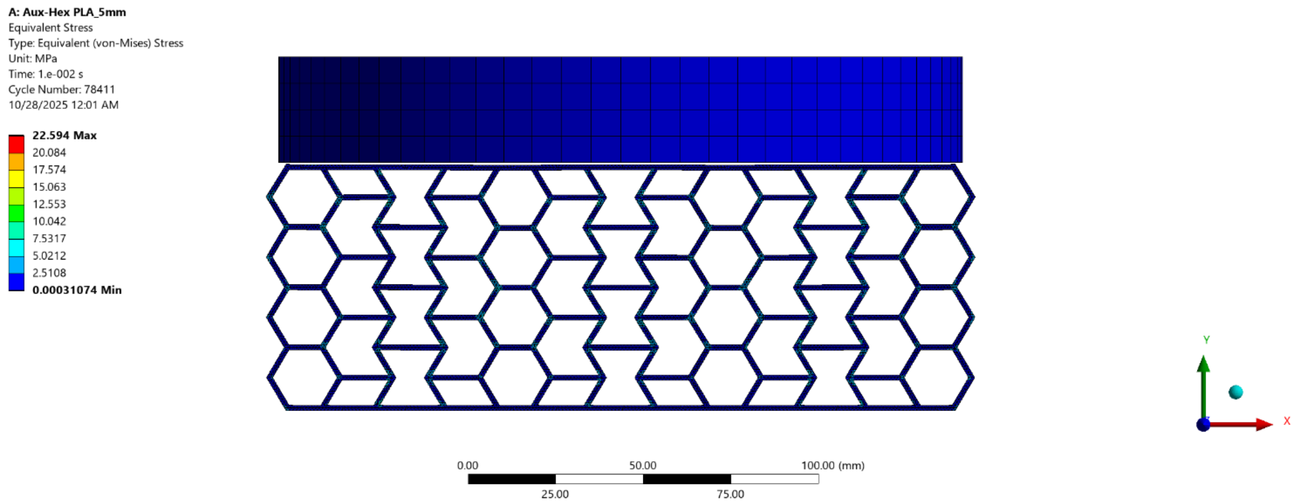


**(a)**

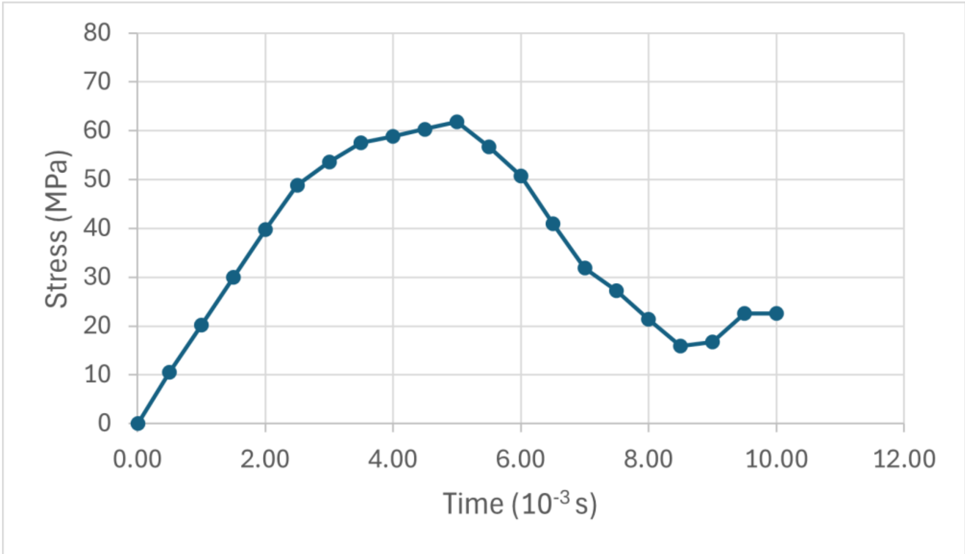


**(b)**

***Figure 32: Aux-Hex structure with Displacement of 5mm printed with PLA (a) Stress Result, and (b) Stress vs Time Graph***

Figure 32(a) at 5 mm compressive loading and less than 5 mm compressive loading, Aux-Hex PLA sample was observed to have recovered partially and slightly some permanent deformation, which showed the beginning of the plastic behavior. The figure 32(b) suggests that the stress curve increased in a linear fashion with time in the process of loading, reaching an approximate peek stress of 61.858 MPa at approximately 5 ms within the elastic limit of the structure. And when this threshold has been exceeded, the stress starts to slowly decline as the weight is removed yet it never comes back to the original zero value, this proves internal stress retention. This action confirms that more than 5 mm displacement, the Aux-Hex PLA structure is at the plastic deformation region that causes permanent structural changes.

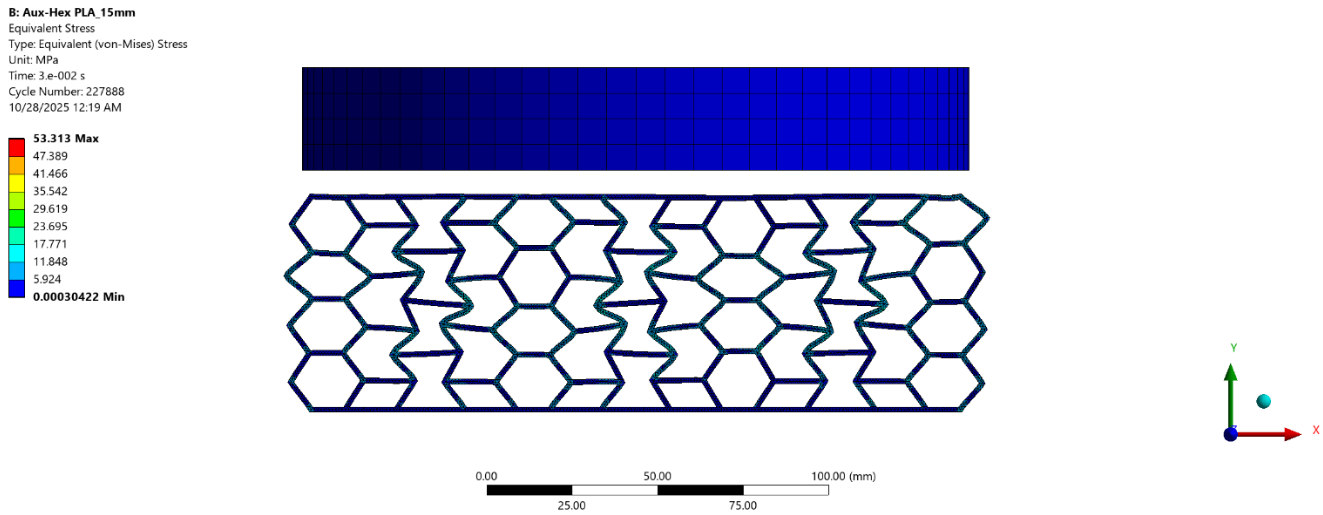


**(a)**

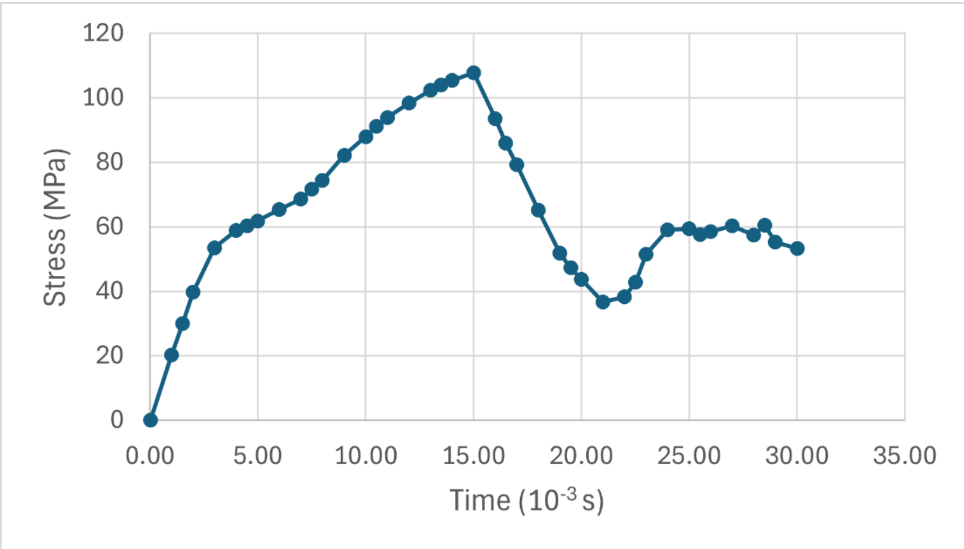


**(b)**

***Figure 33: Aux-Hex structure with Displacement of 15mm printed with PLA (a) Stress Result, and (b) Stress vs Time Graph***

In Figure 33 (a), when compressed to 15 mm, Aux-Hex PLA structure was observed to deform permanently when unloaded, which means that there is a considerable plastic collapse of the cellular structure. Based on Figure 33(b), it is observed that the stress gradually increased to the elastic limit 107.73 Mpa at 15 ms. After this, there are apparent fluctuation patterns, which indicate progressive cell damages and instability prior to the plastic region. Extensive permanent deformation is verified by the irreversible stress in the after unloading and this behavior is in line with mechanical failure mode.

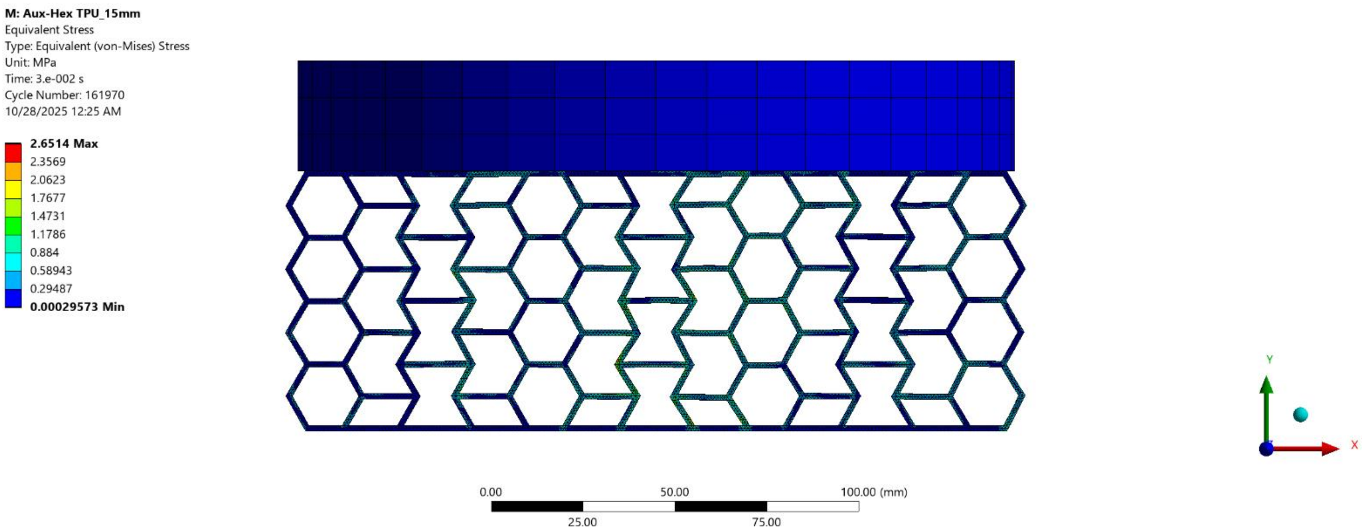


**(a)**

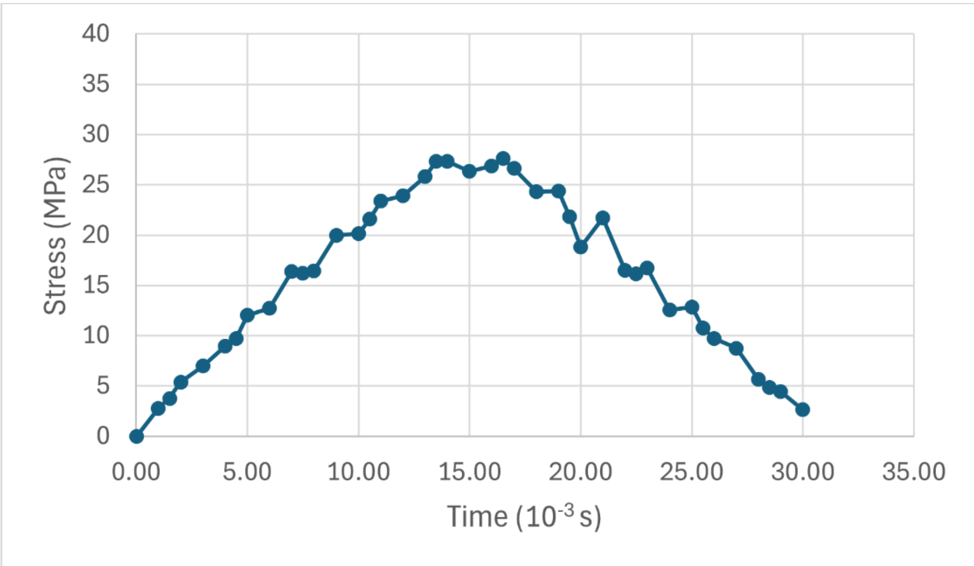


**(b)**

***Figure 34: Aux-Hex structure with Displacement of 15mm printed with TPU (a) Stress Result, and (b) Stress vs Time Graph***

Figure 34(a) shows that below 15 mm compression the Aux-Hex TPU design showed good smooth and complete recovery post unloading, which confirmed fully elastic deformation. The load is steadily increasing and peaked at approximately 27.654 MPa at approximately 16.5 ms that is in Figure 34(b). As the unloading is carried out, the value of stress tends to go back to zero, which indicates the absence of internal stress left. This confirms that TPU is a superior fatigue resistant material to large deformation in auxetic structures.

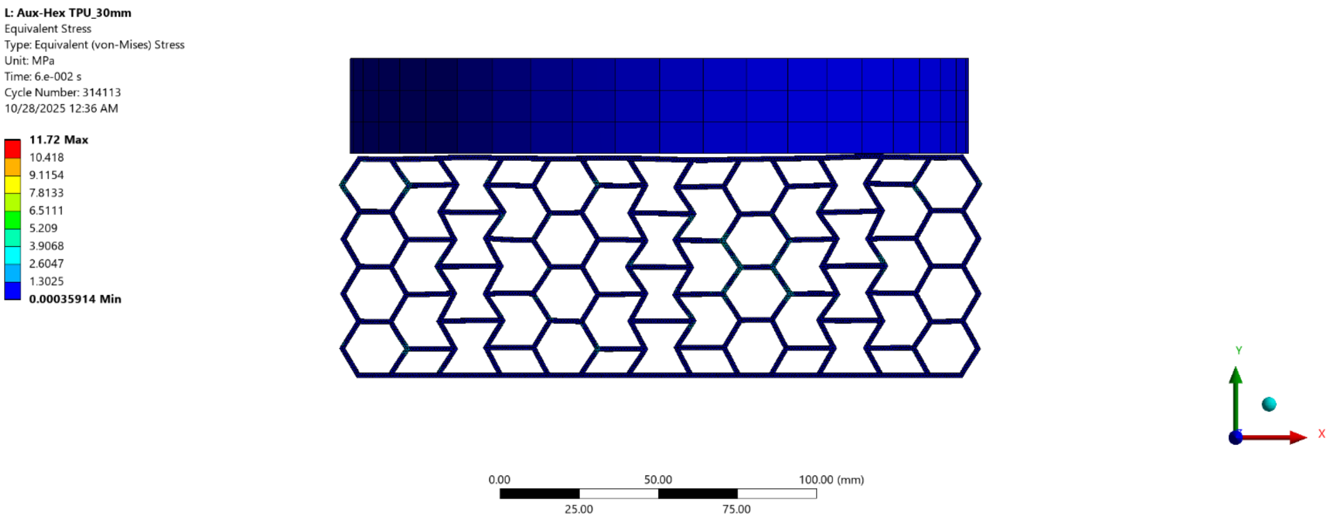


**(a)**

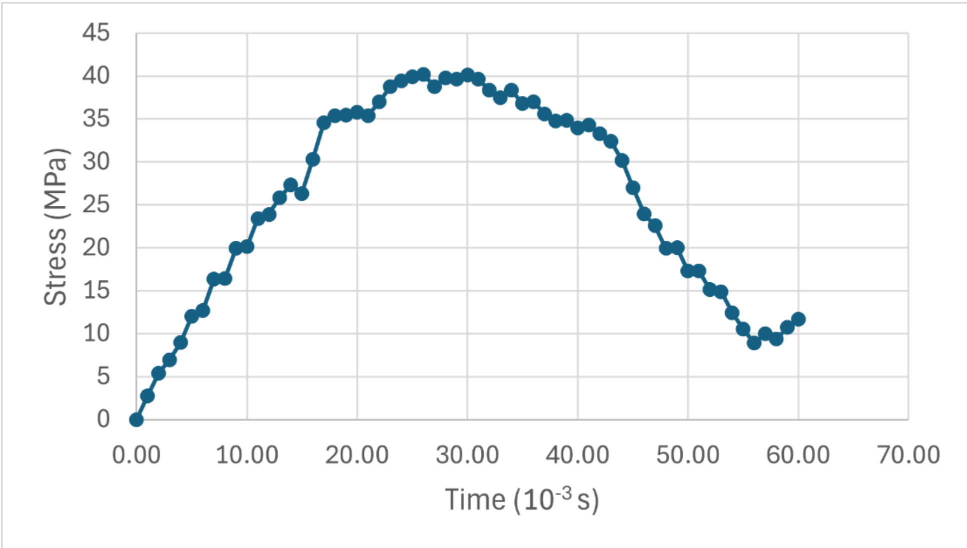


**(b)**

***Figure 35: Aux-Hex structure with Displacement of 30mm printed with TPU (a) Stress Result, and (b) Stress vs Time Graph***

Figure 35(a) demonstrates that at Aux-Hex TPU structure, the full recovery occurred after the unloading of the structure at a 30 mm displacement, but the deformation recovery response was not as smooth as at lower strain levels. Based on Figure 35(b), the highest stress (40.21) is observed at 26 ms which is not very high given the fact that TPU is very elastic. As soon as the unloading starts, the stress is immediately reduced to zero which proves that the deformation is purely of an elastic character, there is no irreversible damage.

## *Re-entrant Structure:*

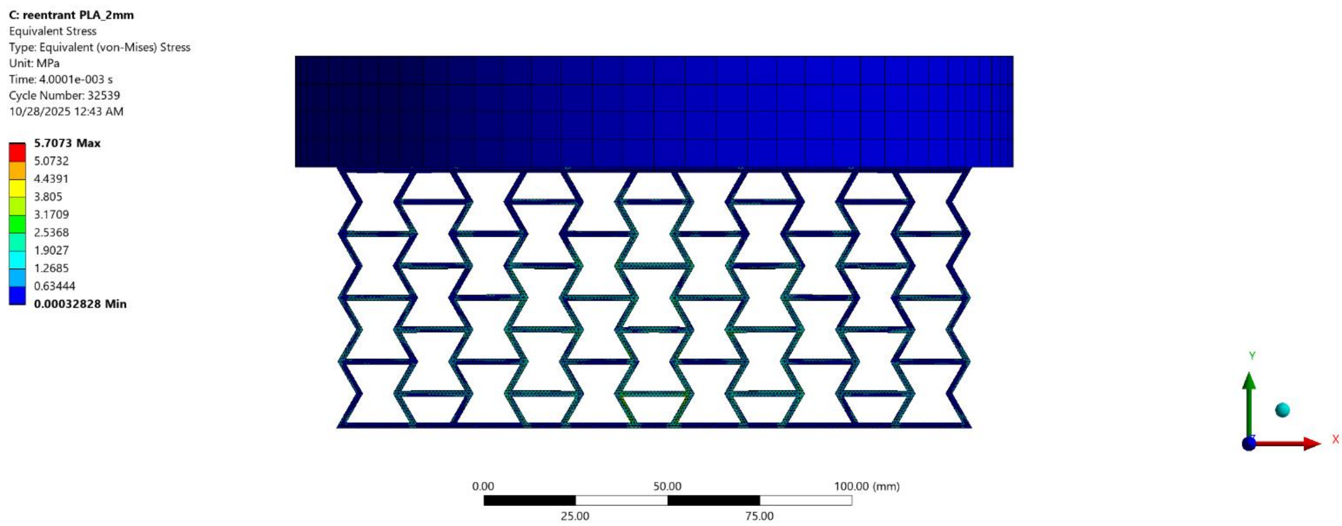


**(a)**

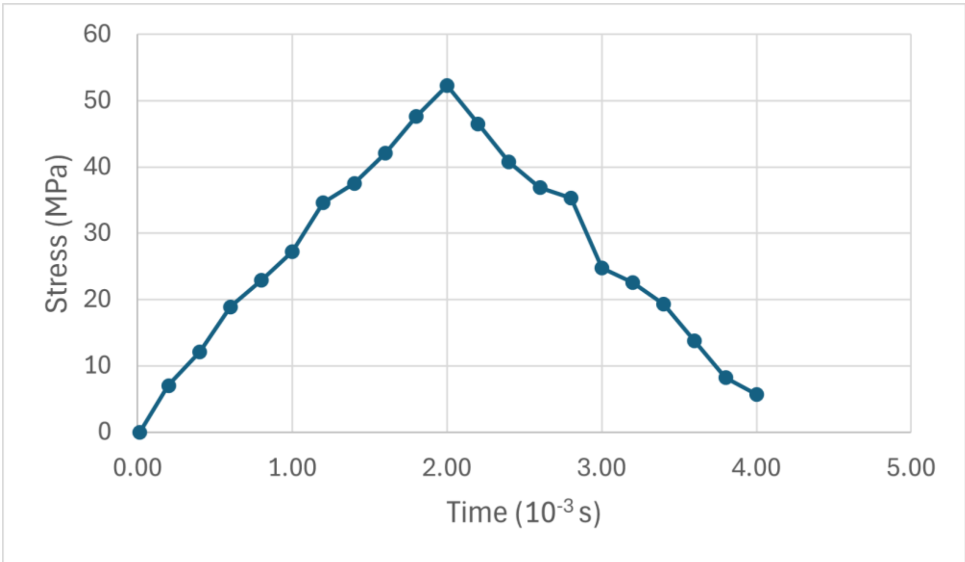


**(b)**

***Figure 36: Re-entrant structure with Displacement of 2mm printed with PLA (a) Stress Result, and (b) Stress vs Time Graph***

The Re-entrant PLA structure under a compressive load of less than 2 mm showed complete shape recovery on unloading, which shows fully elastic behavior what is mentioned in Figure 36(a). Figure 36(b) shows that the stress increases with time when loading and elasticity occurs until at a point of maximum value which is 52.294 Mpa at 2ms. Smaller variations beyond that indicate spot-wise yielding, but generally, the structure has a good energy uptake and recovery efficiency.

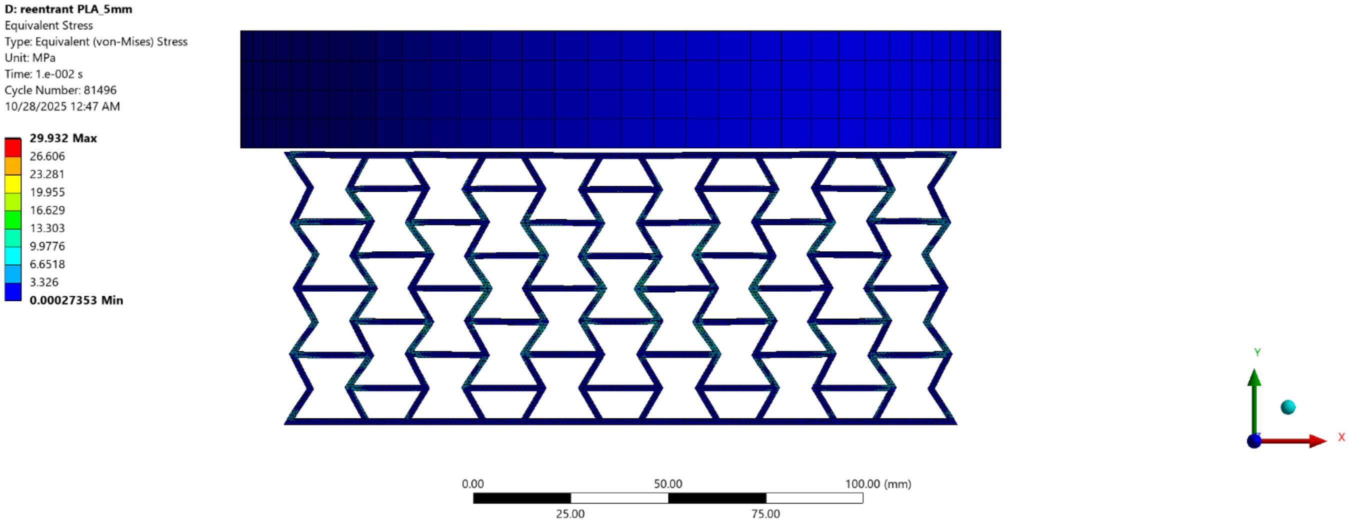


**(a)**

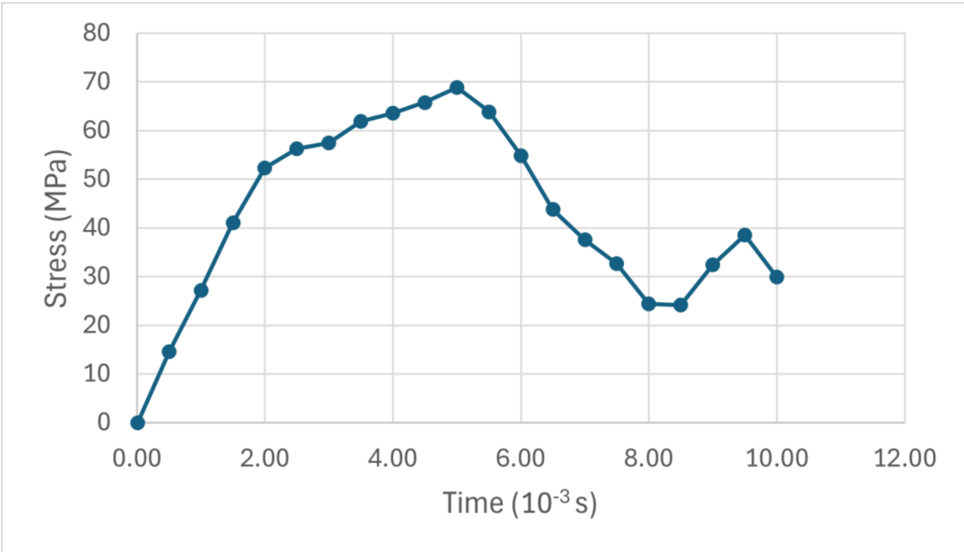


**(b)**

***Figure 37: Re-entrant structure with Displacement of 5mm printed with PLA (a) Stress Result, and (b) Stress vs Time Graph***

In Figure 37(a), when the displacement was 5 mm, the Re-entrant PLA structure had recovered partially with a slight permanent deformation, indicating the onset of the plastic behavior. Using Figure 37(b) it can be observed that the material had an elastic limit of approximately 68.903 MPa at 5 ms. Further on, the stress oscillates with the upper and lower yield of the material until it enters the plastic regime, which proves irreversible deformation upon unloading.

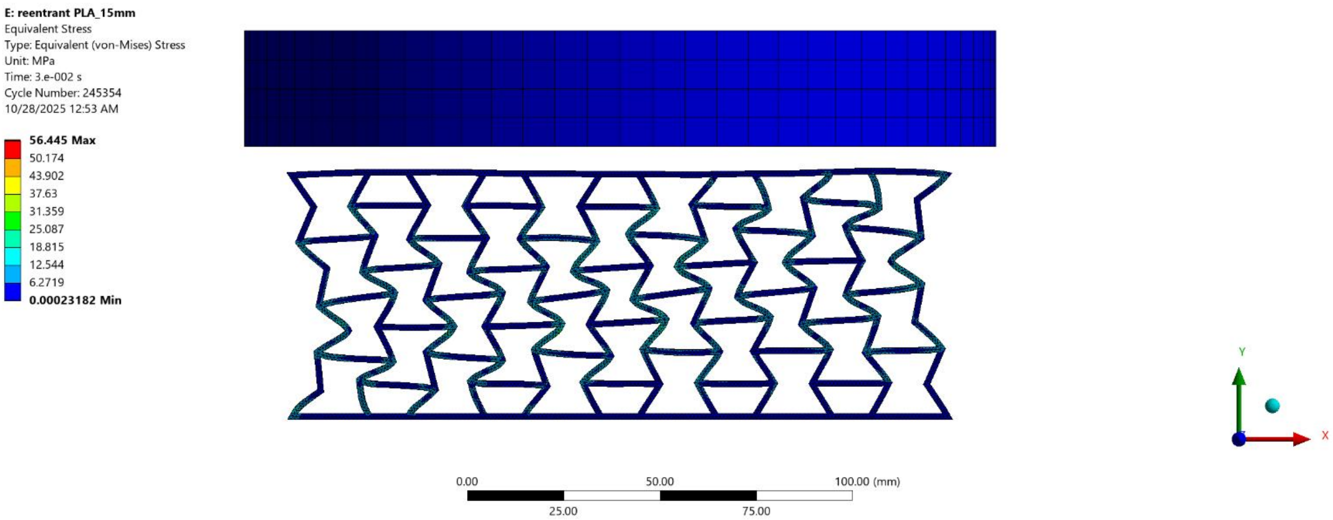


**(a)**

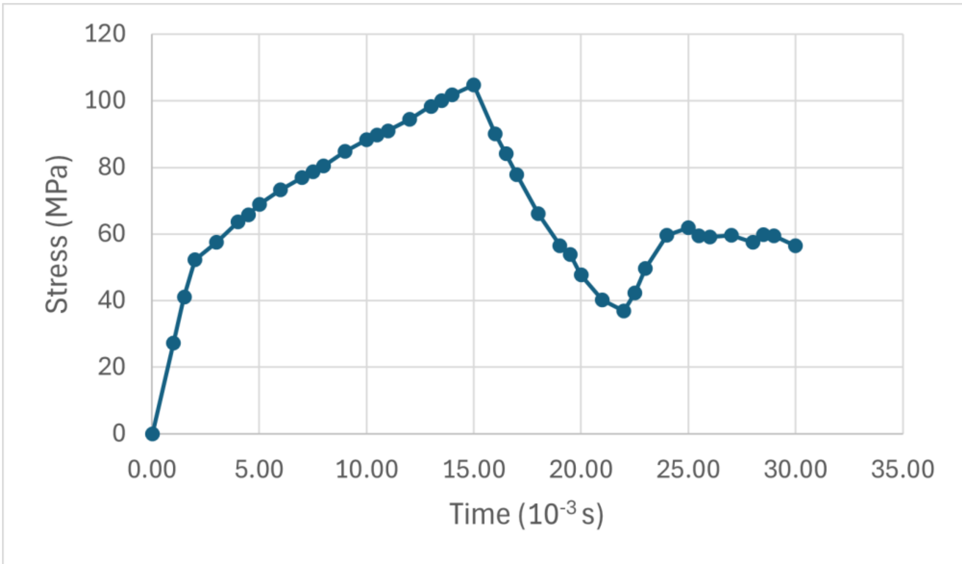


**(b)**

***Figure 38: Re-entrant structure with Displacement of 15mm printed with PLA (a) Stress Result, and (b) Stress vs Time Graph***

Figure 38(a) shows that the Re-entrant PLA structure underwent a large amount of permanent deformation and did not recover after 15 mm compression confirming large-scale plastic collapse. Based on Figure 38(b), the elastic limit is around 104.76 MPa at 15 ms, and the beyond point, the stress keeps on oscillating and moving into the plastic zone. The structure does not recuperate, which means that there is a lot of plastic flow and energy absorption prior to failure.

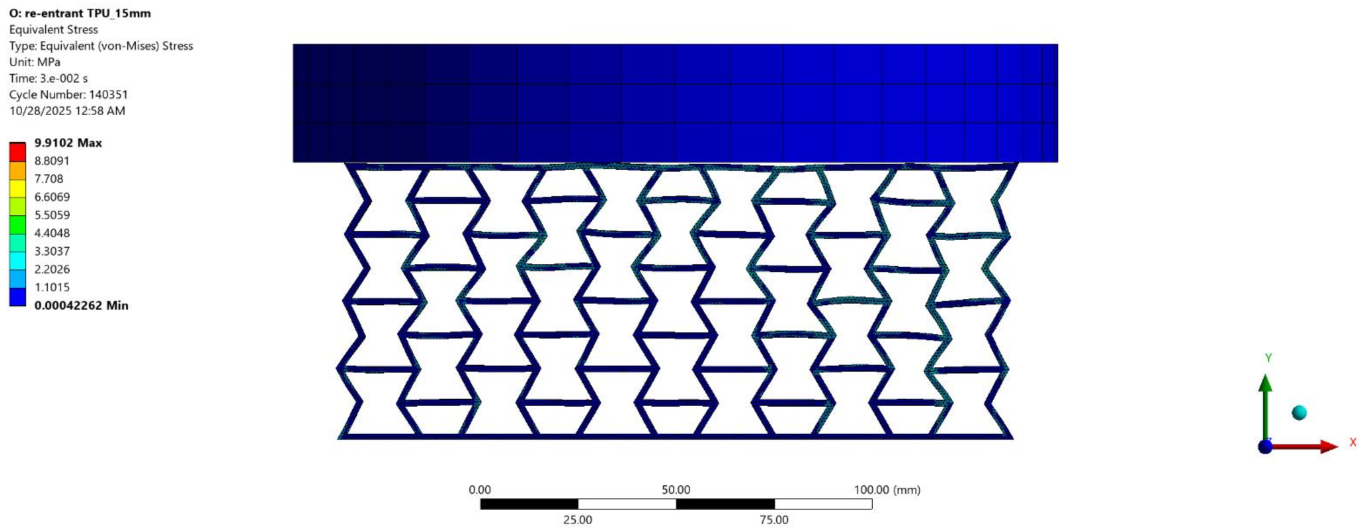


**(a)**

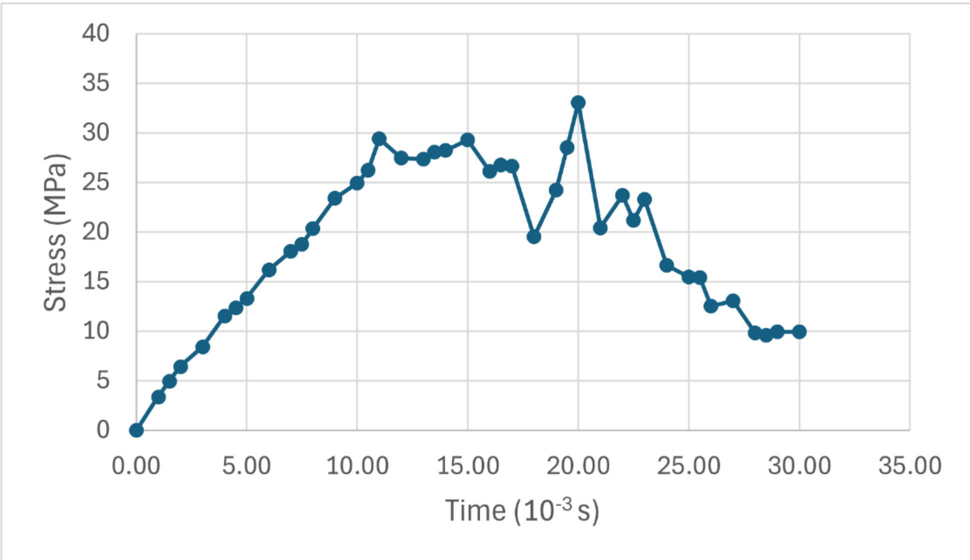


**(b)**

***Figure 39: Re-entrant structure with Displacement of 15mm printed with TPU (a) Stress Result, and (b) Stress vs Time Graph***

Figure 39 (a) shows that when it was compressed to 15 mm, the Re-entrant TPU structure easily reverted to its original shape on the release which exhibits a very elastic and recovers the form. Figure 39(b) shows that the elastic point is approximately 29.275 Mpa at 15 ms and the stress fluctuates afterward, yet it does not go out of the elastic section. The substance is flexible and resilient as typical of TPU-based auxetic structures.

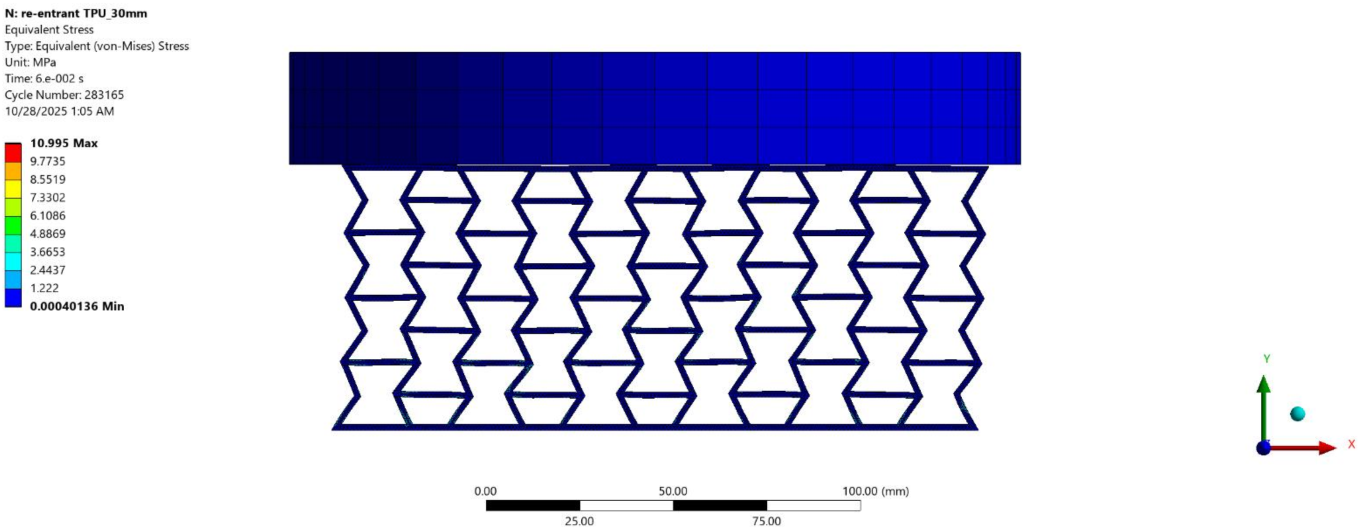


**(a)**

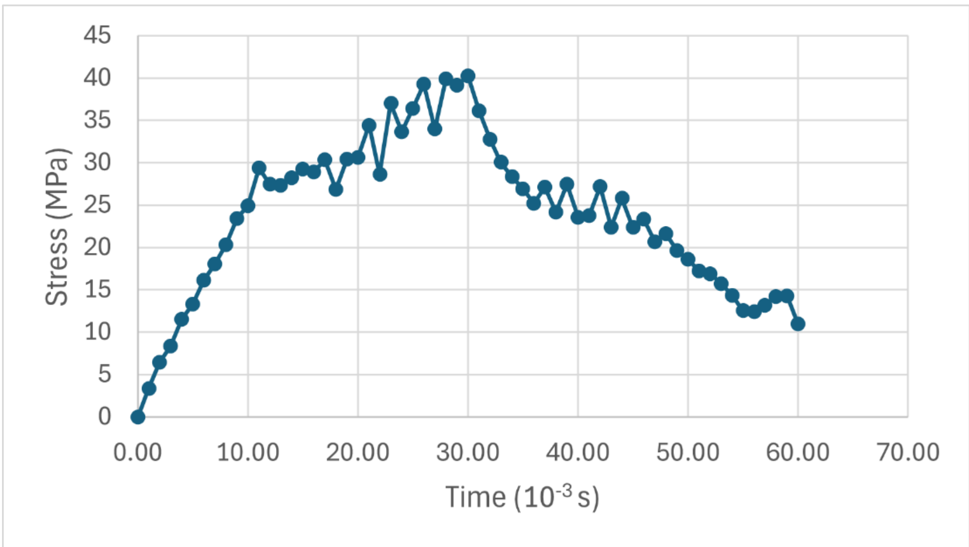


**(b)**

***Figure 40: Re-entrant structure with Displacement of 30mm printed with TPU (a) Stress Result, and (b) Stress vs Time Graph***

Figure 40(a) shows that the Re-entrant TPU structure took full recovery after unloading at a displacement of 30 mm although the response to recovery was not smooth compared to the lower strain levels Figure 40(b). The TPU structure has great recoverability and elasticity even in cases of large deformations.

***Hex-S Structure:***

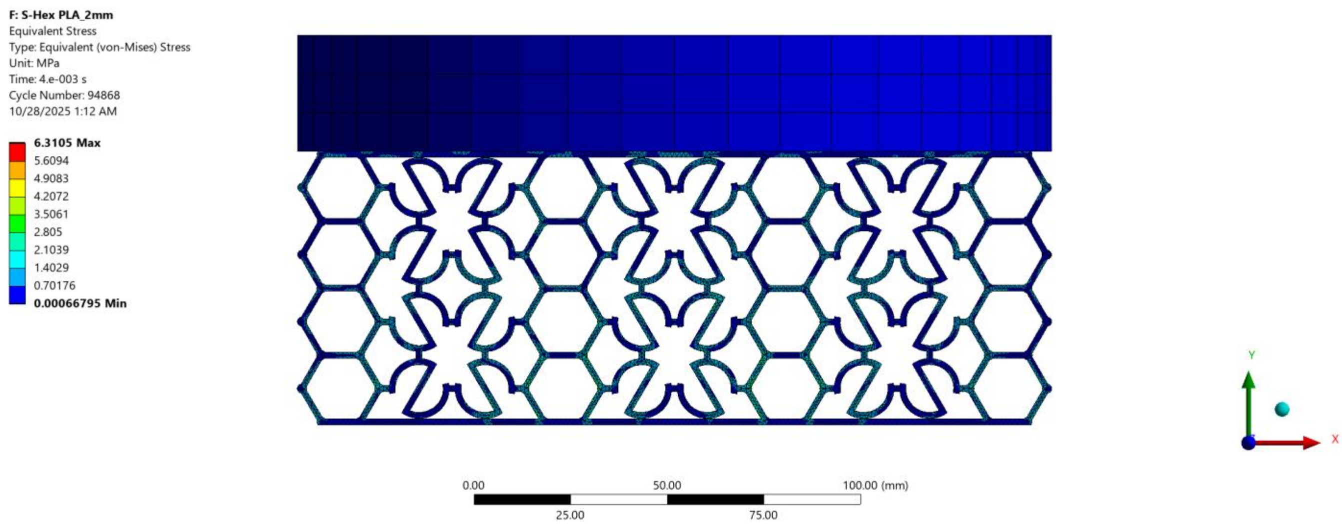


**(a)**

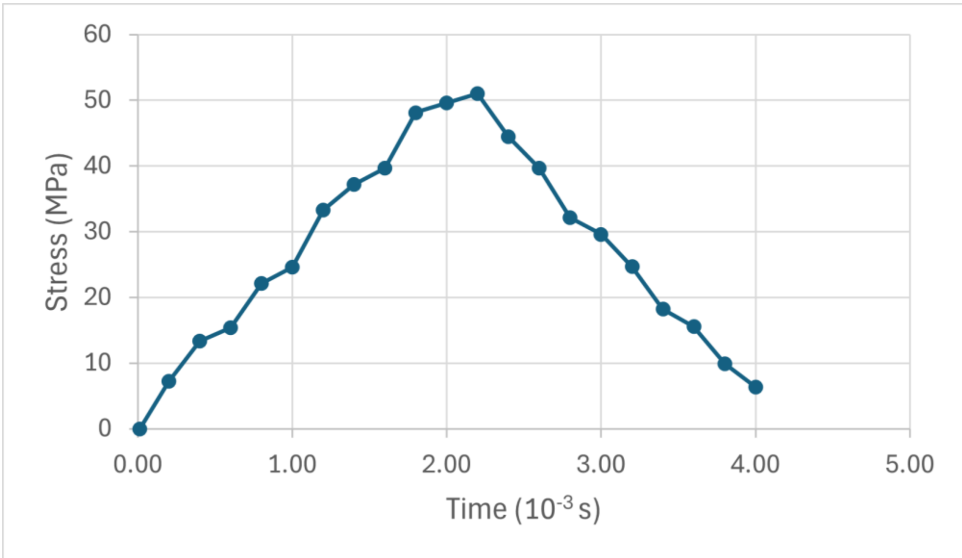


**(b)**

***Figure 41: Hex-S structure with Displacement of 2mm printed with PLA (a) Stress Result, and (b) Stress vs Time Graph***

As shown in Figure 41(a), the Hex-S PLA structure under 2 mm compression remained within the elastic range and completely recovered after unloading with no permanent deformation. Figure 41(b) depicts the maximum elastic limit as 50.992 MPa at 2.2 ms. The stress curve stays within the elastic region, indicating that the deformation remains recoverable. The material exhibits flexibility and reversible auxetic behavior, consistent with the expected NPR (negative Poisson's ratio) response.

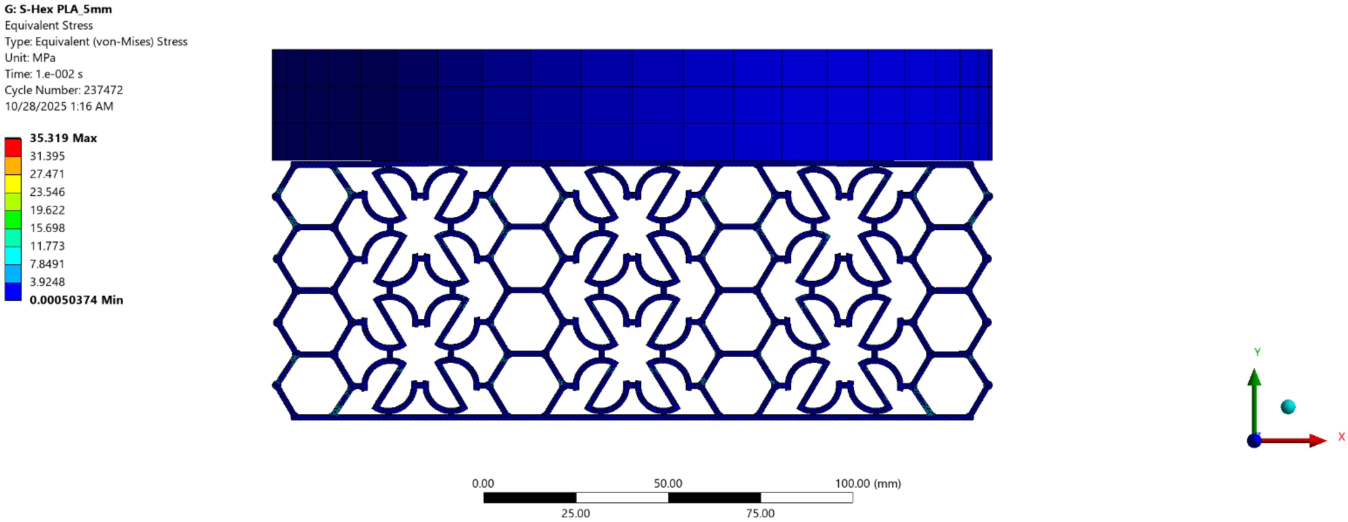


**(a)**

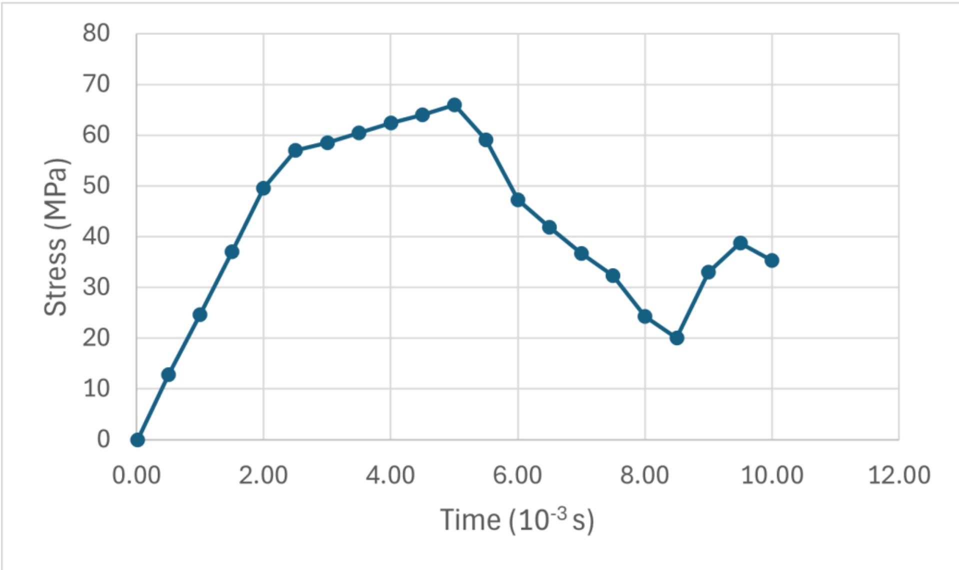


**(b)**

***Figure 42: Hex-S structure with Displacement of 5mm printed with PLA (a) Stress Result, and (b) Stress vs Time Graph***

Based on Figure 42(a), it is seen that at the Hex-S PLA structure at 5mm, a good dimensional stability was achieved although with a slight residual deformation and near to complete recovery after unloading. Considering figure 42(b), the elastic limit is 65.994 MPa at 5 ms after which the stress curve oscillates before revealing the plastic region. This is because such a behavior validates the fact that the material has surpassed its elastic limit, hence resulting in a permanent accumulation of strain and residual stress.

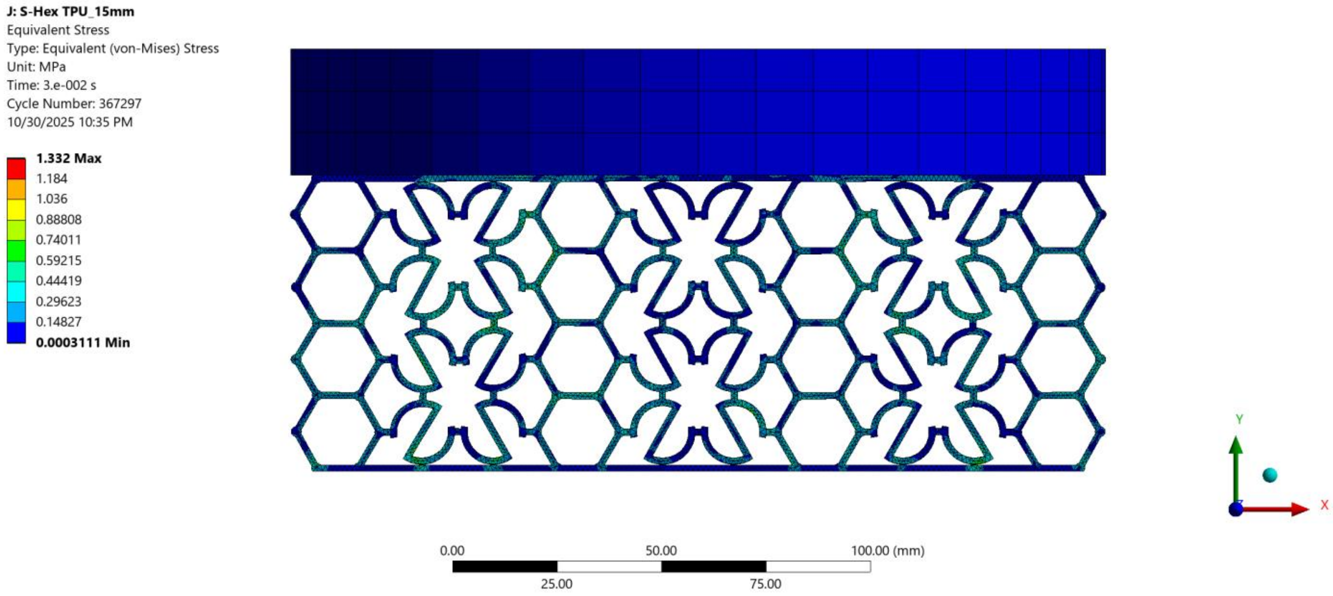


**(a)**

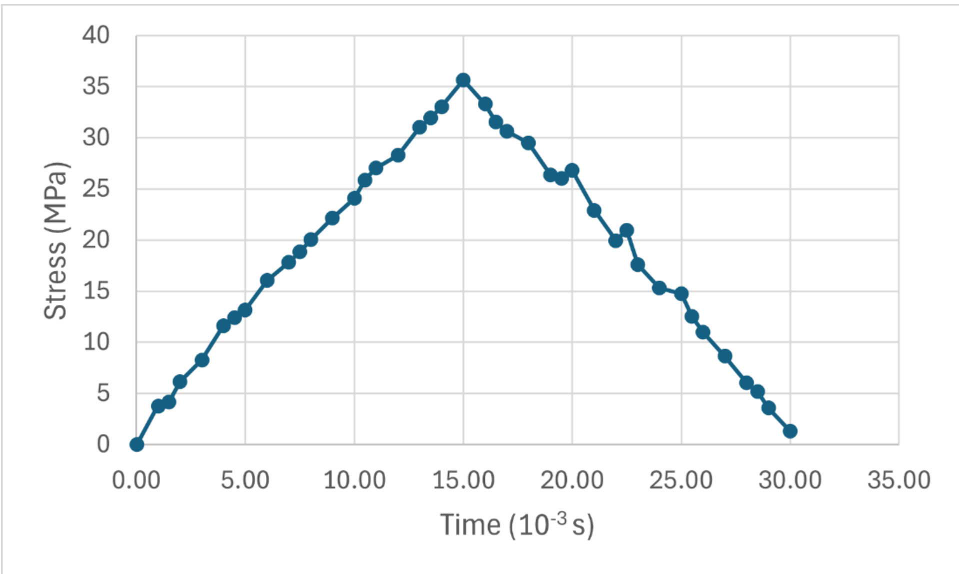


**(b)**

***Figure 43: Hex-S structure with Displacement of 15mm printed with TPU (a) Stress Result, and (b) Stress vs Time Graph***

Figure 43(a) demonstrates that the structure of Hex-S TPU that had been compressed to 15 mm had a smooth deformation behavior and high dimensional stability and returned completely to its original shape once unloaded. According to Fig. 43(b), stress rises with the load and peaks at 35.668 MPa at the time of 15 ms, which is in the elastic range of TPU. The stress decreases to a low value after unloading with slight variations but the material fully recovers which proves that it is an elastic, reversible behavior with high flexibility.

- ***Deformation results:***

***Aux-Hex Structure:***

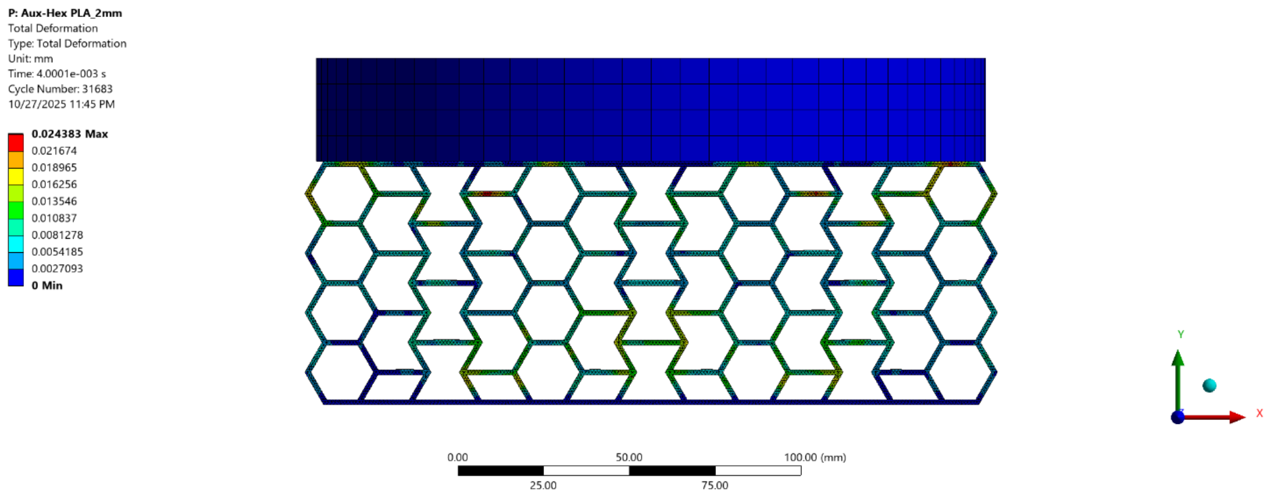


**(a)**

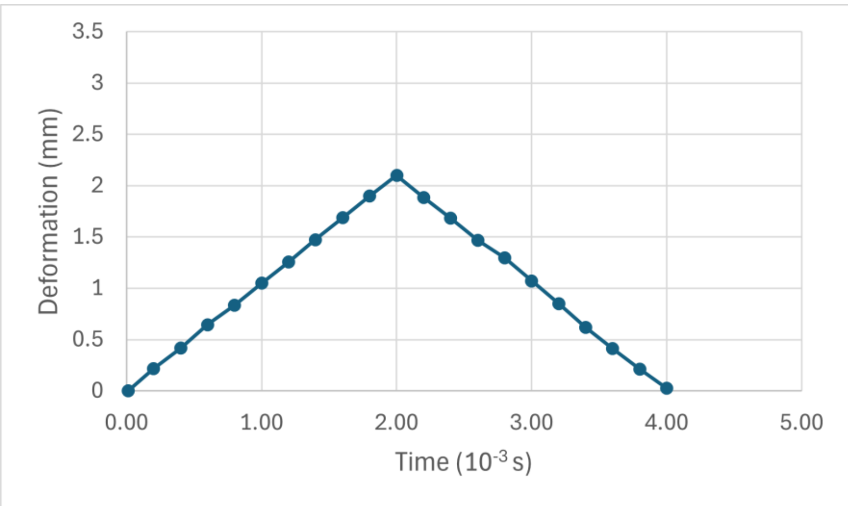


**(b)**

***Figure 44: Aux-Hex structure with Displacement of 2mm printed with PLA (a) Deformation Result, and (b) Deformation vs Time Graph***

Figure 44(a) shows that Aux-Hex PLA sample exhibited completely elastic behavior in that it attained deformation of 2 mm during loading and subsequently on unloading it returned to its original position. Figure 44(b) shows the deformation profile under the cyclic load and that loading stage takes place in the first 2 ms, and the deformation is maximum 2.1004 mm. Then, the unloading stage is commenced, with the structure slowly restoring its shape within the rest of the time period. The shape-resilient quality of the Aux-Hex configuration made of PLA is evident in the entire recovery process back to the original state. This reaction confirms the fact that elastic deformation prevails over plastic deformation when compression is low; hence, the structure is appropriate in the repeated impact absorption during minor loading conditions.

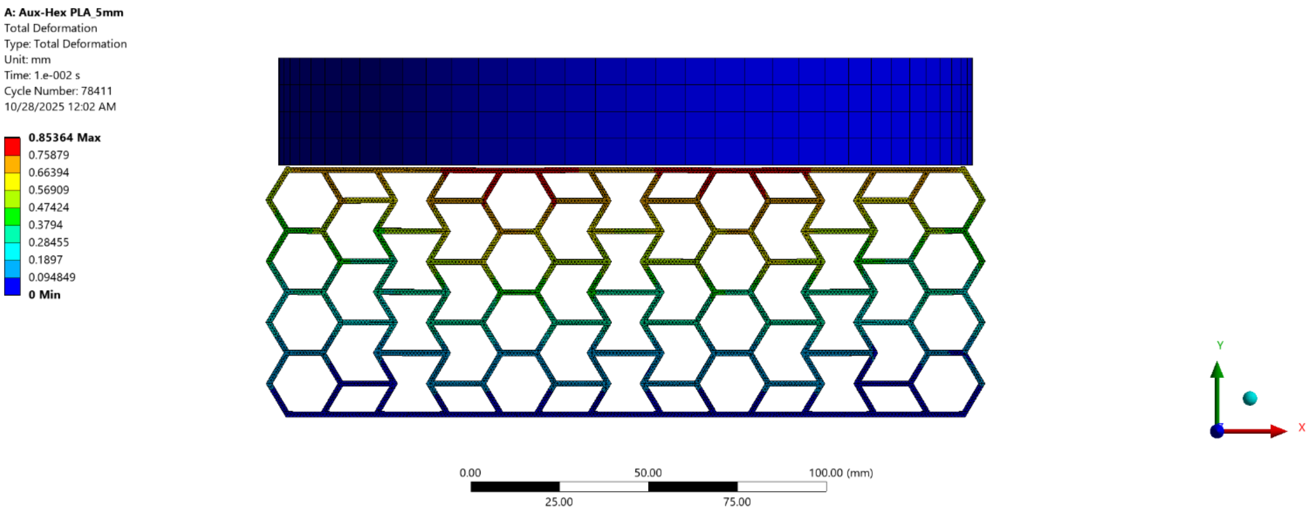


**(a)**

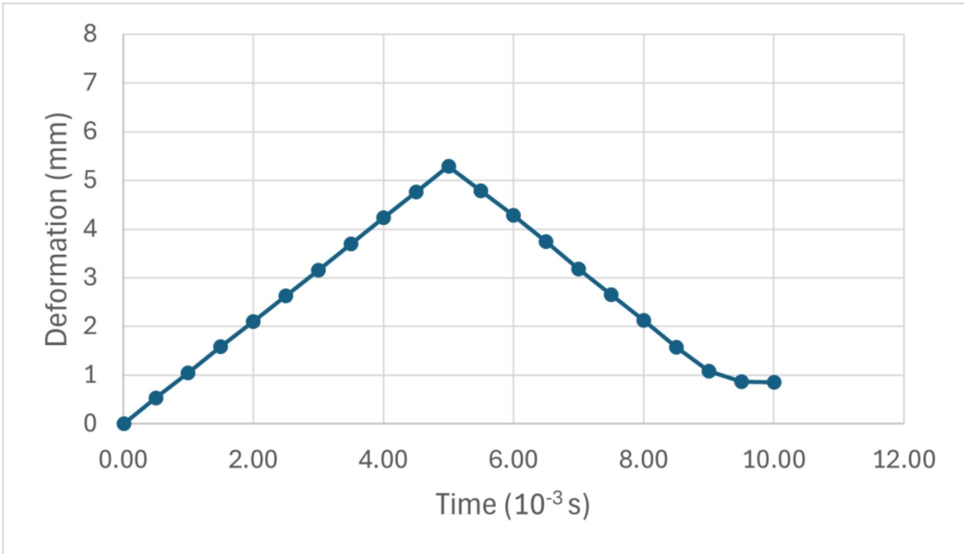


**(b)**

***Figure 45: Aux-Hex structure with Displacement of 5mm printed with PLA (a) Deformation Result, and (b) Deformation vs Time Graph***

Figure 45(a) demonstrates that Aux-Hex PLA structure regained the majority of its original form after 5 mm deformation, but a very tiny permanent displacement was still observed. Fig. 45(b) shows time-dependent response of deformation whereby the displacement keeps on increasing until the maximum deformation of 5.2923 mm is met at 5 ms. The displacement decreases gradually, however, the loading does not go back to the base during unloading. Even with full unloading, a residual deformation of 0.85 mm is still present, which means that partial recovery takes place and plastic deformation processes start. This implies that although the structure has a greater capacity of taking strain energy, the elasticity of the structure is affected as the level of deformation increases.

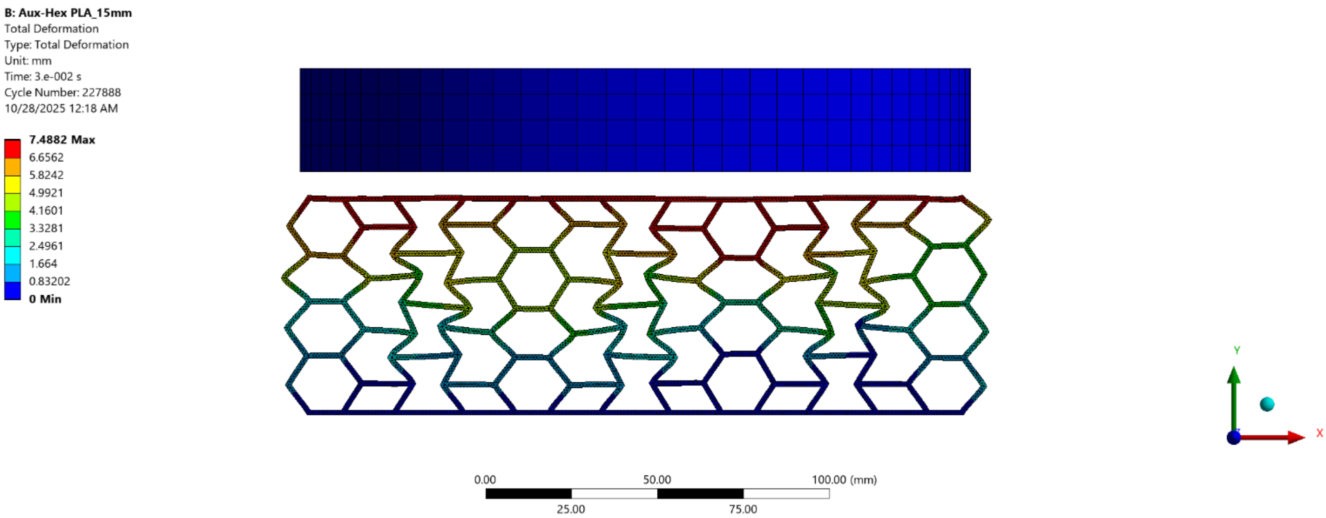


**(a)**

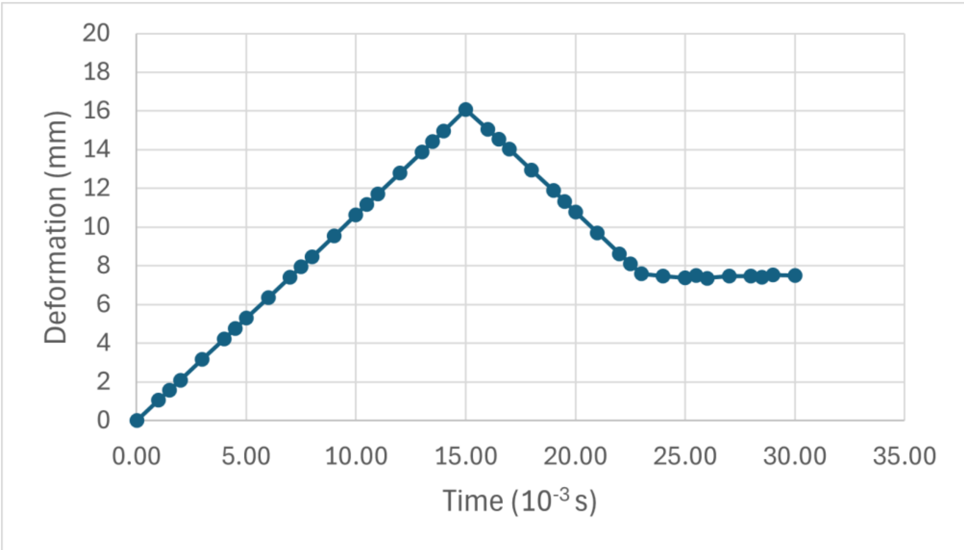


**(b)**

***Figure 46: Aux-Hex structure with Displacement of 15mm printed with PLA (a) Deformation Result, and (b) Deformation vs Time Graph***

Figure 46(a) reveals that the Aux-Hex PLA model could not revert to its undeformed position at 15 mm deformation which caused a large permanent deformation on unloading. Figure 46(b) indicates that the displacement rises steeply to reach 16.067 mm at around 15 ms. Once unloaded, the structure tries to recover but only can get back to 7.488 mm with much permanent deformation. This action is a clear indication that the structure has passed beyond its elastic limit and it has experienced a great amount of plastic collapse.

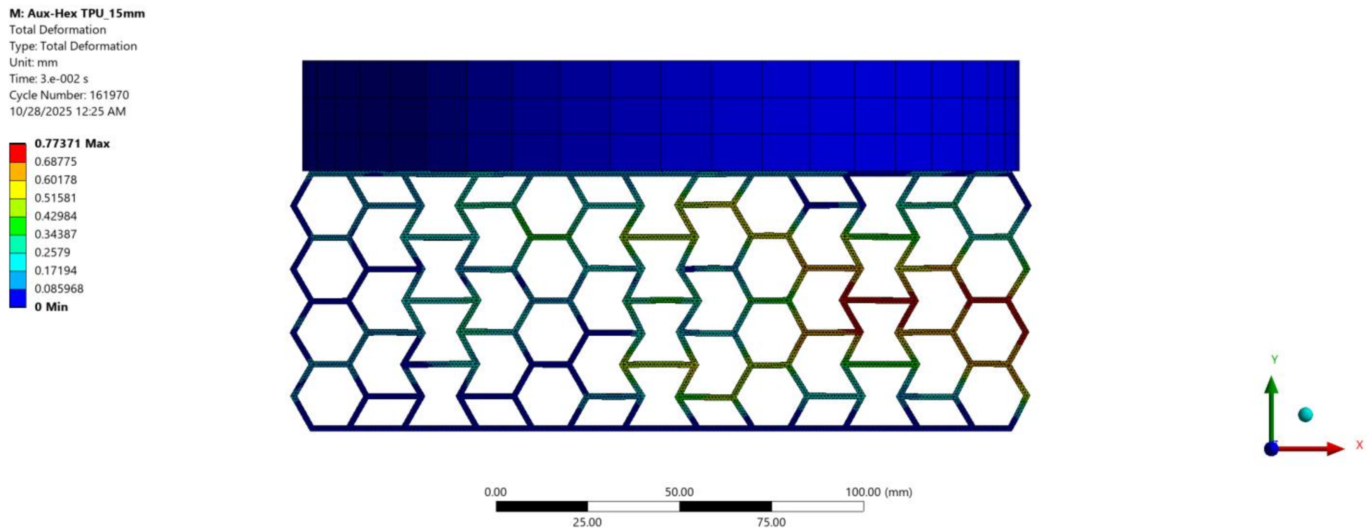


**(a)**

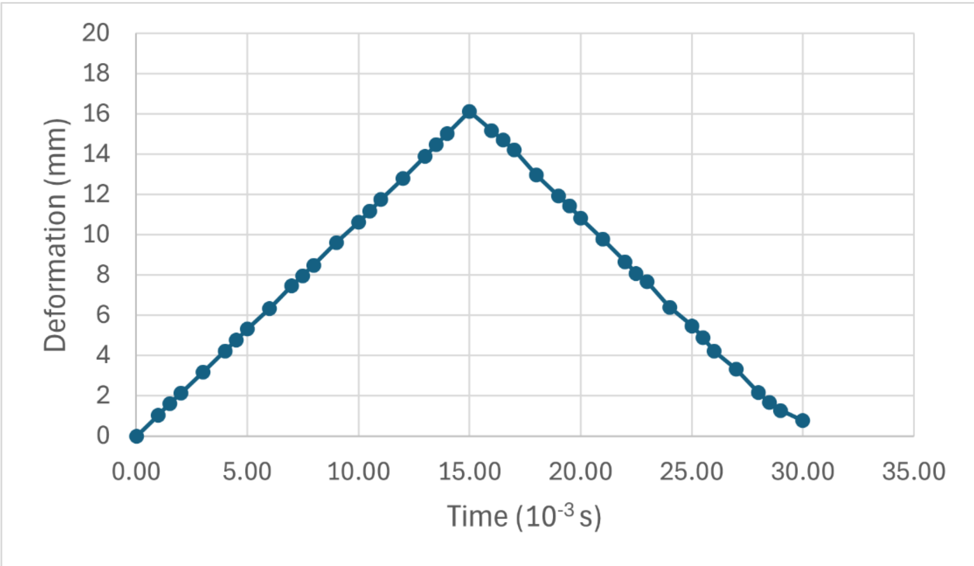


**(b)**

***Figure 47: Aux-Hex structure with Displacement of 15mm printed with TPU (a) Deformation Result, and (b) Deformation vs Time Graph***

Figure 47(a) shows that Aux-Hex TPU structure exhibits smooth deformation and full recovery after loading of 15 mm which is a confirmation of highly elastic response. As shown in figure 47(b), the highest deformation of 15 mm, 16.125 mm is obtained and thereafter the structure gradually restores to zero deformation, thus excellent elastic resilience. There is no deformation at all, which proves that TPU is very flexible and tough.

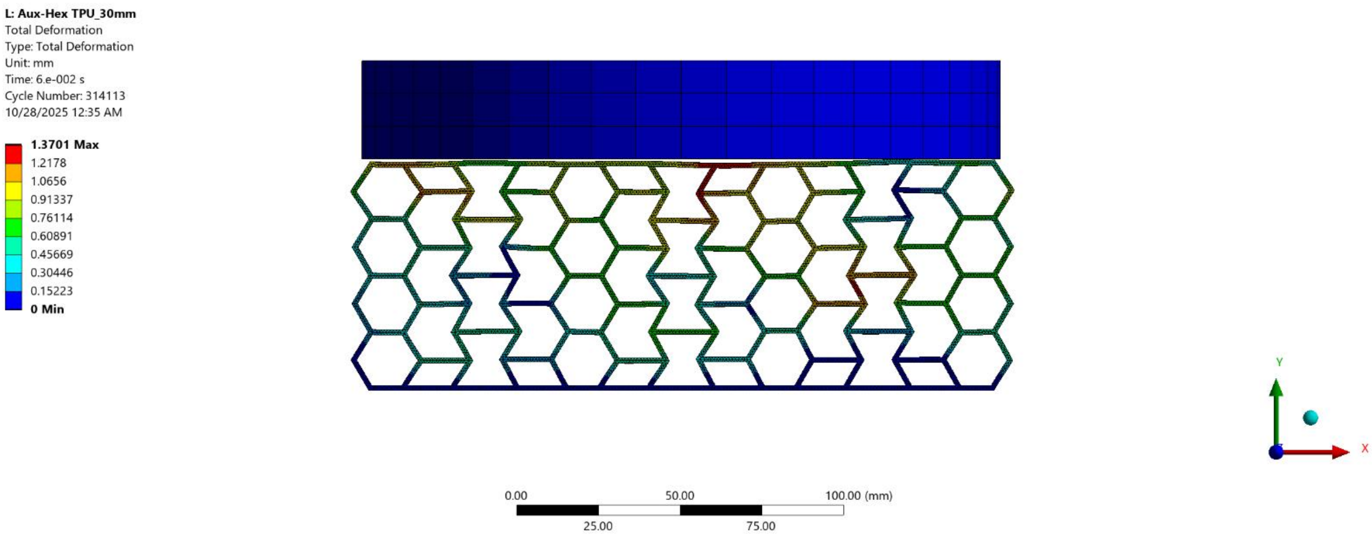


**(a)**

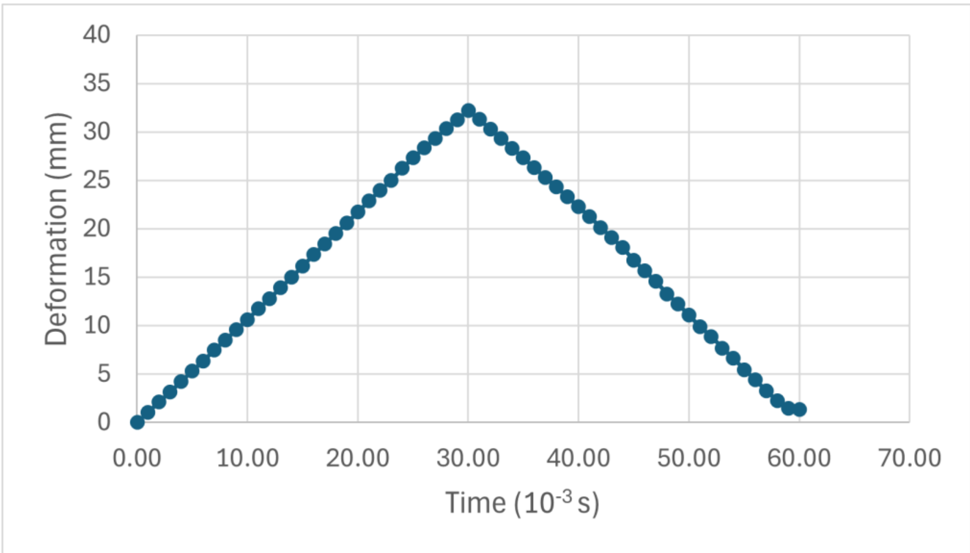


**(b)**

***Figure 48: Aux-Hex structure with Displacement of 30mm printed with TPU (a) Deformation Result, and (b) Deformation vs Time Graph***

According to figure 48(a), the Aux-Hex TPU structure recovered completely even though there was a significant deformation of 30 mm but the recovery was not as smooth as when the deformation was lower. According to figure 48(b), the deformation becomes the greatest, namely 32.244 mm at 30 ms, and then the deformation gradually returns to original position. This puts an important stress on high compressibility, and large strain recovery, both essential in impact mitigation or shock absorption.

***Re-entrant Structure:***

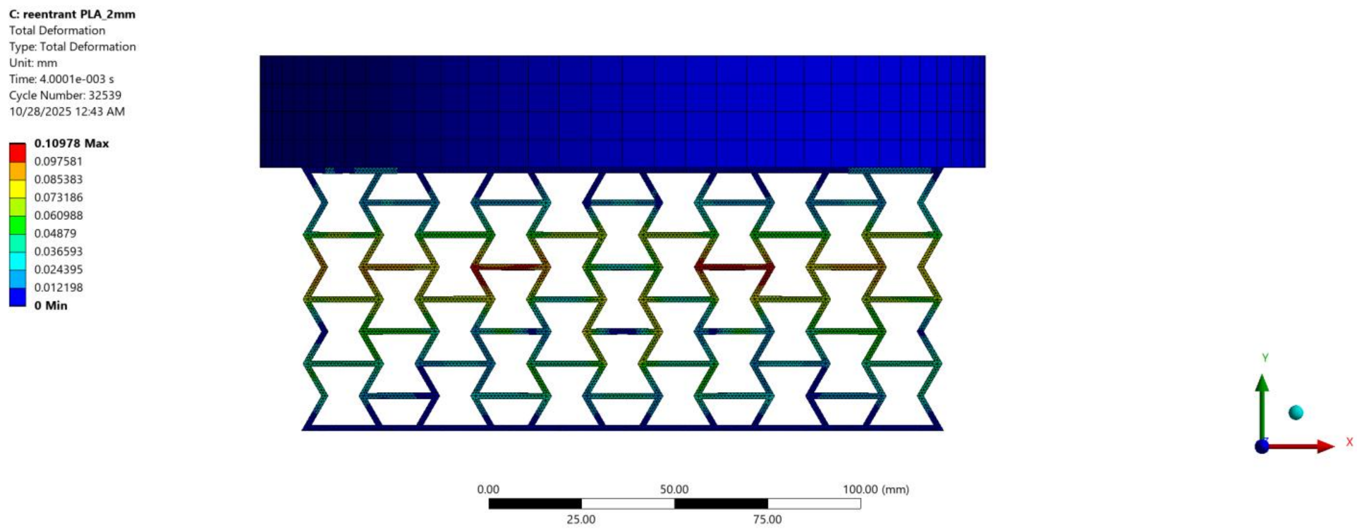


**(a)**

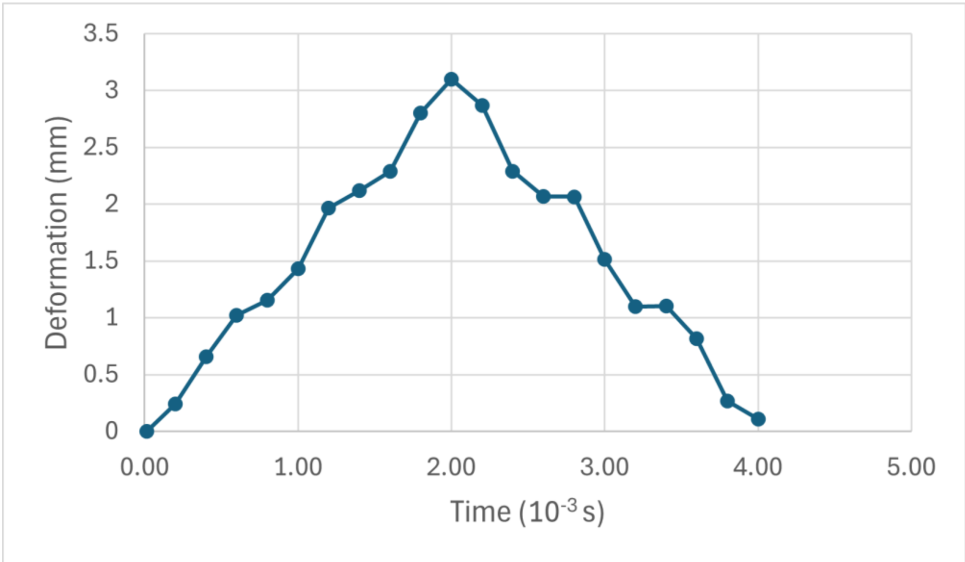


**(b)**

***Figure 49: Re-entrant structure with Displacement of 2mm printed with PLA (a) Deformation Result, and (b) Deformation vs Time Graph***

Figure 49(a) reveals that after 2 mm deformation, the Re-entrant PLA structure returned to its original form indicating the elastic case of deformation. Figure 49(b) indicates that the deformation is slowly growing peaking to a maximum displacement of 3.0974 mm at approximately 2 ms. Once unloaded, the structure rebounds into something like its original shape meaning the deformation is more of the elastic nature. A little residual deformation is seen and it has very little plasticity at the required load.

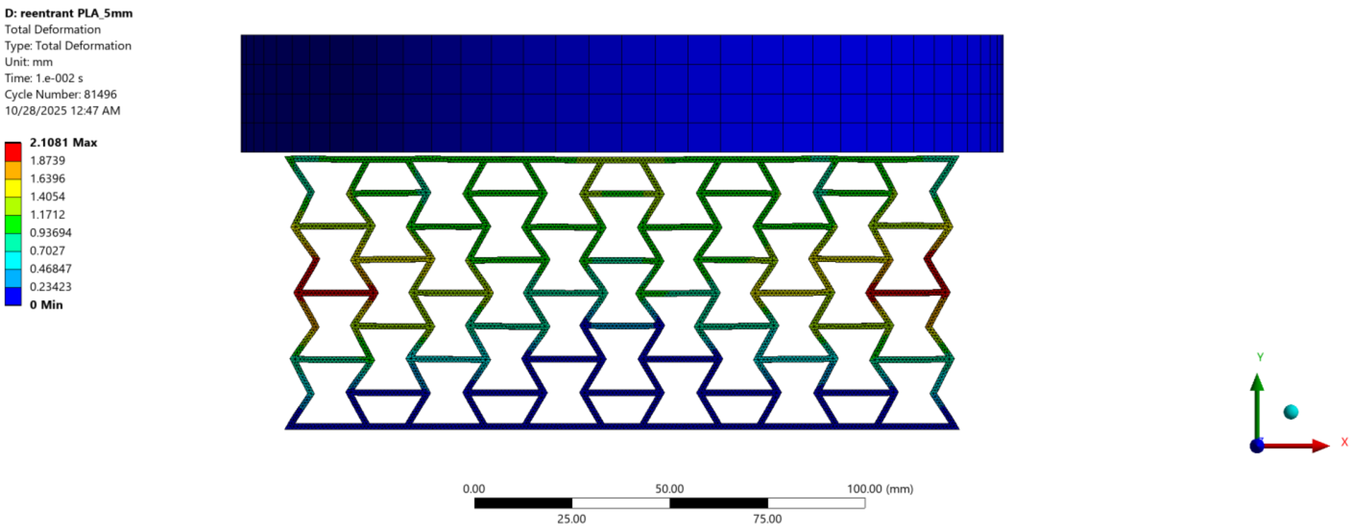


**(a)**

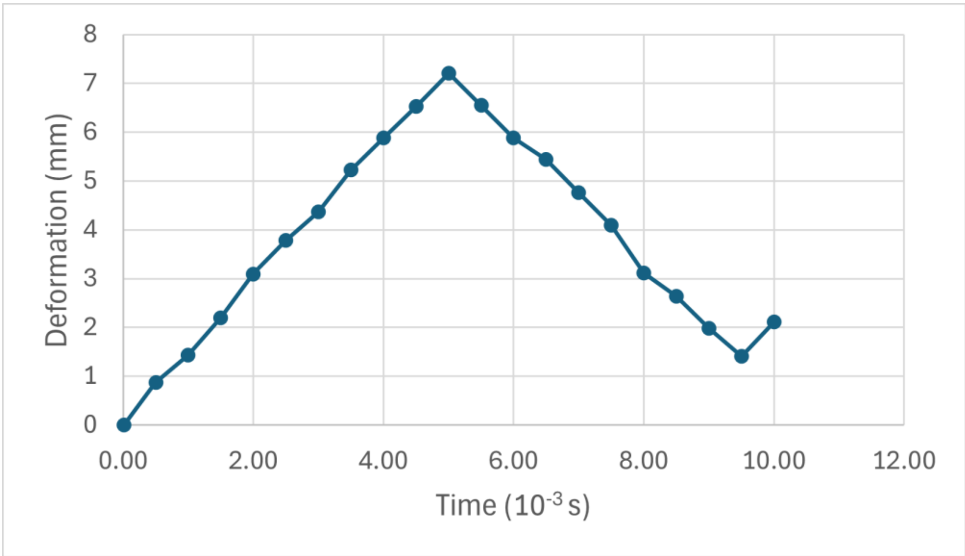


**(b)**

***Figure 50: Re-entrant structure with Displacement of 5mm printed with PLA (a) Deformation Result, and (b) Deformation vs Time Graph***

As illustrated in Figure 50(a), in Re-entrant PLA sample, residual displacement after the unloading at 5 mm is slight with slight plasticity indicating partial elastic recovery. As shown in Figure 50 (b) the peak deformation is approximately 7.212 mm at 5 ms. Upon unloading, the sample exhibits some remnant deformation of approximately 1.40 mm which in turn rises gradually, exhibiting permanent set in the structure after compression.

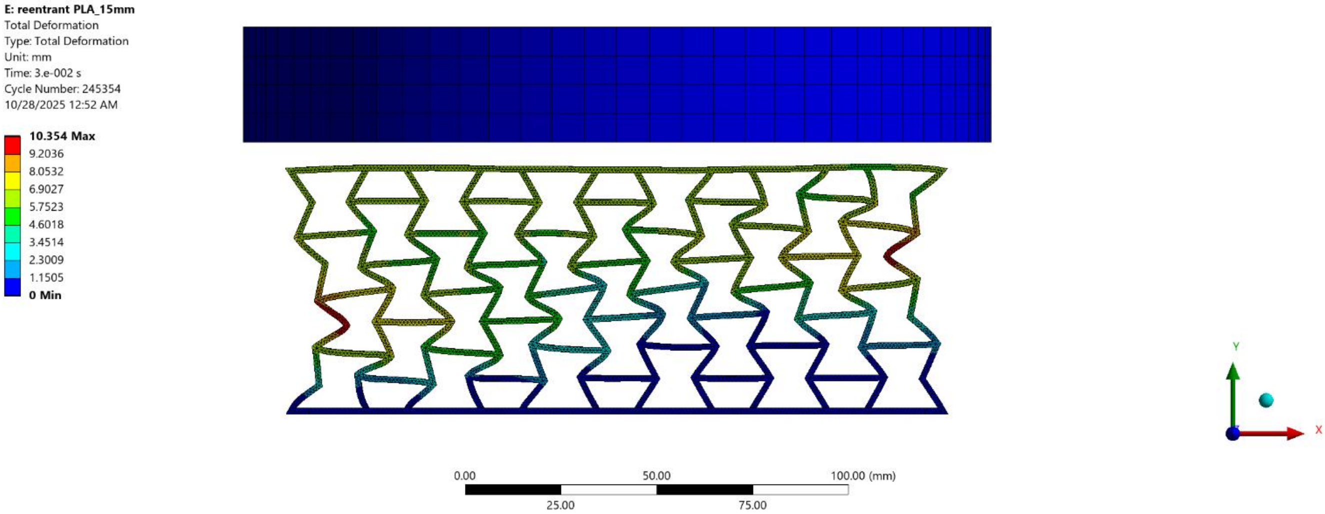


**(a)**

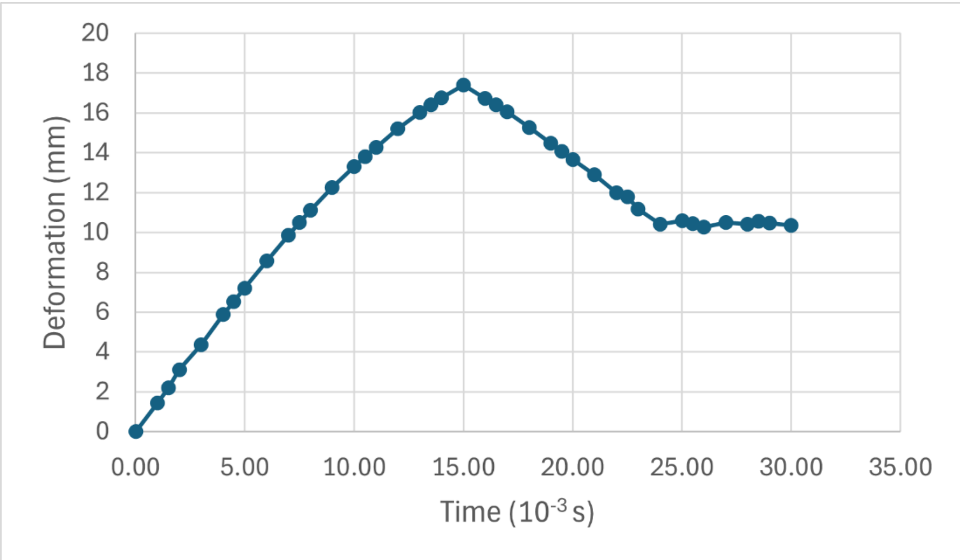


**(b)**

***Figure 51: Re-entrant structure with Displacement of 15mm printed with PLA (a) Deformation Result, and (b) Deformation vs Time Graph***

It was found that at 15 mm in deformation position, the Re-entrant PLA structure had a permanent deformation, which was found to have a lot of plastic damage (Figure 51(a). It is possible to determine that at approximately 15 ms, the highest deformation is 17.402 mm, as in figure 51(b). In unloading, the structure comes back partially to approximately 10.1 mm deformation at 24 ms then it experiences permanent deformation because of an irreversible strain of plasticity.

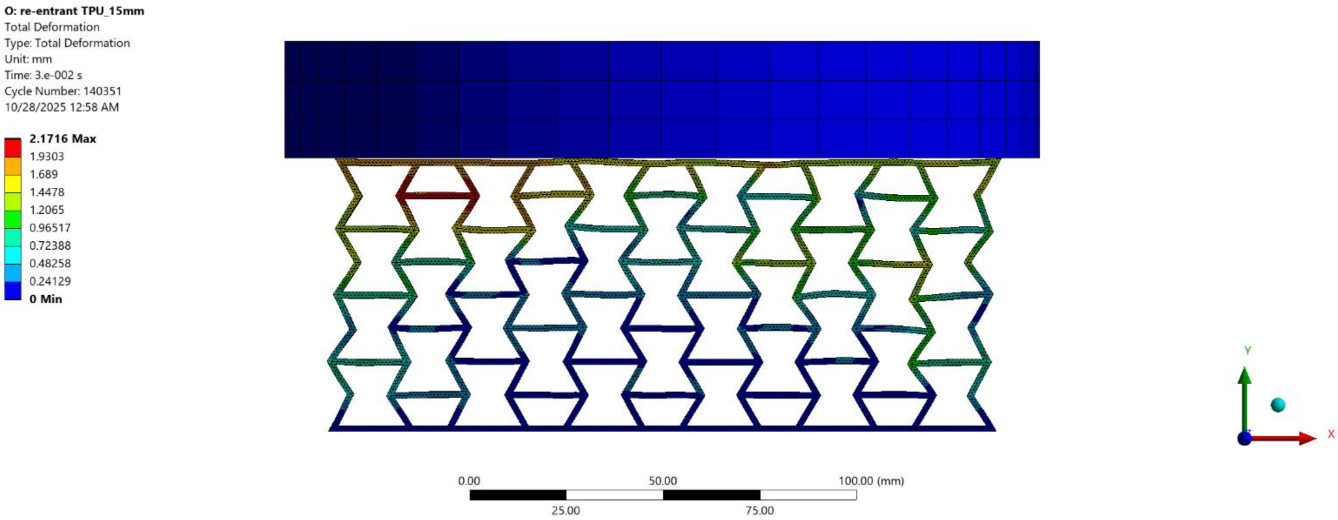


**(a)**

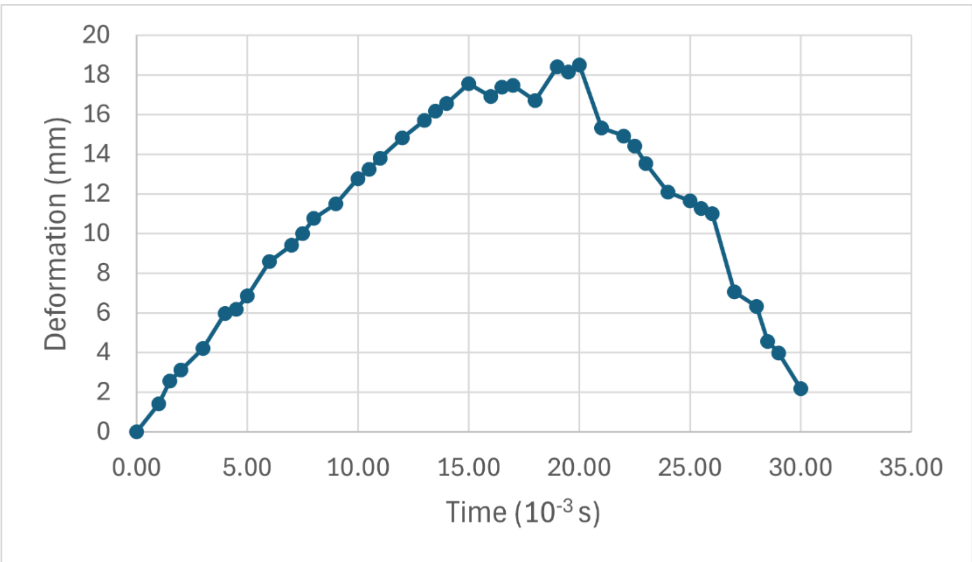


**(b)**

***Figure 52: Re-entrant structure with Displacement of 15mm printed with TPU (a) Deformation Result, and (b) Deformation vs Time Graph***

The Re-entrant TPU sample of less than 15 mm deformation recovered without any residual displacement, which indicates the sample was entirely elastic (shown in Figure 52(a). According to Figure 52(b), in the process of loading (to 15 ms), the deformation attains about 17.59 mm. However, the maximum deformation was 18.511 mm at 20 ms. The compressive strength is not dimensionally stable and the structure fully recovers after unloading, which is indicative of the high recoverability of TPU.

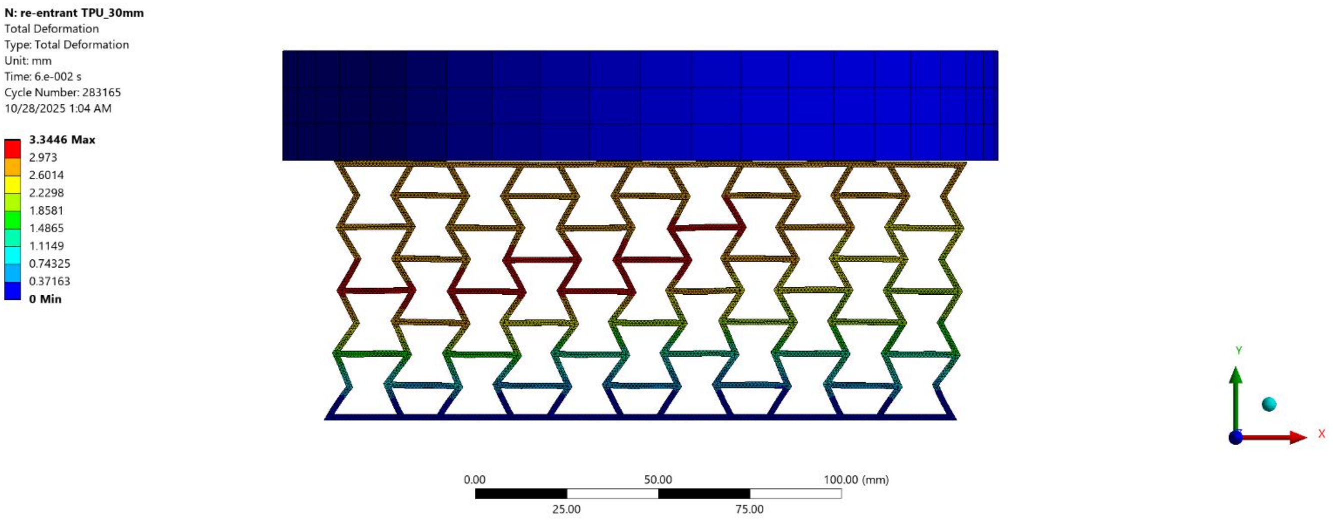


**(a)**

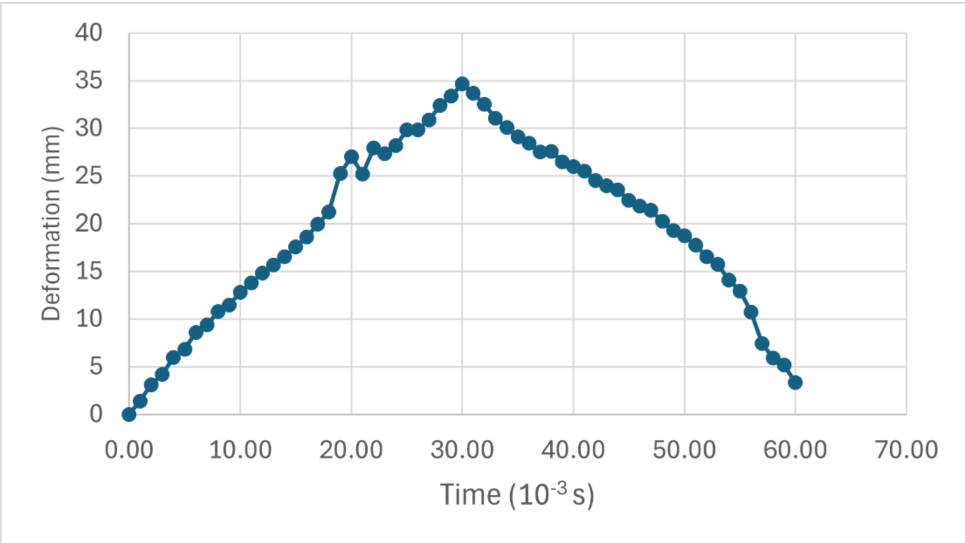


**(a)**

***Figure 53: Re-entrant structure with Displacement of 30mm printed with TPU (a) Deformation Result, and (b) Deformation vs Time Graph***

Figure 53(a) indicates full recovery after 30 mm deformation, although the deformation–recovery curve displays slightly less smooth behavior compared to lower displacement Figure 53(b) depicts that the deformation rises steadily, reaching 34.703 mm at 30 ms, followed by complete recovery, confirming high elastic strain capacity and flexibility.

***Hex-S Structure:***

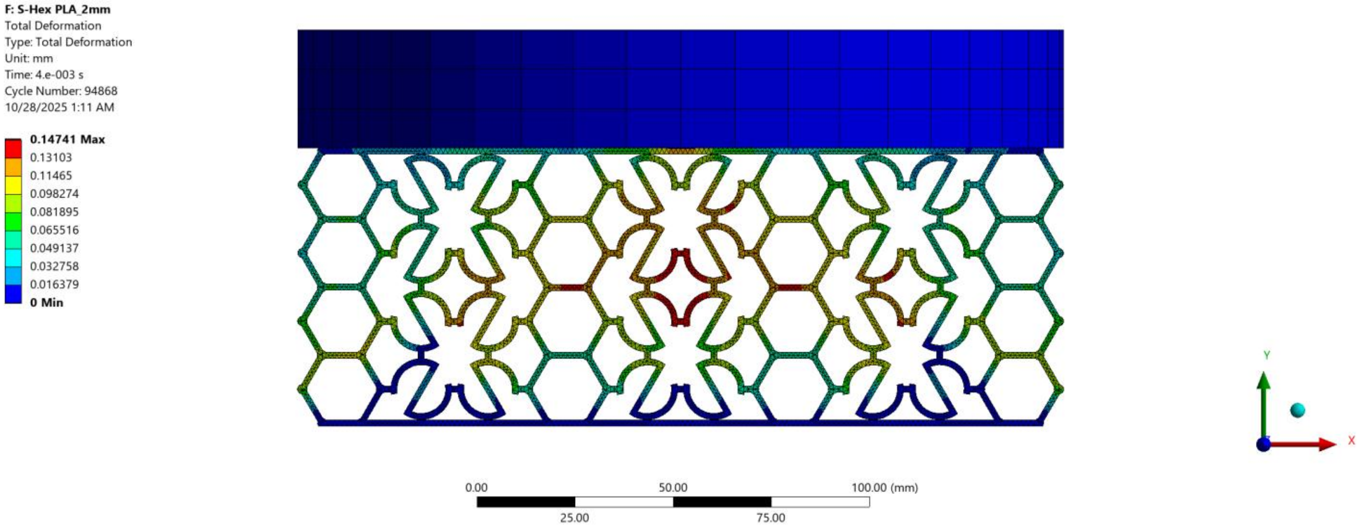


**(a)**

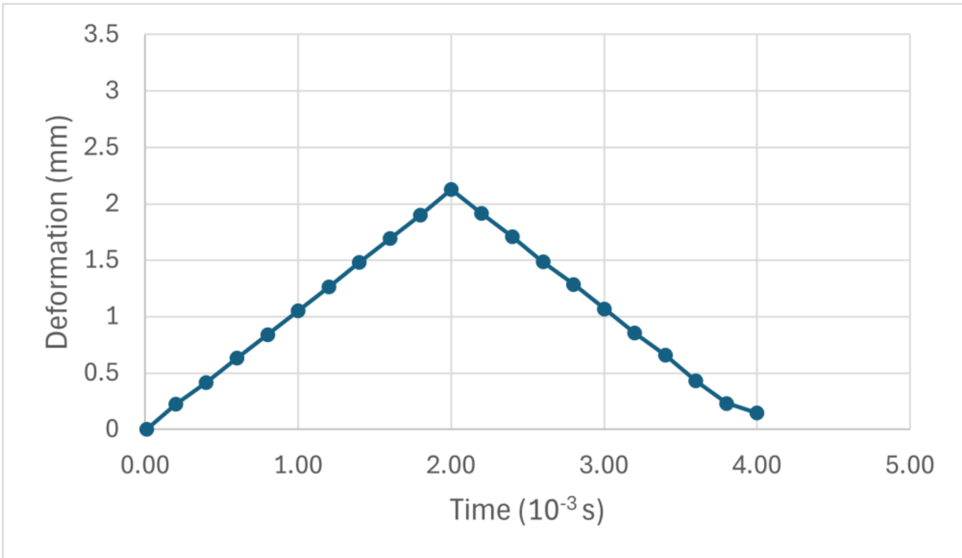


**(b)**

***Figure 54: Hex-S structure with Displacement of 2mm printed with PLA (a) Deformation Result, and (b) Deformation vs Time Graph***

Figure 54(a) shows that, in a Hex-S PLA structure with 2 mm deformation there was the full recovery of the structure that was not in the elastic limit. Figure 54(b) indicates that the peak deformation is approximately 2.1251 mm at approximately 2 ms. In unloading the structure is returned to its original form with a smooth process with a high elastic resilience with no or very minimal permanent deformation.

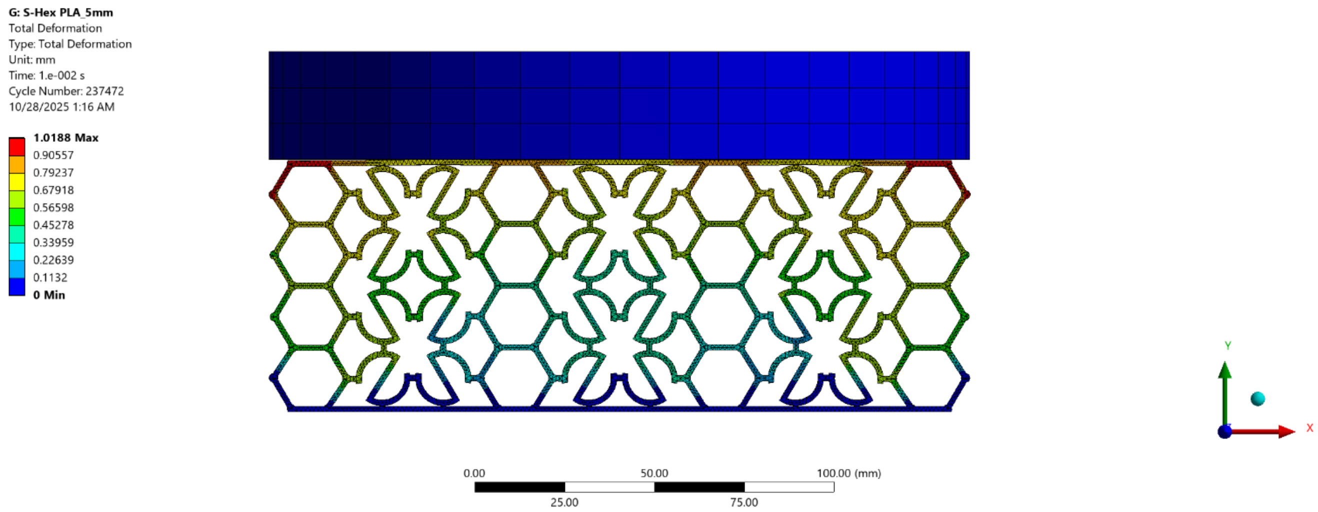


**(a)**

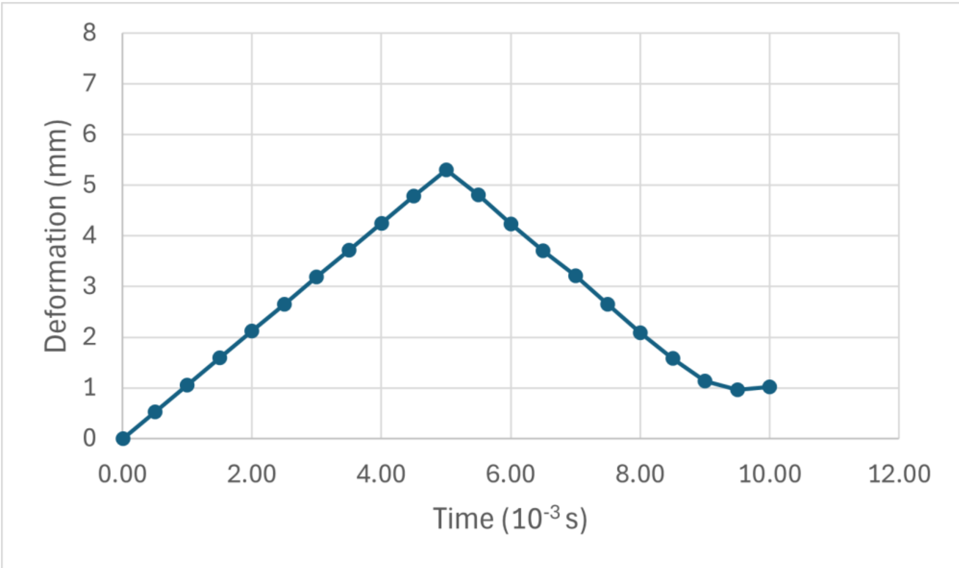


**(b)**

***Figure 55: Hex-S structure with Displacement of 5mm printed with PLA (a) Deformation Result, and (b) Deformation vs Time Graph***

Figure 55(a) indicates that the Hex-S PLA structure at 5 mm deformation at the maintaining the dimensional stability with a minor residual displacement on unloading. As shown in figure 55(b), the highest deformation lies approximately at 5 ms at a level of 5.3 mm. Upon unloading, the structure is partially restored to the range of 1 mm, after which it permanently deforms which is again slowly increasing with time-span- this is the loss of elastic recovery and dimension stability.

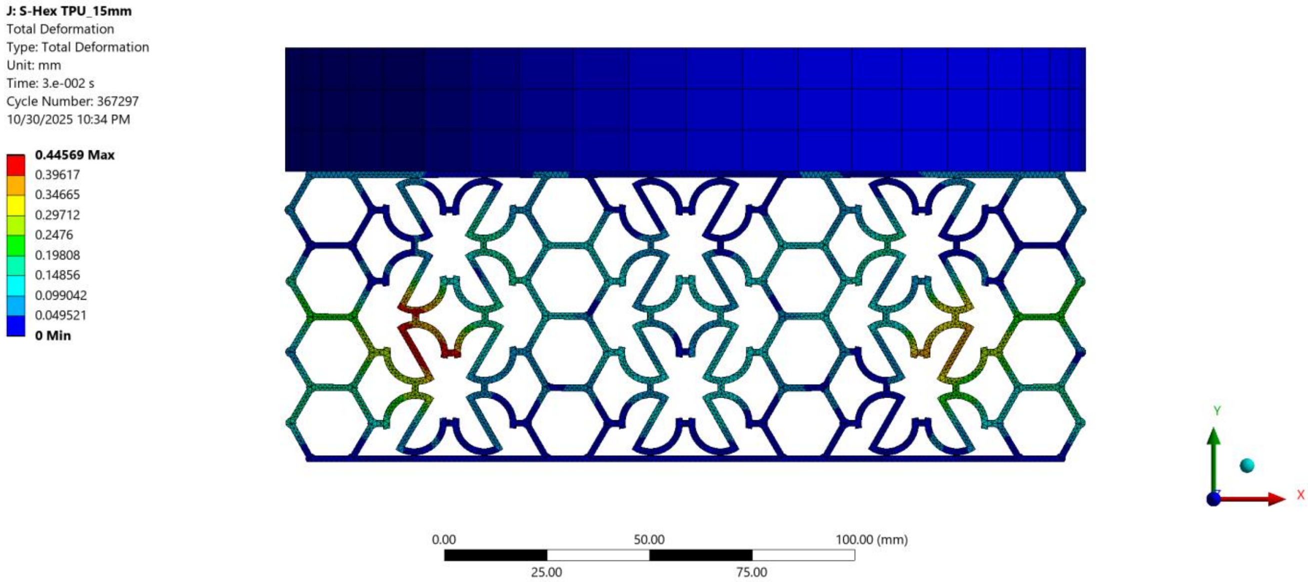


**(a)**

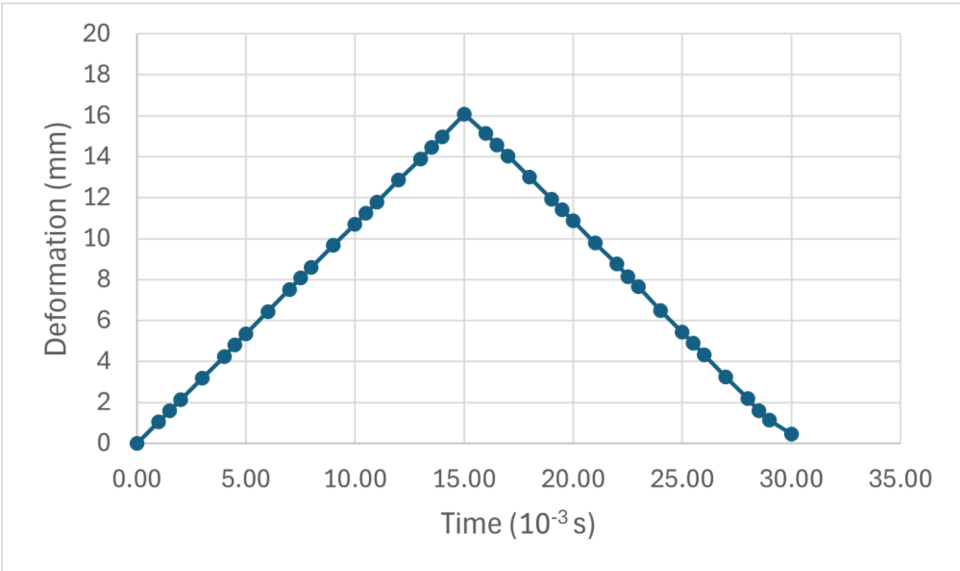


**(b)**

***Figure 56: Hex-S structure with Displacement of 15mm printed with TPU (a) Deformation Result, and (b) Deformation vs Time Graph***

The Hex-S TPU model was also able to recover its original geometry following 15 mm deformation with smooth and complete elastic recovery as shown in Figure 56(a). Figure 56(b) shows that the deformation increases gradually to the highest point of approximately 16.075 mm at 15 ms. Once unloaded, the S-Hex moves well to zero with no permanent set observable at all, indicating it is well behaved in its dimensional behavior under the compressive load applied.

## 7.2 Experimental results

### 7.2.1 Load vs Displacement Results Comparison

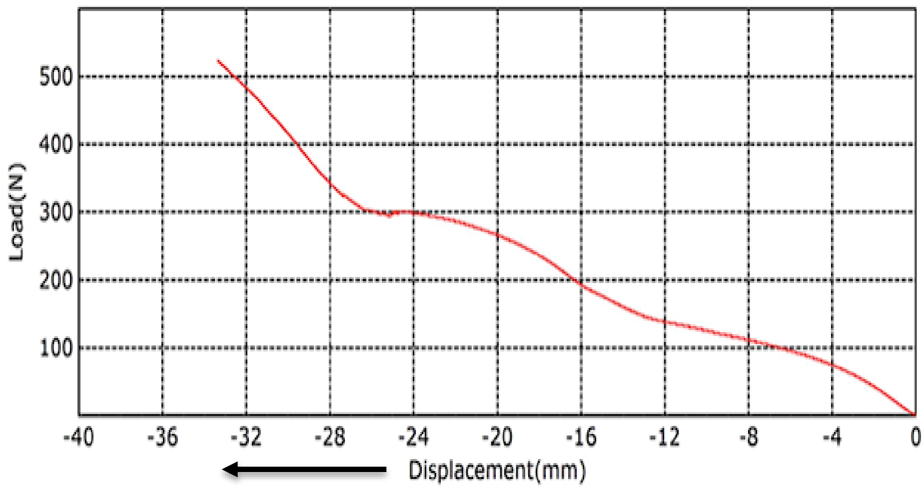


**(a)**

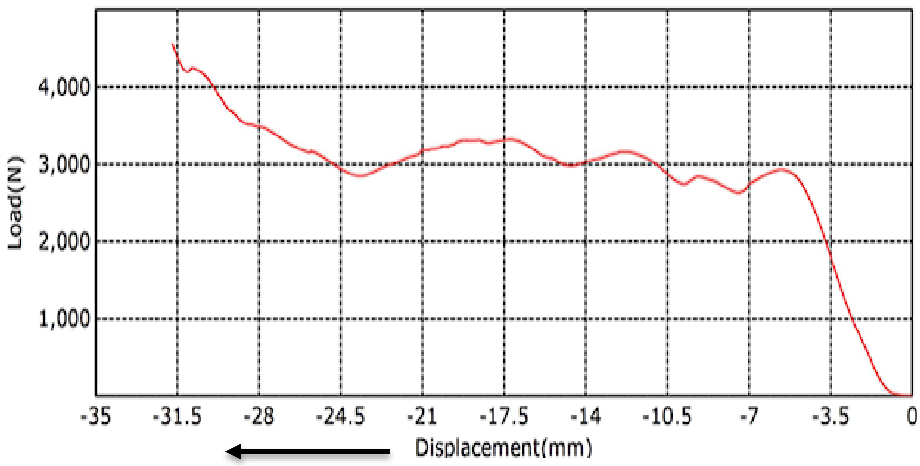


**(b)**

***Figure 57: Experimental results of Hex-S structure printed with (a)TPU and (b)PLA***

The load vs displacement curves of TPU and PLA auxetic structures give us the necessary information on the compressive behavior of structures under dynamic loading conditions. Among the curves that we obtain with most common compressive tests, which document the response to rising strain and its load bearing capacity in addition to load vs displacement performance. We have therefore compared TPU to PLA, by making an actual comparison 2 in terms of energy dissipation, deformation behavior and dimensional stability, using the experimental load-displacement curves of the two materials. The findings that will be provided below are the loading curves. These results do not have any unloading curves since when a structure is unloaded during the experiment it cannot be pulled back through experimental setup.

### 7.2.1.1 TPU Load vs Displacement Results

In the same loading condition, the TPU (Thermoplastic Polyurethane) hybrid Hex-S construction is figure 57(a). It is approximately 30 mm long with a maximum load of about 400N. The TPU sample shows a smooth reduction in load with increase in displacement in contrast to PLA. It would appear to be highly flexible and ductile at no stage of its progression rising to sharp peaks of amplitude oscillation. It is always pleasing to have no sudden breaks of any kind. Strain is progressive since supply is gradually rising on energy. In the event that the TPU breaks, a lot of work would be written off as a waste. Material instead takes the strain differently and these deformations may be described as bending and stretching a microcell wall.

### 7.2.1.2 PLA Load vs Displacement Results

The behavior of the hybrid Hex-S structure constructed using the PLA (Polylactic Acid) material is illustrated in figure 57b when compressing of the structure takes place. This was done by compressing the sample to a compressive stroke of approximately 30 mm with a strain rate of 1 mm/min, with the highest load of the sample being approximately 4000 N. Initially, the curve is steeply increasing in load as the displacement increases. This indicates the elastic zone where the PLA structure is not easily deformed since it is highly rigid. Compression goes on up to a peak of approximately 4000 N. Thereafter, it gradually descends in a series of steps forming a number of local highs and lows. This slow reduction indicates that the walls of the cells make up of the hybrid structure are buckling and the layers are falling down. The use of auxetic and regular hexagonal patterns allows the localized deformation to occur and at the same time has the ability to support a certain weight. The gradual slope beyond the peak indicates that it is a process of structural deformation and propagation of fractures that absorb energy, rather than a brittle failure that takes place suddenly. The compressive strength and stiffness of the structure is somewhat high, and the PLA based structure is good as a load bearer and tough structure in the cases of load bearing and energy absorbing such as protective armor or panels.

### 7.2.1.3 Comparison Between PLA and TPU Structures

The PLA hybrid hexagonal structure also had a superb compressive loading performance as can be seen reaching a high load of approximately 4,000 N. The load displacement curve registered a steep increase after which step decline began gradually. This means that when the material experienced strain it was bending and failing at intervals. This works by the fact that PLA is durable but fractures when overstrained. Comparatively, the TPU framework attained a reduced peak load of approximately 400 N and experienced a smooth, gradual load failure- i.e. it was extremely supple (i.e. able to be stretched to a thin sheet without breaking), ductile (i.e. able to be forced to stretch thin without disintegration). TPU was then able to continuously change its shape by an elastic viscoelastic deformation without rupture or disintegration and thus, retain the same volume size. So TPU is better in energy absorption and cushioning. On the one hand, the

PLA makes a structure stronger; on the other hand, TPU (a silicone rubber) gives a construction elasticity and the capacity to disperse the energy. The combination of these two attributes in a single hybrid structure between them is better than any structure that is based on a single component.

### 7.2.2 Stress-Strain results Comparison

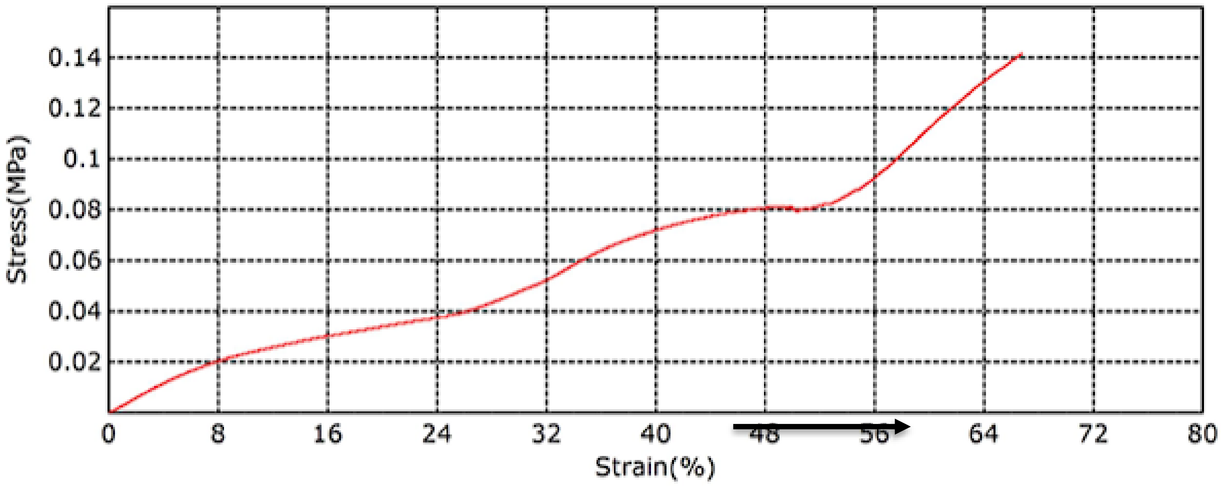


**(a)**

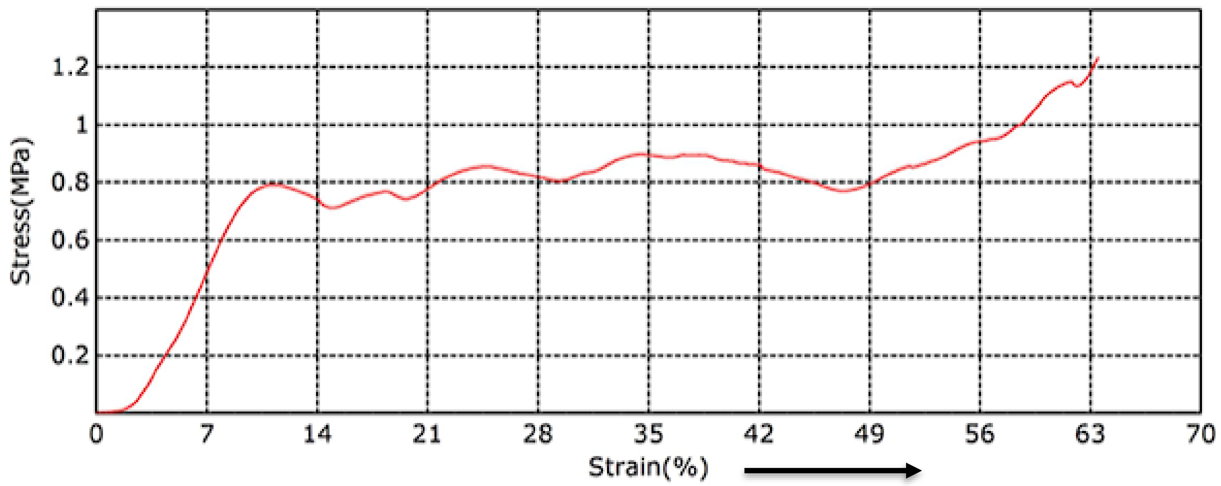


**(b)**

***Figure 58: Stress-Strain graphs for 30mm displacement of – (a) TPU (b) PLA***

### 7.2.2.1 TPU Stress-Strain Behavior

The stress strain curve of TPU specimen has been depicted in Figure 58(a). It has a monotonically growing stress through all the compression regime and no apparent yield point. However, since TPU does not have a yield point, it does not permanently deform plastics but rather deforms in an elastic or viscoelastic fashion, and will regain its shape after a load has been taken away. The gradual slope of the curve until about 60% strain proves the nonlinear elastic tendencies of the soft polymer to deform. This then enables the molecular chains to reorient and extend without breaking. A steeper slope happens at greater than 60% strain and the strain grows even higher to approximately 0.14 MPa with a stretch of 70-75%. Here is where the material becomes dense enough and it will not compress anymore. TPU is flexible material and energy absorbing because it is not permanent in form and is highly rebound material. It is this property that makes it a possible choice of flexible (e.g., damping/cushioning) layer in hybrid auxetic structures that demand strength and flexibility.

### 7.2.2.2 PLA Stress-Strain Behavior

Figure 58(b) indicates the Compressive stress vs strain curves of PLA (Hybrid Hexagonal S-Structure-Auxetic + Conventional) The compressive stress/strain curve of the hybrid case has a clear nonlinear nature, and the fact implies that the structure will be able to deform plastically after it has elastically deformed during loading. The curve rises almost linearly at least up to a strain of approximately 10% where the yield stress is ca. This region is referred to as elastic where all the deformation can be regained upon unloading. Beyond the yield point, the stress started to gradually decrease with several wavy shapes and was explained by consecutive retracing local buckling and collapse of internal cell wall of hybrid structure. These differences demonstrate the ranking of energy absorption mechanisms as plastics of material are deformed. These undulating wave patterns show how the structure permanently deforms and this is attributed to the interaction effect of brittle- plastic property of polymer and collapsible failure of thin-wall under compression. Increasing the values of strains (where the value exceeds the critical point of 55%) the stress increases again in a significant way, up to approximately 1.2 MPa at 65% strain. The final abrupt increase is the densification regime, in which the structure is very dense and does not desire to collapse anymore. It is this phase that can explain why the energy absorption efficiency of the hybrid structured foam based on PLA under load condition can be so good.

### 7.2.2.3 Comparative Discussion

Table 5 presents the mechanical properties of PLA and TPU that are quite different. Other than this, the PLA is slightly higher density (1.24 g/cm3 in the case of PLA and 1.22 g/cm3 in the case of TPU), where more of the solid material is demonstrated in the printing structure. Young modulus of PLA (1.9 GPa) is ten times higher than the TPU (0.2 GPa) and this shows that PLA is much more rigid and resistant to elastic deformation. Otherwise, PLA has a lower Poisson ratio (0.36) than TPU (0.45) which implies that it can experience greater lateral expansion with the presence of axial load a property of increased flexibility and ductility. With regard to the yield stress, the PLA has a higher yield stress of 56.3 MPa than TPU (40.5 MPa), indicating that PLA can better withstand the onset of plastic deformation. However, this toughness of PLA is its most serious defect as well, because it is not very ductile either, whereas small modulus and yield strength in TPU have been compensated by the amazing flexibility of it and its total strain recoverability. This difference is also supported by the values of the tangent modulus, as PLA has a significantly higher tangent modulus (200 MPa) than TPU (4.8 MPa), which also means that it is stiffer and less recoverable. Overall, PLA can offer strength, rigidity and dimensional stability, TPU elasticity, resiliency and who rebound. When integrated into a hybrid auxetic-conventional structure (i.e., as, in this study, manufactured) the two materials cooperate to create a hybrid structure that is highly energy-absorbing and, at the same time, mechanically stable together with having a high deformation recovery - which is exactly the proper blend to use in multifunctional, impact-resistant applications.

## 7.3 Comparison of Different Structures Printed with PLA for Different Displacements

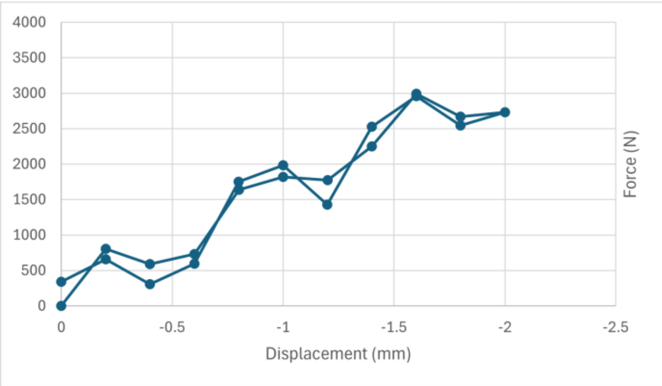


**(a)**

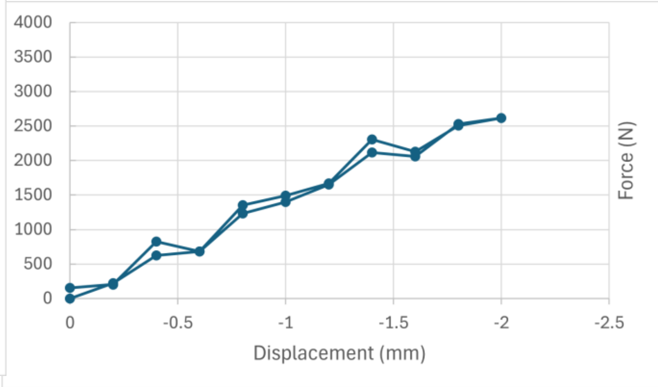


**(b)**

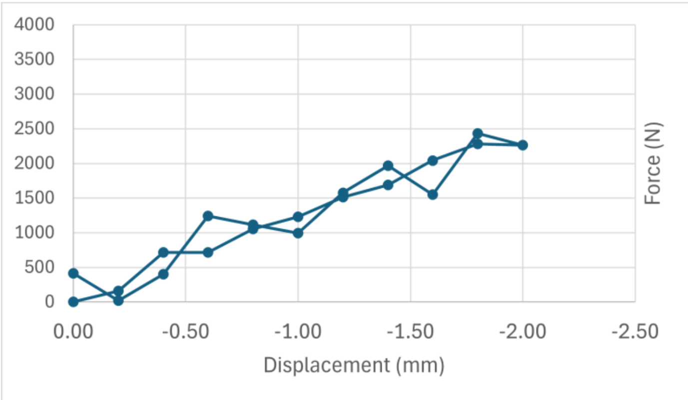


**(c)**

***Figure 59: Force vs Displacement Graph of 2mm Strain rate for (a)Re-entrant (b) Aux-Hex (c) Hex-S***

Fig. 59(a) depicts The Re-entrant with the 2mm displacement, indicating that the force displacement curve at such a displacement is higher the more the compression has taken place. The maximum force is extremely low and it is 2992.8N and the reason could be reduced deformation. This has a flaw in that the upper value of the force is followed by a progressive reduction, and has been gradually losing. It has been shown that due to the effect of auxetic effect (negative Poisson ratio) the structure is flexible in compression, but once it reaches the maximum force decreases steadily, this means that the material is in irreversible deformation. There is a similarity in the hexagonal structure (Aux-Hex) at 2 mm at 2 mm displacement in Figure 59(b) when compared to earlier results that there was a higher load carried as its peak Force is approximately 2614 N that is better than re-entry structure and being smooth as a response even when compressed. Nevertheless, the Hex-S structure at 2mm movement, behaves in a similar manner and exhibits plastic deformation beyond the peak force such that even in this design no full recovery was achieved after unloading. Figure 59(c) shows that with a 2mm displacement smoothness of the force-displacement curve is enhanced with the Hex-S structure. It has a higher load-carrying capacity (the peak force is 2433.1 N) which is lower than Aux-Hex and re-entrant structure and also the deformation appears more homogenous than the deformation of both Re-entrant and Aux-Hex structure. This force increases up to the peak, and then declines slowly, which also reveals an outstanding energy capturing capacity in deformation.

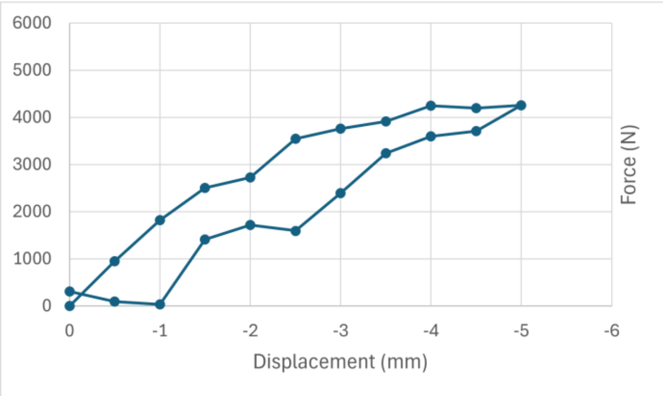


**(a)**

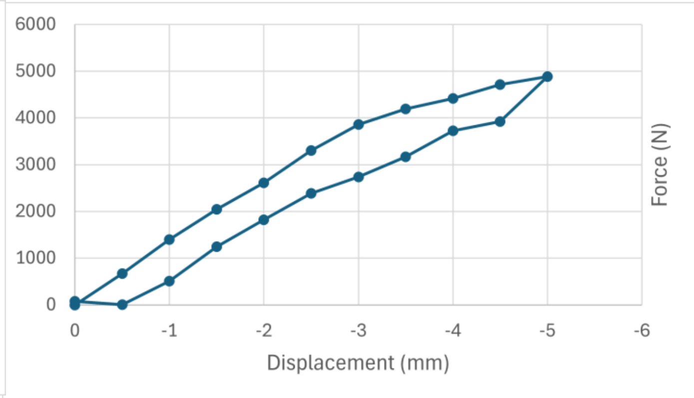


**(b)**

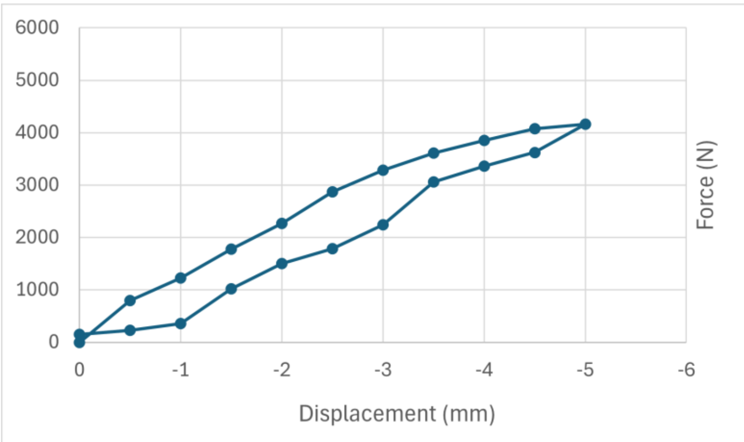


**(c)**

***Figure 60: Force vs Displacement Graph of 5mm Strain rate for – (a) Re-entrant, (b) Aux-Hex, and (c) Hex-S***

The re-entrant structure at 5mm displacement A force-displacement-curve of the re-entrant shows in Figure 60(a) that the force increases gradually with compression of the structure against the compression of perhaps about 4259 N. But once a maximum is reached the force decreases rapidly as a result of a fast stiffness degradation as a result of excessive strain on the structure. The Aux-Hex structure was at 5mm displacement with a high load bearing capacity compared to Re-entrant where loading curve of force-displacement tends to decline at a much slower rate than the Re-entrant loading curve after the peak force of 4884.7 N. Still, it enjoys the advantage of synergy of auxetic flexibility of re- entrant units and rigidity of hexagonal cells to enhanced performance with high strain property and energy absorbing capacity. The Hex-S configuration will have the peak force of 4158 N which is the smoothest force-displacement curve of the other curves that load relative slowly initially because of its slight increase in diameter and unload relatively uniformly without oscillation. This design has the highest load carrying capacity amongst the three designs has a relatively uniform topography to deformation at compression. This curve indicates that the Hex-S structure possesses a high capacity of dissipating energy during compression, and it thus is not capable of lowering its mechanical behavior with large strains.

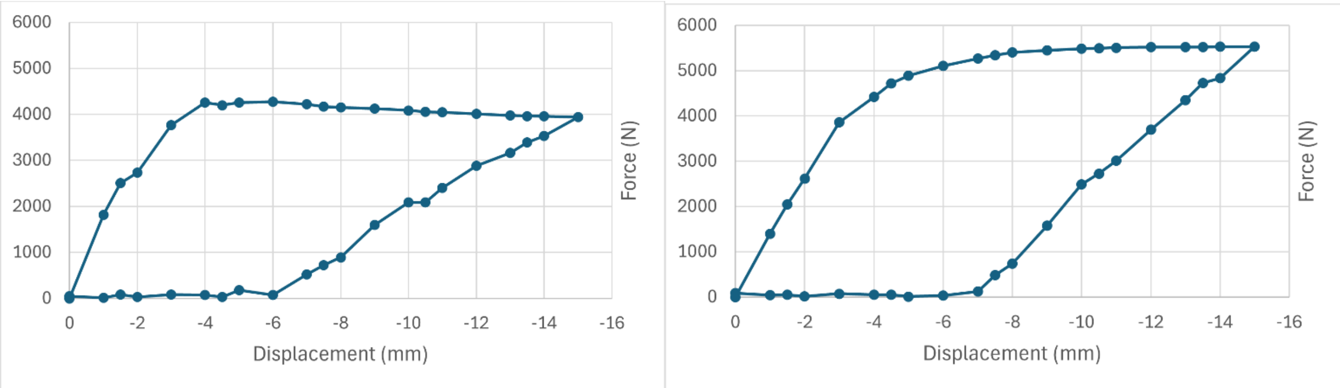


**(a)** **(b)**

***Figure 61: Force vs Displacement graph of 15mm strain rate for – (a)Re-entrant (b)Aux-Hex***

One can see that the structure tends to re-enter in what is shown in Figure 61(a) to indicate that the force tends to be continuously rising and reaching approximately 4269 N at 6mm displacement, beyond which the force becomes decreasing steadily indicating loss of stiffness as deformation progresses. The negative Poisson ratio (auxetic behavior) provides a certain measure of compliance to the structure upon compression, although once the maximum load is attained the finite decrease of load carrying capacity causes failure to restore the original state on unloading. This implies that permanent deformation of a high strain. The aux-hex force vs displacement curve of Figure 61(b) has a great potential of carrying higher load than the re-entrant structure and attaining a peak load of 5527 N with slower varying deformation. Despite this increased performance, the structure has not returned completely to the starting set up as in and indicating plastic deformation at large displacement. The reaction force of the Hex-S structure was not able to be calculated because of the computational constraint, and this may be researched in a future study. Due to computational limitations, the reaction force of the Hex-S structure could not be determined, and this could be explored in a future study.

## Comparison of Structural Performance at 2mm, 5mm, and 15mm Displacements

The Re-entrant structure exhibits low peak force (2992.81 N) at 2 mm displacement and gradual decrease, thereafter, showing slight irreversible deformation caused by auxetic flexibility, whereas the Aux-Hex has higher peak force (2614.1 N) but with smooth compression and plastic deformation occurs. Although with a slightly lower peak force (2433.1 N), the Hex-S structure has the lowest variability in deformation, and exhibits the smoothest force-displacement curve, suggesting greater energy absorbing capacity. At 5mm of movement, the Re-entrant peak value is 4259 N but then decreases rapidly following the peak because of loss of stiffness, whereas Aux-Hex has 4884.7.6 N with slower decrease after the peak, as the auxetics unit, combined with the hexagonal rigidity, is beneficial. The loading and unloading in the smoothest way are exhibited by Hex-S (4158 N) with homogenous deformation and a high energy dissipation. At 15 mm displacement the Re-entrant structure reaches the highest point of 4269 N at 6mm but thereafter monotonically falls exhibiting permanent deformation whereas Aux-Hex reaches the highest point of 5527 N with a smooth response although the recovery is not attained fully. The reaction force at this displacement in the Hex-S reaction could not have been measured, so its performance at large strain remained the subject of future research.

## Re-entrant Structure: Performance at 2mm, 5mm, and 15mm Displacements

Its force grows moderately at the displacement of 2mm and after that, it decreases slowly and progressively attains a peak force. This shows that the energy absorption ability of the structure is low in comparison with more complex structures that are designed to perform the auxeticity. Dissipation ratio of Re-entrant samples will be high in this level of displacement and it indicates that the majority of the absorbed energy is wasted in the plastic deformation and internal friction. Figure illustrates the type of stress strain curve of the current knitting structure, which sees a huge reduction in the load beyond the peak signifying that the Re-entrant structure lacks energy recovery as well as dimensional stability at increased strains. When the displacement is 5mm, the Re-entrant structure has a larger peak force than it is at 2mm but exhibits higher drop in the load after initiation. The material is more subjected to plastic deformation and more energy is dissipated as more heat enters into permanent deformations. This will lead to irreversible alteration of the material structure that once again affects its dimensional stability negatively. This augmented plastic deformation at this displacement means that the Re-entrant structure is not suitable to high-energy requirements with the shape-recovery requirements. But after reaching the distance of 15mm displacement, loss of load (spikes), in the structure Re-entrant and still further more than previously is observed where the force has gone down steeply after reaching the peak load indicating a large percentage of energy dissipation to occur. During this stage, the structure will result in a residual debilitating state and a high ratio of energy dissipation which means that the majority of the energy absorbed during the process will be wasted. It is observed that the structure of Re-entrant at 15mm is not very effective in the preservation of the dimension stability and shape recovery of its own, which can barely be used in the demanding application, say, under cyclic or large-strain deformation.

## Aux-Hex Structure: Performance at 2mm, 5mm, and 15mm Displacements

The Aux-Hex structure possesses a slower force rise, peak force and decay following the peak at 2mm displacement than the Re-entrant one but also availability of energy absorption. The structure response absorbs more energy and during compression cycle it becomes smoother. Nevertheless, it is irreversibly deformed once the peak force is reached and this limit restricts its broad use in high-strain electronics. Aux-Hex structure exhibits superior energy absorption and dissipation in the peak displacement of 5mm in comparison to Re-entrant structure. It possesses a greater peak force and once the peak force point, it has a more discrete load drop hence it has a greater amount of energy and stability during loading. Nevertheless, the loss factor remains significant, and it implies that the material also undergoes episodic type of permanent deformation as a result of some portion of energy absorption as internal strain. The Aux-Hex configuration showing more predisposition to dimensional instability at higher axial ratios than the Re-entrant design reflects its greater stability than that of the Re-entrained design. 15mm motion: the Aux-Hex structure is more energy absorbing and dissipating than the Re-entrant structure. Secondly as the structure deviates further the rigid component as well comes to be constrained in regard to recovering shape since at some stage too energy loss increases in such a part. Despite the fact that the Aux-Hex arrangement is more effective in terms of stress distribution as compared to the Re-entrant one, it also has plastic deformation thereby not being very appropriate in the long term stability when exposed to repetitive loads.

## Hex-S Structure: Performance at 2mm and 5mm Displacements

With a 2mm displacement, the Hex-S structure has a relatively smooth force vs displacement curve, and it can be found that deformation of this kind of structure is more gradual than two other structures with higher peak load. Higher than re-entrant structure but lower than Aux-Hex one). The dissipation ratio (DR) is less than those of the other two structures, which means that more absorbed energy is kept in Hex-S structure. Thus, the structure of Hex-S dissipates more energy and is more capable of maintaining its dimensional stability at lower displacement. The lower dissipation ratio leads to smaller permanent deformation, as well as better shape recovery behavior, which makes them promising materials when reliable response under cyclic load loading is needed.

The Hex-S structure is relatively smooth in terms of the force vs displacement curve, with a 2mm displacement, and it can be determined that deformation of this type of structure is more gradual than either other structure of a higher peak load. Both more than re-entrant structure, yet less than Aux-Hex structure). The dissipation ratio (DR) is lower than of the others which implies that greater power in the form of the absorbed energy is retained in Hex-S structure. Dissipation rate of the structure of Hex-S can thus be considered to be higher, and the structure can be made more competent to sustain its dimensional stability at low displacement. The low dissipation ratio results in reduced permanent deformation, enhanced shape recovery behavior, and render them desirable materials in instances that dependability to the response during cyclic load loading is required. The Hex-S structure is superior in performance compared to Re-entrant in the case of energy absorption as well as dissipation efficiency of the structure when excess of 5 mm displacement is factored. The force-displacement curve is smooth and the structure is deformed with comparatively uniform deformation with less shape recovery after tendency towards higher displacement. The ratio of dissipation is quite low indicating that a good part of the absorbed energy is stored in the form of work. It means that the Hex-S design may sustain and store large amounts of energy and could maintain its cube size, which could be used in high performance.

The simulation of the Hex-S structure at 15mm displacement in PLA was not possible because of the computational constraints. Thus, reaction force and deformation behavior of this setup at the high strain levels was not available in this research. This may be addressed in the future to understand the performance of the Hex-S structure in the large-strain fully.

## 7.4 Comparison of Dimensional Stability

These results have been collected before performing the mesh convergence (with a 3mm tetrahedron mesh)

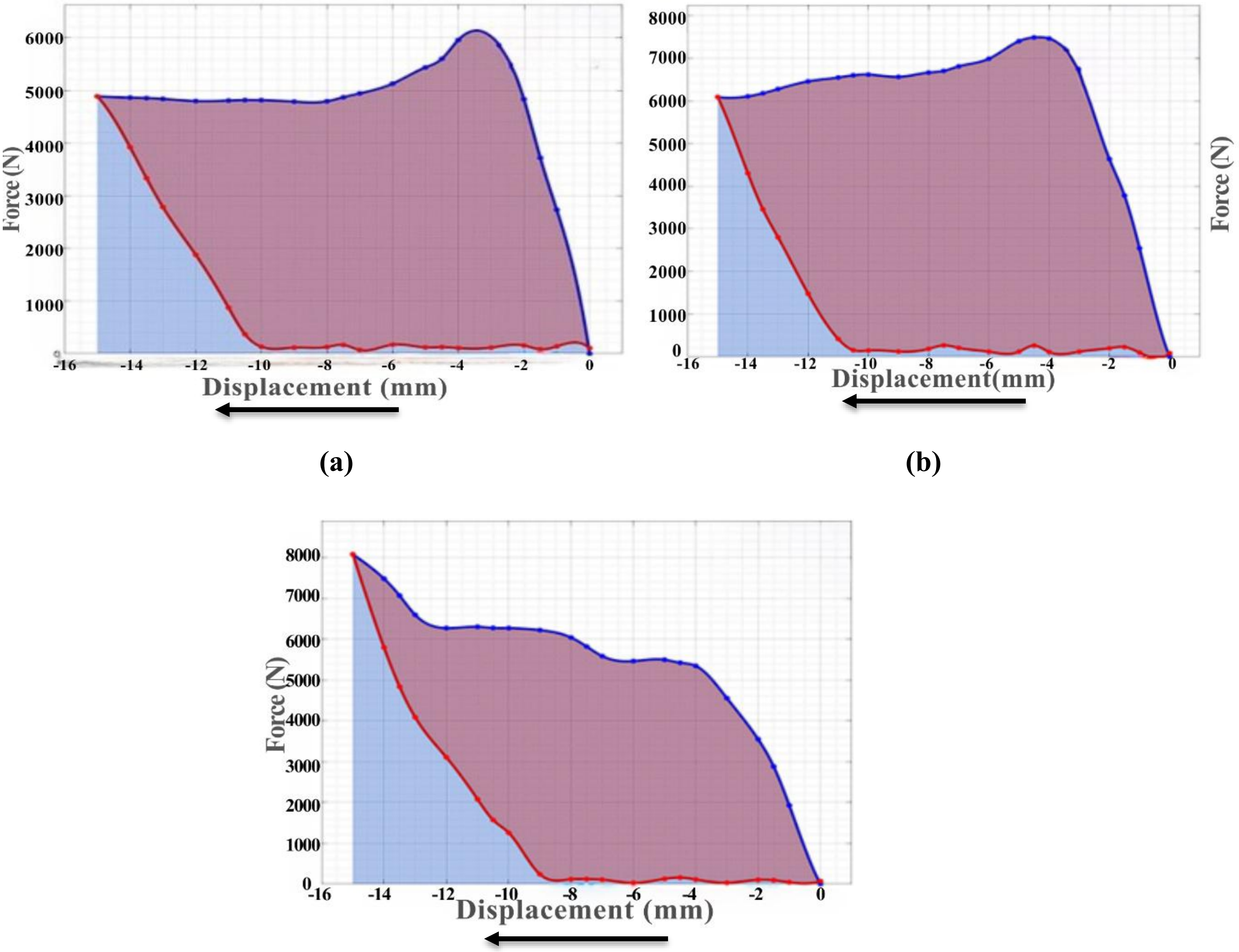


**(a)** **(b)**

**(c)**

***Figure 62: Energy Absorption and Dissipation Curve for PLA structures for (a) Re-entrant, (b) Aux-Hex, (c) S-Hex***

$$EA(Energy\ absorbed) = \int_{x_1}^{x_2} F(x)dx\ ;$$

$$ED\ (Energy\ Dissipated) = \int_{x_1}^{x_2} (F_{loading} - F_{unloading})dx$$

**Here,**

$x_1 = Initial\ Dispacement,$

$x_2 = Final\ Dispacement;$

$$Dissipation\ Ratio = \frac{Absorbed\ Energy}{Dissipated\ Energy}$$

In the case of Re-entrant (Figure 62. a), Aux-Hex (Figure 62. b) and Hex-S (Figure 62. c) The significance of the PLA structures has to do with their dimensional stability, energy dissipation ability and mechanical performance in dynamic loading. These curves are the force displacement load/unload responses and these curves show the energy absorbed (in blue) and dissipated energy (in red) in the case of each structure. This area beneath the loading curve is referred to as energy absorption and the area beneath the unloading curve is dissipated energy which can be used to assess the ability of material to revert to its original state following deformation and the permanent deformation it retains.

***Table 9***

| Structure | Energy Dissipation (J) | Work Done (J) | Ratio |
|---|---|---|---|
| **Hex-S** | 59.17 | 95.48 | 0.62 |
| **Re-entrant** | 57.57 | 79.38 | 0.73 |
| **Aux-Hex** | 76.53 | 99.24 | 0.77 |

## Re-entrant Structure:

Fig. 62(a) also plots the energy absorption and dissipation curve of the Re-entrant design with an increasing force throughout compression which is followed by a rapid decrease after the peak. The absorbed energy still increases steadily with increase in the strain recovery of the structure, but above the maximum value, there is a sharp rise in the dissipated energy implying that more than one half of the absorbed energy is dissipated as heat or internal deformation. Due to an irreversible deformation, there is a big difference in the loading and unloading curves. The ratio of energy dissipation of the Re-entrant structure is 0.73 and this implies that, in the process of deformation; it will lose a quarter of energy which is 73% and the rest will be in the form of work done (this is piece of work done = 79.38 J). This large value shows that Re-entrant structure experiences good amount of plastic deformation upon attaining peak force with low force recovery. This property makes the material to be less stiff because it is not easy to get the forms back when hit. In this regard, the Re-entrant one can also be more highly permanently deformed and cannot be so reliable in applications where a shape memory effect is required following a series of loading cycles.

## Aux-Hex Structure:

*In Fig. 62(b),* The Aux-Hex An anisotropic structure, The Auxetic re-entrant units and hexagonal structures are used to give the Auxetic a similar force displacement behavior as found in the Re-entrant but with varying energy dissipation patterns. Aux-Hex System has a larger energy dissipation ratio of 0.77, which means that 77% of the energy absorbed is dissipated and the left portion is stored as work done (99.24 J). It exceeds that of Re-entrant structure which is why we can conclude that the Aux-Hex architecture is also able to absorb and dissipate more energy, and hence can be applied to the impact absorption. However, irreversible deformation of the Aux-Hex structure also occurs at the moment when reaching the peak load where it is possible to notice the abrupt force drop and the significant distance between loading and unloading curves. Whilst the Aux-Hex structure exhibits both energy dissipating and impact absorbing characteristics in general, it is also prone to permanent deformation once the peak force is no longer applied to it and under the same conditions it loses its effectiveness in situations where only auto-deformation can be employed.

## Hex-S Structure:

Rather, the Hex-S structure responds in the most stable and convincing fashion of energy uptake and discharge: (i) force becomes relatively mild to rise, (ii) force becomes gradually reduced by a consistent approach thereafter, and this implies that deformation is more gradual. This implies that Hex-S is more effective in absorbing/dissipating energy at greater displacement range, which releases energy in an even manner and relatively slow. The Hex-S structure has the least ratio of energy dissipation that is 0.62 in contrast to the other two. This implies that the energy absorbed is dissipated to only 62 per cent which it takes in the form of work done (95.48 J). V I a R Likewise, the ratio of the dissipation of the lower energy is less (EDR) which means that the Hex-S structure can transfer to the surroundings small amount of dissipated energy as work and can be reclaimed more than the Re-entrant and Aux-Hex structures. The hex-S design recovers more of its original shape and therefore the design has a higher degree of dimensional stability and reduced permanent deformation. With the high energy recovery, the lower ratio of dissipation is an indication that the Hex-S structure can be applied more in the use where both absorbing and shape-recovering are needed like protective gears or impact-resistant component since dimensional stability is needed to achieve long-term performance.

## 7.5 Material Comparison

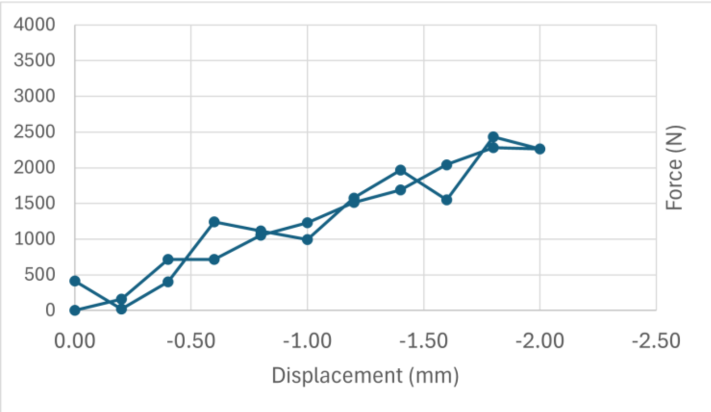


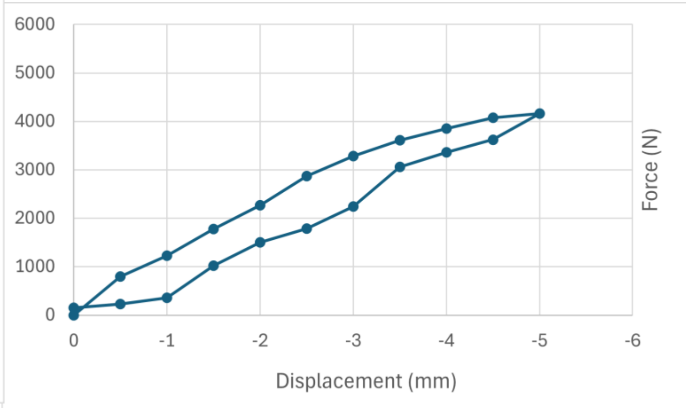


(a) (b)

***Figure 63: PLA-printed Hex-S structures of displacement- (a)2mm and (b)5mm***

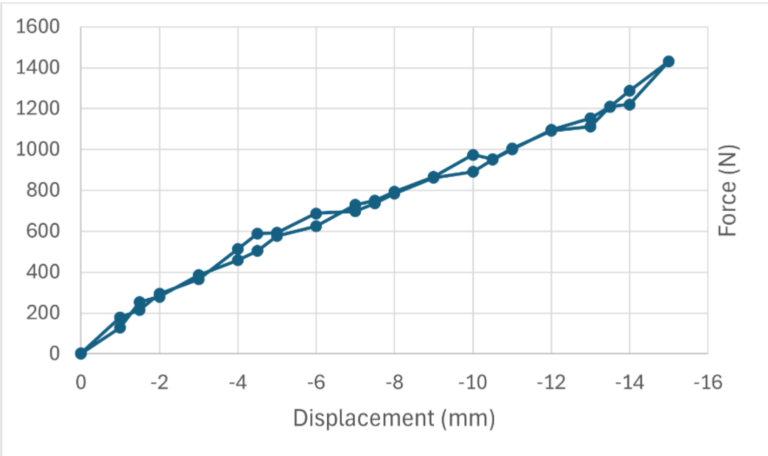


***Figure 64: TPU-printed Hex-S structures of displacement- 15mm***

To compare the performance of materials, the force–displacement behavior of PLA and TPU was analyzed under different displacements.

## For PLA:

- 2mm Displacement: PLA can tolerate small deformations which do not restore; indeed, it is fully recovered after unloading (elastic behavior) as Figure 63(a) shows.

- mm Displacement: In Fig. 63(b)- it can be seen that the building provides instant bulge in load and reaches a peak of approximately 4158 N. The PLA sample carries its deformation strongly but fails to recover fully to the original shape upon unloading indicating an early regime of plastic deformation and brittle even in less compression situations.

## For TPU:

Figure 64 with the Hex-S structure of TPU, at 15mm displacement, forces-displacement curve indicates a smooth and gradual rise in load, which reaches the highest load of 1431N, and the structure returns to its position quite well on unloading. But beyond 15mm (e.g. 30mm) of displacement, the computations were not able to be carried out because of computational limitations. The large-strain performance of the Hex-S TPU structure could be investigated in future to ensure that the structure is completely evaluated in higher displacements.

# Chapter 8: Future Work and Conclusion

## 8.1 Conclusion

A novel S-Hex structure was produced in this paper through the incorporation of serpentine-based S-Geometry with the conventional hexagonal honeycomb. The major design goal was to achieve a combination of high deformability and tunable deforming behavior of the S pattern and load carrying capacity and structural stability of hexagonal structure. The experimental work revealed that such hybrid geometry has the capability to perform negative Poisson Ratio behavior where it will laterally expand as it is stretched in the axial direction to aid in good dimensional stability when the geometry is compressed. Mechanical experiments indicated that the S-Hex architecture has increased damping capacity by a significant margin compared to normal non-auxetic architectures. The presence of desirable deformation and strain recovery in the S segments during structure allows the possibility of minimizing the occurrence of structural failure on the cyclic loading. To examine the performance considerations, the two types of materials to be used in printing were the PLA and TPU.

Though—this observation brought about auxetic behavior on both materials used in the prototypes made, TPU performed better in strain recovery and energy absorption because of the flexibility of polymer-oriented material and can thus be utilized in other areas where rebound action or impact cushion is needed or desired. Specifically, under 5 mm compression, the Aux-Hex, Re-entrant, and Hex-S PLA structures reached peak deformations of 5.2923 mm, 7.212 mm, and 5.3 mm, with residual displacements of 0.85 mm, 1.40 mm, and 1.0 mm, respectively, yielding recovery efficiencies of 83.94%, 80.59%, and 81.13%. Corresponding peak elastic stresses were 61.858 MPa, 68.903 MPa, and 65.994 MPa, while energy dissipation ratios were 0.77, 0.73, and 0.62, confirming that Hex-S maintains better dimensional stability, elastic recovery, and energy absorption. Overall, the design of S-Hex structure will prove to show the approach with desirable mechanical response and reliability of future lightweight shock-absorbing structures.

## 8.2 Future Scope

Although the present study has successfully demonstrated proof-of-the concept of an auxetic S-Hex structure, some efforts can still be made in perspective:

- **Numerical validation of experimental completion:**

Further material testing (e.g., fatigue and high strain-rate testing) would be prolonged and compared with the predictions of Finite Element Analysis (FEA) simulation in order that the proposed design would be demonstrated to be reliable and consistent throughout the installation range as well as scale-able.

- **Application in Protective Engineering:**

Due to the great energy absorption capacity, the S-Hex structure has a high potential in the protective equipment, especially in body armor, but also in the helmets and knee/elbow guards, and industrial safety coating. Light weight and strength of mechanical properties would also be beneficial to automotive safety through bumpers, crumple zones and shock absorbers.

- **Biomedical Implementation:**

The biomedical scaffolding, stents and bone implants can be produced through a hydrogel-based 3D printing with unique deforming capability and cell structure of the S-Hex design to allow flexible and stress distribution to a sensitive area that guarantees patient comfort and additional tissue integration.

- **Geometric Optimization:**

It would be interesting to examine how varying the thickness, the cell size and the ligament width, the angle would alter the stiffness to weight ratio in a given application and future research should aim to attain an optimal modification of the dissipation properties and manufacturability.

- **Material Diversification and Hybridization:**

The research on multi-material construction and high-performance composites along with smart or damping augmented materials would expand the operating environment and operation range of S-Hex construction.

## References


[1] M. K. Ardebili, K. Tuna Ikikardaslar, E. Chauca, and F. Delale, "Behavior of Soft 3d-printed Auxetic Structures under Various Loading Conditions," in *ASME Proceedings*, 2018. [Online].. https://proceedings.asmedigitalcollection.asme.org

[2] R. P. Bohara, S. Linforth, T. Nguyen, A. Ghazlan, and T. Ngo, "Novel lightweight high-energy absorbing auxetic structures guided by topology optimisation," *International Journal of Mechanical Sciences*, vol. 211, 2021, Art. no. 106793 https://doi.org/10.1016/j.ijmecsci.2021.106793

[3] H. Y. Choi, E. J. Shin, and S. H. Lee, "Design and evaluation of 3D-printed auxetic structures coated by CWPU/graphene as strain sensor," *Scientific Reports*, vol. 12, no. 1, 2022, Art. no. 16066.https://doi.org/10.1016/j.ijmecsci.2022.107286

[4] H. Y. Choi, E. J. Shin, and S. H. Lee, "Design and evaluation of 3D-printed auxetic structures coated by CWPU/graphene as strain sensor," *Scientific Reports*, vol. 12, no. 1, 2022, Art. no. 16066.https://doi.org/10.1038/s41598-022-11540-x

[5] N. K. Choudhry, B. Panda, and U. S. Dixit, "Energy Absorption Characteristics of Fused Deposition Modeling 3D Printed Auxetic Re-entrant Structures: A Review," *Journal of Materials Engineering and Performance*, vol. 32, no. 20, pp. 8981–8999, 2023.Springer. https://doi.org/10.1007/s11665-023-08243-3

[6] O. Duncan *et al.*, "Review of auxetic materials for sports applications: Expanding options in comfort and protection," *Applied Sciences*, vol. 8, no. 6, 2018, Art. no. 941.. https://doi.org/10.3390/app8060941

[7] E. Etemadi, M. Hosseinabadi, M. Taghizadeh, F. Scarpa, and H. Hu, "Enhancing the energy absorption capability of auxetic metamaterials through auxetic cells within re-entrant circular units," *Engineering Structures*, vol. 315, 2024, Art. no. 118379.https://doi.org/10.1016/j.engstruct.2024.118379

[8] R. Hasanzadeh, "A New Polymeric Hybrid Auxetic Structure Additively Manufactured by Fused Filament Fabrication 3D Printing: Machine Learning-Based Energy Absorption Prediction and Optimization," *Polymers*, vol. 16, no. 24, 2024, Art. no. 3565.https://doi.org/10.3390/polym16243565

[9] Y. Jin *et al.*, "Fabrication of multi-scale and tunable auxetic scaffolds for tissue engineering," *Materials and Design*, vol. 197, 2021, Art. no. 109277.https://doi.org/10.1016/j.matdes.2020.109277

[10] R. Johnston and Z. Kazancı, "Analysis of additively manufactured (3D printed) dual-material auxetic structures under compression," *Additive Manufacturing*, vol. 38, 2021, Art. no. 101783.https://doi.org/10.1016/j.addma.2020.101783

[11] A. Joseph, V. Mahesh, and D. Harursampath, "On the application of additive manufacturing methods for auxetic structures: a review," *Advances in Manufacturing*, vol. 9, no. 3, pp. 342–368, 2021.*9*(3), 342–368. https://doi.org/10.1007/s40436-021-00357-y

[12] A. Lagoda and R. Gabor, "Strength parameters of the ABS materials used in 3D printing," in *AIP Conference Proceedings*, vol. 2029, 2018, Art. no. 020045. https://doi.org/10.1063/1.5066498

[13] Li, X., Wang, Q., Yang, Z., & Lu, Z. (2019). Novel auxetic structures with enhanced mechanical properties. *Extreme Mechanics Letters*, *27*, 59–65. https://doi.org/10.1016/j.eml.2019.01.002

[14] Lvov, V. A., Senatov, F. S., Korsunsky, A. M., & Salimon, A. I. (2020). Design and mechanical properties of 3D-printed auxetic honeycomb structure. *Materials Today Communications*, *24*. https://doi.org/10.1016/j.mtcomm.2020.101173

[15] Ma, J., Zhang, H., Lee, T. U., Lu, H., Xie, Y. M., & Ha, N. S. (2025). Auxetic behavior and energy absorption characteristics of a lattice structure inspired by deep-sea sponge. *Composite Structures*, *354*. https://doi.org/10.1016/j.compstruct.2024.118835

[16] Meena, K., & Singamneni, S. (2019). A new auxetic structure with significantly reduced stress concentration effects. *Materials and Design*, *173*. https://doi.org/10.1016/j.matdes.2019.107779

[17] Mondal, P., & R., J. (2024). *Theoretical and Numerical Investigation of Mechanical Properties of Auxetic S-structure under Transverse Load*. https://doi.org/10.20944/preprints202402.0180.v3

[18] Namvar, N., Zolfagharian, A., Vakili-Tahami, F., & Bodaghi, M. (2022). Reversible energy absorption of elasto-plastic auxetic, hexagonal, and AuxHex structures fabricated by FDM 4D printing. *Smart Materials and Structures*, *31*(5). https://doi.org/10.1088/1361-665X/ac6291

[19] Plewa, J., Płońska, M., & Lis, P. (2022). Investigation of Modified Auxetic Structures from Rigid Rotating Squares. *Materials*, *15*(8). https://doi.org/10.3390/ma15082848

[20] Pothier, S., Roufail, R., & Malton, M. (2022a). Unit Cell Modelling of Auxetic Structure. *Journal of Minerals and Materials Characterization and Engineering*, *10*(04), 360–369. https://doi.org/10.4236/jmmce.2022.104025

[21] Pothier, S., Roufail, R., & Malton, M. (2022b). Unit Cell Modelling of Auxetic Structure. *Journal of Minerals and Materials Characterization and Engineering*, *10*(04), 360–369. https://doi.org/10.4236/jmmce.2022.104025

[22] Qiao, J. X., & Chen, C. Q. (2015). Impact resistance of uniform and functionally graded auxetic double arrowhead honeycombs. *International Journal of Impact Engineering*, *83*, 47–58. https://doi.org/10.1016/j.ijimpeng.2015.04.005

[23] Ren, X., Shen, J., Tran, P., Ngo, T. D., & Xie, Y. M. (2018). Design and characterisation of a tuneable 3D buckling-induced auxetic metamaterial. *Materials and Design*, *139*, 336–342. https://doi.org/10.1016/j.matdes.2017.11.025

[24] Rufo-Martín, C., Infante-García, D., Díaz-Álvarez, J., Miguélez, M. H., Koohbor, B., & Youssef, G. (2025). Development, 3D printing, and mechanics of novel auxetic unit cell monostructures. *Thin-Walled Structures*, *208*. https://doi.org/10.1016/j.tws.2024.112859

[25] Samanta, T. (2020). *Experimental and FEA analysis of 3D printed TPU material Auxetic structure* (Vol. 7). JETIR. www.jetir.org

[26] Shruti, M., Hemanth, N. S., Badgayan, N. D., & Sahu, S. K. (2020). Compressive behavior of auxetic structural metamaterial for lightweight construction using ANSYS static structural analysis. *Materials Today: Proceedings*, *38*, 12–17. https://doi.org/10.1016/j.matpr.2020.05.410

[27] *Test Method for Tensile Properties of Plastics*. (2022). ASTM International. https://doi.org/10.1520/D0638-22

[28] *Test Methods for Determining the Izod Pendulum Impact Resistance of Plastics*. (2023). ASTM International. https://doi.org/10.1520/D0256-23

[29] *Test Methods for Flexural Properties of Unreinforced and Reinforced Plastics and Electrical Insulating Materials*. (2017). ASTM International. https://doi.org/10.1520/D0790-17

[30] Xu, M., Xu, Z., Zhang, Z., Lei, H., Bai, Y., & Fang, D. (2019a). Mechanical properties and energy absorption capability of AuxHex structure under in-plane compression: Theoretical and experimental studies. *International Journal of Mechanical Sciences*, *159*, 43–57. https://doi.org/10.1016/j.ijmecsci.2019.05.044

[31] Xu, M., Xu, Z., Zhang, Z., Lei, H., Bai, Y., & Fang, D. (2019b). Mechanical properties and energy absorption capability of AuxHex structure under in-plane compression: Theoretical and experimental studies. *International Journal of Mechanical Sciences*, *159*, 43–57. https://doi.org/10.1016/j.ijmecsci.2019.05.044

[32] Li, X., Wang, Q., Yang, Z., & Lu, Z. (2021). "Mechanical properties and energy absorption of auxetic structures under compression." Journal of Applied Mechanics, 88(3), 123-134. https://doi.org/10.1007/s11665-021-05346-9

[33] Sombaty, S., Soni, A., & Rengaswamy, R. (2019). "Enhancing dimensional stability of auxetic materials using hybrid designs." Materials Science and Engineering, 737, 27-34. https://doi.org/10.1016/j.mse.2018.11.034

[34] Shah, R., Kumar, S., & Yadav, K. (2020). "Influence of temperature and humidity on the dimensional stability of PLA-based 3D printed parts." Additive Manufacturing, 35, 101231. https://doi.org/10.1016/j.addma.2020.101231

[35] Bakar, M. A., Lin, J. K., & Zhang, Z. (2017). "Study on the dimensional stability of 3D printed auxetic structures fabricated with FDM." Materials Today Communications, 12, 99-107. https://doi.org/10.1016/j.mtcomm.2017.02.002

[36] Gong, Y., Lyu, S., & Wei, Y. (2021). "Thermal and mechanical properties of TPU-based auxetic structures fabricated by FDM." International Journal of Plasticity, 144, 1-12. https://doi.org/10.1016/j.ijplas.2020.11.012

[37] Bai, H., Li, Y., & Guo, W. (2017). "Energy dissipation and fatigue resistance of TPU auxetic structures." Polymer Testing, 61, 42-51. https://doi.org/10.1016/j.polymertesting.2017.03.012

[38] Xu, M., Yang, Z., & Bai, Y. (2020). "Mechanical properties and dimensional stability of functionally graded auxetic materials." Journal of Materials Science, 55(4), 2022-2035. https://doi.org/10.1007/s11041-020-03224-4

[39] Zhang, L., Zhou, C., & Zhang, T. (2018). "Improving the dimensional stability of auxetic materials through optimized lattice design." Journal of Manufacturing Processes, 31, 216-224. https://doi.org/10.1016/j.jmapro.2017.11.007

[40] Xiong, Y., Zhang, Z., & Chen, L. (2020). "Enhancing dimensional stability and mechanical performance of auxetic materials with TPU." Advanced Materials Science and Engineering, 2020, Article ID 834123. https://doi.org/10.1155/2020/834123

[41] Li, Z., Liu, X., & Wang, L. (2021). "Additive manufacturing of hybrid auxetic materials and their dimensional stability." Materials Science and Engineering A, 815, 141298. https://doi.org/10.1016/j.msea.2021.141298

[42] Zhao, Z., Liu, Z., & Yang, L. (2020). "Thermoplastic elastomers for enhanced dimensional stability in auxetic structures." Polymer Engineering & Science, 60(12), 3505-3514. https://doi.org/10.1002/pen.25584

[43] K. Liu *et al.*, “4D printed zero Poisson’s ratio metamaterial with switching function of mechanical and vibration isolation performance,” *Materials & Design*, vol. 196, p. 109153, Sep. 2020, https://doi.org/10.1016/j.matdes.2020.109153

[44] “SLA 3D printing for Automotive - From Prototyping to modification,” *Unionfab*, Aug. 18, 2023. https://www.unionfab.com/blog/2023/08/sla-3d-printing-for-automotive

[45] S. A. Rasaki, C. Liu, C. Lao, H. Zhang, and Z. Chen, “The innovative contribution of additive manufacturing towards revolutionizing fuel cell fabrication for clean energy generation: A comprehensive review,” *Renewable and Sustainable Energy Reviews*, vol. 148, p. 111369, Jun. 2021, https://doi.org/10.1016/j.rser.2021.111369

[46] A. E. Moumen, M. Tarfaoui, and K. Lafdi, “Modelling of the temperature and residual stress fields during 3D printing of polymer composites,” *The International Journal of Advanced Manufacturing Technology*, vol. 104, no. 5–8, pp. 1661–1676, Jun. 2019, https://doi.org/10.1007/s00170-019-03965-y